3.8.2 H_2O and OH on semiconductors

W. JAEGERMANN, TH. MAYER

3.8.2.1 Introduction

In this data collection the adsorption and adsorbate properties of H_2O and OH on well defined semiconductor surfaces in UHV are summarized. The adsorbate induced changes of substrate properties are only considered, if they are intrinsically related to the adsorption process. They are subjects of other parts of this LANDOLT-BÖRNSTEIN III/42A2. Here only those effects are mentioned which are absolutely necessary to understand the basic adsorbate properties. Reactions with the substrate are only covered, if they are immediately connected with dissociative adsorption below or at room temperature. Thermally induced reactions at elevated temperatures, usually an oxidation of the semiconductor substrate and details about the involved mechanisms, are not presented here in any detail, despite the fact that many papers dealing with H_2O adsorption are motivated by this process and contain results in this respect. A number of review articles have been published in the past, which present and discuss the interaction of H_2O with semiconductor surfaces (see e. g. [87F, 88F, 95W1]).

The interaction of H_2O with semiconductor surfaces is studied to achieve a fundamental understanding of solid/liquid interfaces involving aqueous solutions. Such interfaces are the essential part of semiconductor based devices as (photo)electrochemical and (photo)catalytic cells and sensors. They are also of central importance in wet chemical etching and processing steps in semiconductor microelectronics as e.g. in passivating oxide formation. Usually the number of reactants is rather large in these applications and the interface interactions may become very complex. As a consequence the electronic properties of the interfaces may vary depending on the processing steps strongly influencing the operation of the devices. In many cases the microscopic origin of the involved changes are not very well understood, as the species interacting with the semiconductor surfaces have not been identified and their electronic interactions remain unclear. As H_2O is often the main constituent with high surplus in the solution its interaction with the semiconductor must be understood in very detail. Thus, H_2O as an adsorbate on defined semiconductor surfaces is of basic interest and also a key ingredient to a fundamental understanding of wet-chemical processes in many technological applications.

In contrast to metals the bonding interactions of semiconductors are governed by localized and directional chemical bonds. Therefore the adsorption process as well as the adsorbate properties are in general strongly influenced by the structure and chemical composition of the substrate surface, which again depends on the preparation procedure used for a specific semiconductor [92B, 95M]. The atomic structure of semiconductor surfaces deviate considerably from bulk truncated surfaces as most semiconductors undergo severe surface relaxations and reconstructions to minimize their specific surface energies. Thermodynamic driving force is the attempt to minimize the number of energetically unfavourable surface dangling bonds produced by the loss of translational symmetry across the surface. Furthermore compound semiconductors exhibit surface atoms of different polarity adding electrostatic potentials and different dangling bond energies to the surface energy. As a consequence the adsorption is strongly dependent on the specific surface orientation and the kind of semiconductor used for investigation. In addition, the procedure of surface preparation and the obtained defect concentration may vary in different investigations which also influences the adsorption process. Therefore the data and conclusions given in literature may differ due to these effects. These factors will be discussed in more detail in section 3.8.2.2 and 3.8.2.3.

Different surface terminations imply very different surface electronic structures ([92B, 94H, 94S2, 95M] and LANDOLT-BÖRNSTEIN III/24B, chapter 3.2 by Calandra and Manghi). Already on clean semiconductor surfaces the energetic position and dispersion of surface states and surface resonances strongly influences the charge distribution between semiconductor bulk and surface. Local dipoles involve only the surface atoms, but extended space charge layers lead to extended layers of ionized dopants in the bulk. As the adsorption of H_2O as an electron donating adsorbate induces charge transfer from its occupied molecular orbitals to the semiconductor, the electronic structure of the surface changes with adsorption. On the other hand a dissociative adsorption will lead to surface bound OH and H groups

which may be neutral or partially negatively/positively charged. Depending on their bonding properties and surface molecule energy states the charge transfer between the bulk and the surface may change again. As a result adsorbed H_2O or OH and H may strongly change the electronic surface potentials and, vice versa, the given surface potentials of the semiconductor substrate controlled by its doping may influence the adsorption process. A more detailed discussion on these effects is given in section 3.8.2.4.

The variation in structural and electronic properties of different semiconductors with their specific surface terminations leads to strongly varying adsorption properties and bonding interactions. The interaction with adsorbates as H_2O and its dissociation products will depend on the number, distances and relative orientations of specific surface atoms and related bonding sites. Due to adsorption the substrate structure and electronic structure will change again in most cases. It turns out that depending on the experimental conditions as e.g. temperature and dosage the exposure of most semiconductors to H_2O does not only lead to adsorption but the adsorbate species may further react with surface and subsurface atoms. These surface reactions following the adsorption step lead to oxidation and etching, which may already be initiated at low sample temperatures. Therefore, it is hardly possible to prepare identical adsorption stages in different experiments. Many contrary interpretations on H_2O adsorption on semiconductors are probably related to this effect that adsorption and subsequent reaction steps occur in parallel.

Most of the work on water adsorption on semiconductors has been performed with Si surfaces. This is evidently in part motivated by the fact that Si is the best established semiconductor material, which can rather easily be prepared in different surface orientations and defined reconstructions. In addition, it is the semiconductor most important in technology. Especially the interaction with H_2O is of interest for etching processes, the formation of H-terminated surfaces, and oxide growth. A large number of investigations have been performed using different surface science techniques. For the technically important Si(100) surface and to a lesser extent for the Si(111) surface the interaction of H_2O (OH) as an adsorbate is well studied and reasonably well understood. In cases where some uncertainties may still exist these are given in the text and added as remarks in the tables. For all other semiconductors the number of investigations is much smaller. In these cases there is no general agreement on H_2O adsorption, yet. Even the most simple question on the mode of adsorption – dissociative or molecular – is still not clarified for many semiconductors. For these semiconductor substrates it is attempted to give a survey of the performed experiments and the main conclusions, as given in the original contributions. We do not attempt to draw any final conclusions on the mode of adsorption and the adsorbate properties. In cases, where parts of the results seem to be questionable based on other and more recent investigations, remarks will be added in the text and as a comment in the tables.

List of Acronyms and Symbols used in this chapter

Acronyms

AES	Auger electron spectroscopy
ARUPS	angle resolved UPS
CNDO	complete neglect of differential overlap of atomic orbitals on the same atom
DB	dangling bond
DAS	dimer adatom stacking fault
DFT	density functional theory
ELS	energy loss spectroscopy
EHT	extended Hückel theory
ESDIAD	electron stimulated desorption ion angular distributions
HREELS	high resolution electron energy loss spectra
IR	infrared
IRAS	infrared absorption spectroscopy
LCAO	linear combination of atomic orbitals
LDA	local density approximation
LDFT	local density functional theory
LDFT/LDA	LDFT within the local density approximation

LEED	low energy electron diffraction
LEIS	low energy ion scattering
LITD	laser induced thermal desorption
MNDO	modified neglect of diatomic overlap
MO	molecular orbital
ODA	outer dimer atom
PED	photo electron diffraction
PSID	photon stimulated ion desorption
PYS	photoemission yield spectroscopy
SIMS	secondary ion mass spectrometry
STM	scanning tunneling microscopy
SXPS	soft XPS or synchrotron induced XPS
TDS	thermal desorption spectroscopy
TPD	thermal or temperature programmed desorption
TOF-SARS	time of flight scattering and recoiling spectrometry
UHV	ultra high vacuum
UPS	ultraviolet photoelectron emission spectroscopy
XPS	x-ray photoelectron emission spectroscopy

Symbols

$\Delta\phi$	change of workfunction
χ	electron affinity
$\Delta\chi$	change of surface dipol
ΔE_B	change of binding energy
E_B	binding energy
E_B^F	binding energy referenced to E_F
E_B^{vac}	binding energy referenced to vacuum level
E_B^{VBM}	binding energy referenced to valence band maximum
E_F	Fermi level
E_{vac}	vacuum level
eV_{bb}	band bending
E_{VBM}	valence band maximum
θ	coverage
θ/θ_{sat}	relative coverage
θ_{sat}	saturation coverage
H_{ads}	adsorbed hydrogen
L	Langmuir (1×10^{-6}Torr × 1s = 1.33×10^{-6}mbar × 1s)
ML	monolayer
O_{ads}	adsorbed oxigen
OH_{ads}	adsorbed OH
RT	room temperature
Si_{ad}	adatom of Si(111)7×7 reconstruction
Si_{rest}	restatom of Si(111)7×7 reconstruction
S	sticking coefficient
S_0	initial sticking coefficient for $\theta \rightarrow 0$
S/S_0	relative sticking coefficient
100 K	sample temperature in K
→300 K	adsorption at low temperature, measurement taken after annealing to 300 K

3.8.2.2 Surface preparation

The adsorption of H_2O on semiconductor surfaces evidently depends on the type of semiconductor, its surface orientation, and the procedure applied to prepare clean and defined substrate surfaces. For this reason some early experiments on H_2O adsorption on powdered/crushed semiconductors published in the literature will not be considered in this data collection (see e.g. [68E]). The different techniques known for the preparation of metal surfaces in UHV, namely thermal cleaning, ion bombardment, ion bombardment and annealing, and in situ deposition by any vacuum deposition process cannot be applied with the same success to most semiconductor surfaces. The different surface orientations of elementary semiconductors like Si and Ge are usually prepared by cleaving in vacuo or by ion bombardment and annealing. Also starting from chemically etched surfaces is possible, which is followed by a thermal cleaning process. In general, there are well established procedures available, which allow to prepare surfaces of comparable quality.

For compound semiconductors the surface preparation may be very complex depending on the specific surface orientation under consideration. High quality substrate surfaces are obtained for the cleavage planes, which are the non-polar surfaces of the substrate material. For compound semiconductors with Zinkblende structure as e.g. GaAs these are the (110) planes. All other surface orientations are usually prepared by several ion bombardment and annealing cycles, which may result in many different surface reconstructions or facetting. In principle, it is also possible to obtain high quality surfaces of most surface orientations by in-situ MBE growth or by transferring epitaxial films from any growth chamber using shielding surface layers, which can be heated off at elevated temperatures. To our knowledge such surfaces have hardly been used for the investigation of H_2O adsorption. Therefore, adsorption studies on compound semiconductors suffer from different surface pre-treatments and for this reason from differing surface properties.

High quality defect free and chemically inert substrate surfaces can be prepared from the (0001) van der Waals cleavage plane of layered chalkogenide semiconductors. The chemically saturated hexagonally closed packed cleavage plane allows physisorption of H_2O at low sample temperatures only.

Some general information on preparation methods used for the different semiconductor surfaces can be found in the following references [83K1, 92B, 95L, 95M], see also LANDOLT-BÖRNSTEIN III/24A. Details on the preparation of the substrates are usually given in the experimental part of the cited papers.

3.8.2.3 Surface structure: relaxation and reconstruction

Clean semiconductor surfaces of a defined crystallographic plane do usually not exist in their bulk truncated structure. Assuming homonuclear cleavage of bonds in surface formation unsaturated directional dangling bonds are formed which are only occupied with a single electron. In order to minimize the surface free energy these semiconductor surfaces exhibit a pronounced tendency to surface relaxation or reconstruction, which may involve a severe structural rearrangement of surface atoms. Thermodynamic driving force is the reduction of the number of energetically unfavourable dangling bonds and/or of their electronic character by charge redistribution. Whereas relaxation processes and also some surface reconstructions can occur spontaneously, some of the thermodynamically more stable surface reconstructions need the thermal activated diffusion of surface atoms. Therefore, the structural rearrangement on the idealized surface is also influenced by the substrate temperature profile used within the preparation sequence. As a consequence different surface terminations are known to exist for elementary and compound semiconductors depending on the preparation sequence used, which are listed in several reviews [83K1, 92B, 95L, 95M] and a previous LANDOLT-BÖRNSTEIN III/24A. The reader should refer to this article for the representation of the structural arrangement of a certain surface, given in the established notation of its superstructure as e.g. found in LEED. The number of dangling bonds, their distance and orientation to each other, as well as their atomic origin deviate considerably on the different semiconductor surfaces. As these dangling bonds act as adsorption sites one expects strong variations in H_2O adsorption properties on different semiconductor surfaces.

The semiconductor substrates considered in this review are:

- the elementary semiconductor surfaces Si(100), Si(100)2×1, Si(100)2×1 vicinal, Si(111)7×7, Si(111)2×1, Si(113)3×1, Si(113)3×2, Ge(100)2×8, Ge(100)2×1, Ge(111)2×8, Ge_xSi_{1-x}(100)2×1;
- the 3-5 compound semiconductor surfaces GaAs(100), GaAs(100)2×4, GaAs(100)4×6, GaAs(110), InP(110), InP($\bar{1}\,\bar{1}\,\bar{1}$), AlAs(100)1×1;
- the chalcogenide semiconductor surfaces GaSe(0001), InSe(0001), $MoSe_2$(0001), MoS_2(0001), WSe_2(0001); pyrite FeS_2(100);
- and the ternary compound semiconductor surface $CuInSe_2$(011)

Furthermore, the adsorption also is influenced by the ideality (structural quality) of the prepared surface. The number of defects depends on the detailed experimental procedure used for the preparation. The experimentally observed results may be governed by these defects, which may act as adsorption and dissociation sites on otherwise inert surfaces. For more complex surface terminations the „intrinsic“ adsorption properties of a specific surface orientation can hardly be discerned, if the number of defects after preparation is large. But the number of defects, which are actually obtained, are hardly known for most investigations (besides when using techniques like STM) and are usually not quantified. A summary of possibly formed defects on semiconductor surfaces is also given in LANDOLT-BÖRNSTEIN III/24A, chapter 2.3 by Henzler and Ranke.

3.8.2.4 Surface electronic structure and surface potentials

The electronic structure of different semiconductor surfaces may also vary depending on the type of semiconductor surface and the existing reconstruction. The energy levels of dangling bonds formed on the surface may be situated in the bulk bandgap forming surface states or may be outside the gap forming surface resonances. As a consequence the semiconductor substrate has different surface electronic properties. In some cases e.g. with Si(111)7×7 the surface is metallic; in other cases e.g. for the perfect GaAs(110) cleavage plane a semiconducting surface is found without electronic states in the bandgap. Also the charge carried by different surface atoms may be different. This is evident for compound semiconductors: on GaAs(110) the surface relaxation is accompanied by a partial electron transfer from Ga to As dangling bonds. But also for elementary semiconductors differently charged surface atoms exist: On the Si(100)2×1 surface the outer dimer atom is negatively charged whereas the inner dimer atom is positively charged. On Si(111)7×7 the adatoms are positively charged whereas the neighboring rest atoms are negatively charged. Polar surfaces as e.g. GaAs (100) or (111) are usually strongly reconstructed with a surface excess of one atomic species, which then dominates the surface electronic structure. Thus, one may expect the adsorption of H_2O as nucleophylic species and subsequent dissociation to occur on different surface sites. The reader should refer to [88H, 94H, 94S2, 95M] and LANDOLT-BÖRNSTEIN, III/24B, chapter 3.2, where the electronic surface properties of clean semiconductor surfaces have been summarized in very detail. It should be noted at this stage that similar to the structural properties of semiconductor surfaces also the electronic properties depend very much on the quality of surface preparation. Defects or contaminations may introduce extra surface states and surface resonances, which do not exist on the perfect surface.

The energetic positions of the semiconductor band edges in reference to the vacuum level are given by the values of the ionization potential $I_p = (E_{vac} - E_{VB})$ and electron affinity $\chi = (E_{vac} - E_{CB})$ of a specific semiconductor surface. For different surface orientations these values only depend on changes of the localized surface dipole extending about a few monolayers. This surface dipole is determined by the polarity of the surface bonds. The surface position of the Fermi level in reference to the semiconductor band edges and thus the work function $\phi = (E_{vac} - E_F)$ additionally depends on the relative position of the bulk Fermi level and the energetic level and occupation of surface states [95M, 96J]. The bulk Fermi level

is given by the type of doping states (acceptor states: p-type; donor states: n-type) and their concentrations. Flat band conditions, which correspond to the lack of extended space charge layers, can only be expected for surfaces free of surface states. In this case the work function of a p-doped semiconductor is larger than that of an n-doped one by the difference of the bulk Fermi level positions. Active surface states may lead to band bending eV_{bb} in the surface region of the semiconductor typically in the range of 100 to 10^4 Å (inverse proportional to bulk doping). Vice versa the work function is changed by the shift of the Fermi level given by eV_{bb} versus the band edges. Acceptor (donor) like surface states will accept (donate) electrons from (to) the bulk of the semiconductor, if their energy position is below (above) the bulk Fermi level. For high concentrations of surface states the surface Fermi level is pinned at the energetic level of the surface states; as a consequence p- and n-doped semiconductors show the same work function. The electronic properties of clean semiconductor surfaces are summarized in Ref. [88H, 94H, 94S2, 95M] and LANDOLT-BÖRNSTEIN III/24A, chapter 3.2. With adsorption and depending on the bonding properties the electronic surface states or resonances may change their character (acceptor or donor) and/or energy position in respect to the band edges. As a consequence the band bending and surface dipole will usually be changed.

The value of the binding energy E_B of electronic states measured e.g. for adsorbed species by photoemission depends on the reference level used. If the Fermi level is used as common reference level (E_B^F) a shift of binding energy value may occur with adsorption, which is related to a change of semiconductor band bending corresponding to a surface Fermi level shift. This band bending can be related to a charge transfer from the bulk to the adsorbate or may be induced by the adsorbate due to passivation of electronically active surface states originally present in the bulk bandgap of the material. As a consequence the binding energy values E_B^F may change with coverage without any change in the adsorbate electronic state. The induced band bending will also influence the changes of the work function $\Delta\phi = eV_{bb} + \Delta\chi$, with $\Delta\chi$ as the change in electron affinity due to changed surface dipole potentials. To avoid changes due to band bending the binding energy values are also referred to the valence band maximum E^{VBM}. In this case only surface dipole potentials showing up between the adsorbate and the substrate may shift the relative binding energy values of adsorbate vs. substrate lines. If the vacuum level is taken as reference level, the binding energy values E_B^{vac} are affected by band bending eV_{bb} and surface dipoles [95M, 96J] e.g. by the overall shift of work function $\Delta\phi$. The changes of surface potentials are not specifically covered in this part of the LANDOLT-BÖRNSTEIN series on adsorption but in the contribution of Jacoby and Nilsson et al. (LANDOLT-BÖRNSTEIN III/42A2, chapters 4.2 and 4.3). But for presenting the electronic properties of adsorbate states the different reference values and their influence on the experimentally determined binding energy values always have to be kept in mind. In principle, the different binding energy scales can be referred to each other, but, unfortunately, the necessary data on band bending and work functions are not given in all papers presented in this work.

One may also expect a strong influence of semiconductor bulk doping on H_2O adsorption. If charge transfer from the bulk to the adsorbate is involved, the type of doping and the related band bending defines, which type of charge carrier, electron or hole, is more easily available in the adsorption process. This has been extensively discussed in older work on ionosorption (ionic adsorption) of adsorbates on oxide semiconductors [55H, 63W, 77M], but has not been studied in any detail in more modern work with defined semiconductor surfaces. As in many cases even the doping of the semiconductors are not given in the cited papers, we did not specifically address this point in this data summary.

3.8.2.5 Methods of investigation

For the investigation of H_2O adsorption on semiconductor surfaces all relevant techniques of surface science have been applied during the last years. Only experiments performed in UHV have been considered thus excluding e.g. scanning probe experiments at air or in solutions. The principles of the most important methods of investigations are described in detail in LANDOLT-BÖRNSTEIN III 42/IA2. chapter 2. General information on experimental techniques can also be found in other LANDOLT-BÖRNSTEIN volumes as III/24 and in many monographies on surface science techniques. We use the standard abbreviations without further explanations. They are summarized in section 3.8.2.1. Also theoretical calculations using different methods were applied. For details and limitations the reader may refer to the original literature.

We also want to note that the application of a certain technique may disturb the adsorption process and the obtained results. In general, the degree of disturbance decreases from ions to electrons to photons, and also from high energies to small energies. Especially with semiconductors the formation of defects may already be introduced by the use of high energy photon beams of high brilliance as e.g. given by synchrotron radiation. These effects may be even more severe, if adsorbates are present. It is usually expected that spectroscopic techniques as UPS and IR do not disturb or modify the surfaces. But in any case changes of spectral features with time may indicate probe induced surface processes. Also the thermal excitation of the adsorbate by hot filaments must be taken into account. For well defined experiments pressure measurements are performed in clear separation from the substrate. This could not be verified for all of the quoted experiments. A discussion on probe induced modification of the adsorption process was part of the controversy on molecular and dissociative H_2O adsorption on Si surfaces.

3.8.2.6 Adsorption mode

For all semiconductors and their different surface terminations there was a long lasting controversial discussion in literature, if the mode of H_2O adsorption is dissociative or molecular. This controversy seems to be settled now at least for Si(100), Si(111), and Ge, for which the experimental results clearly support dissociative adsorption at room temperature saturating the surface dangling bonds (see Table 1). On Si even at low temperatures dissociation occurs. On top of the dissociative adsorption layer molecular H_2O may be condensed as H-bonded physisorbed ice layer, at substrate temperatures below 150 K. At elevated temperatures above RT the oxidation of the surface sets in after complete dissociation of H_2O into O_{ads} and $2H_{ads}$. This process is (at least partly) already observed at RT or even below.

The adsorption mode of H_2O on 3-5 semiconductors seems to be less clear. Some data suggest an initial dissociative adsorption even at low temperature, whereas others support a dissociative adsorption only at RT and some authors conclude on strongly chemisorbed H_2O (Table 1). The reactivity may also depend on the surface orientation and the applied preparation conditions. The orientation dependence of H_2O adsorption on 3-5 semiconductors has not been systematically studied, yet.

The layered chalcogenides with their chemically inert van der Waals (0001) surfaces seem to be the only system identified so far, for which physisorbed H_2O (ice layer) is condensed at low temperatures (<150 K). It is completely desorbed without dissociation above this temperature.

We do not include in Table 1 results from theoretical calculation as they are only significant in comparison to experimental results (see Table 2 and 6).

Si (100) and its reconstructions

All the earlier investigations were mainly addressed to the question whether water adsorption on Si surfaces is either molecular or dissociative. According to ellipsometry data, it was proposed [71M] that H_2O dissociates into 2H and O to saturate all the surface dangling bonds. Early UV photoemission spectra were interpreted to be due to molecular adsorption [81F1, 81F2, 83S2] but could not be confirmed later on. UPS measurements performed later give different spectra [84O, 89F], which now are attributed to OH and H groups saturating the Si(100)2×1 dangling bonds. HREELS and IR spectra clearly prove dissociative chemisorption forming Si-OH and Si-H surface molecules [82I2, 84C1]. There is now general agreement that the dominating process below about 400 K is dissociation into OH and H species which saturate two dangling bonds (DBs) of the 2×1 reconstructed surface (Fig. 1, Fig. 12). STM work [93A, 93C2] shows that the reconstructed dimer bonds of the substrate are not broken which was also concluded from the LEED observation of retaining the (2×1) superstructure [82I2, 84S1, 85C, 87L2].

At low temperatures (below 140 K) molecular water may be condensed on top of the dissociated layer. Above 400 K chemisorbed OH species begin to react further forming atomically adsorbed oxygen [96R2, 97W].

Si (111) and its reconstructions

There is now general agreement that on Si(111)7×7 adsorbed H_2O initially dissociates into OH and H adsorbate species even at about 80 - 90 K, which saturate two neighboring adatom-restatom pairs in the DAS model of the 7×7 surface reconstruction. This conclusion is now consistently supported by HREELS [82I2, 83K1, 85N, 86N, 86S2], UPS [89F], SXPS [95P] and STM [91A, 97S1] data. Early UPS experiments [79F, 81F1, 81F2] were never reproduced in this way and the observed spectra are probably due to the onset of oxidation. Later UPS results [85R1, 85R2, 86S2] show spectra dominated by OH_{ads} due to dissociatively adsorbed H_2O, which have been misinterpreted. Depending on coverage and temperature different dangling bond states are involved leading to different stages of adsorption in the range of about 0.12 and 0.19 ML. It is suggested that OH occupies the adatom sites and H the restatom sites [91A, 97S1], but theoretical calculations also propose a reverse occupation of bonding sites [97E]. The energy and angle dependencies of the vibrational modes in HREELS indicate a preferential orientation of the Si-OH and Si-H bond nearly normal to the surface and of the SiO-H bond tilted by 75° from the surface normal [86N]. The 7×7 reconstruction remains unchanged during the initial adsorption process. At room temperatures and high exposures a slow saturation of all surface dangling bonds is found and subsequently a thermally activated reaction with Si back bonds and complete dissociation into O_{ads} and $2H_{ads}$ is evident. At this stage the surface reconstruction is lost and the oxidation of Si sets in [85N, 85R1, 89K, 95P, 96F, 97S1].

The adsorption of H_2O on laser annealed Si(111)1×1 surfaces also leads to a dissociative adsorption in a much higher surface concentration, which is related to the increased number of surface dangling bonds on this surface [95W2].

The adsorption mode on Si(111)2×1 is less clear. Also here a dissociative adsorption is experimentally found, which is accompanied by a loss of the π–bonded chain structure [84S1].

Ge in different surface orientations

H_2O is suggested to be molecularly adsorbed on Ge(100)2×1 and Ge(111)2×8 surfaces at low temperatures (110 K) or as mixture of dissociative and molecular adsorption. [84C2, 87K2, 87K3, 89L, 91L1, 91L2, 91P1, 92C, 93R1, 93R2]. At RT dissociative adsorption is found for all orientations. The OH_{ads} and H_{ads} species saturate the surface dangling bonds available at the surfaces. The surface reconstruction is lost due to adsorption as deduced from the loss of superstructure diffraction spots in LEED. At elevated temperatures the surface is at least partly oxidized [87K3, 91P1].

3-5 semiconductors in different surface orientations

Only a small number of H_2O adsorption studies with 3-5 semiconductors have been performed so far and no conclusive results on the mode of adsorption for different compounds and surface orientations can be given up till now. Adsorption studies have been performed either with the unreconstructed but relaxed (110)1×1 cleavage plane or with the reconstructed (100) and (111) planes. Based on SXPS data some authors have suggested an initial dissociative adsorption even at low temperatures on (110) surfaces forming Ga(In)-OH and As(P)-H pairs in correspondence to the related Si and Ge surfaces [96H, 97H, 00H]. Others suggest physisorbed and chemisorbed molecular adsorption but the obtained UPS spectra do not agree to the expected emission pattern observed later on other substrates [79B]. On (100) surfaces molecular adsorption is suggested at low temperatures, which is followed by thermally activated dissociation [97M1, 97M2, 98C]. Dissociation always leads to the formation of group 3-OH and group 5-H bonds as the group 5-OH and group 3-H bonds are thermodynamically unfavorable. In all cases the long range surface structure as given by LEED remains unchanged during initial adsorption.

Miscellaneous semiconductors

The van der Waals (0001) surfaces of layered chalcogenides are composed of a close packed array of chemically saturated chalkogenide surface atoms free of dangling bonds. Thus H_2O is only adsorbed molecularly as condensed ice layer at low temperatures (< 150 K) and is completely desorbed at temperatures above. No oxidation is found despite on step edges. For FeS_2 (100) and $CuInSe_2$ (011) at low temperatures a preferential adsorption of molecular H_2O is suggested on Fe and Cu sites, respectively. The stable molecular adsorption was related to the coordination type bonding to transition metal sites.

3.8.2.7 Thermodynamic data of adsorption

There are no recent attempts published to measure thermodynamic data quantitatively e.g. in calorimetric experiments (adsorption isotherms), due to the thermal activated reactivity of most semiconductors with the adsorbate species H_2O and OH. Older data as given in [68E] suffer from an insufficient characterization of the surface structure and composition. Informations on adsorption energies are thus only available from kinetic experiments. But also in such studies the determined activation energies on desorption may be affected by the parallel process of thermally activated reactions of the chemisorbed species with the semiconductor substrates (oxidation). At elevated temperatures most semiconductors form oxides before the chemisorbed adsorbates (H_2O and OH) desorb. Only for multilayer coverage (ice formation) at low temperatures the physisorbed layers will be desorbed at typical temperatures above 150 K. Data on adsorption energies are also available from theoretical calculations, which give bonding energies as calculated for isolated adsorbate/substrate surface molecules.

As an example, on the Si(100)2×1 surface dissociation is observed even at low temperatures (80 - 100 K) [84C2, 85R1] indicating that a possible activation barrier, if existing at all, is quite low. Engler used a theoretical calculation (empirical potential method) to argue that the energy difference between molecular and dissociative adsorption is small, though he predicted a large activation barrier between these states [90E]. In an LDA-DFT calculation the enthalpy change accompanying dissociative chemisorption of one H_2O molecule was calculated to be 3.9 eV [95V].

Using other DFT calculations and cluster models of the surface the energy and mechanism of adsorption, the stability of the dissociated products, and the minimum energy reaction path (Fig. 1) were calculated by Konecny et al. [97K]. In agreement with experimental data they found evidence for a weakly bound molecular precursor but no net activation barrier for adsorption. The values given for the adsorption energy from the different applied methods are summarized in Table 2.

3.8.2.8 Kinetic data of adsorption/desorption, surface diffusion and surface reactions

The kinetics of adsorption are usually determined by the relative sticking coefficient S/S_o (S_o: sticking coefficient for $\theta \rightarrow 0$) versus relative coverage θ/θ_{sat}. (θ_{sat}: saturation coverage). These curves are derived from adsorbate coverages versus exposure. For all well studied semiconductors the experimentally observed sticking coefficients and saturation surface coverages depend strongly on the experimental conditions as surface orientation, temperature, and pressure regime. The changes in relative adsorbate coverage for different surface orientations have been clearly demonstrated with cylindrical single crystals of Si [85R3] (Fig. 2a) or Ge [87K3] (Fig. 6) or with lensshaped samples of Si [90S]. The shape of the adsorption curves cannot be explained by Langmuir adsorption, but are typical for an adsorption process with a mobile precursor state [96R2] as treated by Kisliuk [57K, 58K]. In this model impinging molecules may migrate both over occupied and unoccupied regions of the surface and are finally chemisorbed on two adjacent unoccupied dangling bond sites. It is now well accepted that for the most often studied semiconductor surfaces of Si and Ge initially a fast and nearly activation free dissociative adsorption occurs on bonding sites in close neighborhood to each other. Subsequently, substrate surface bonds are attacked in a thermally activated process, which is accompanied by further adsorption of additional H_2O

molecules. This process is related to the disruption of reconstruction bonds and back bonds. Thus, the adsorption kinetics depend on the number and distances of specific dangling bonds as given by the surface reconstruction of the semiconductor surface.

There are no data available on the desorption kinetics of adsorbed H_2O and OH besides the desorption of condensed ice layers covering the first adsorbate layer. This is due to the fact that after dissociative adsorption of H_2O the surface species react in a thermally activated process with semiconductor substrate atoms to form oxides, which involves the complete dissociation of H_2O with the intermediate step to OH_{ads} and H_{ads} and finally to O_{ads} and $2H_{ads}$. Thus, in thermal desorption spectra first the desorption of H_2 is observed at elevated temperatures which is followed by the desorption of SO_x species (S = surface atom). H_2O adsorption studies on semiconductor surfaces and subsequent activated formation of oxides is motivated by the interest in understanding the basic processes involved in the high temperature wet-oxidation of semiconductors used in electronic device processing. Detailed studies on the thermally activated wet oxidation following adsorption of H_2O is found for example in the following papers (Si: [85N, 89K, 96F] Ge: [87K3, 91P1] 3-5: [93C1, 96H, 97M1, 98C, 00H]). In this data collection the substrate oxidation is considered only if it occurs in adsorption/desorption experiments of adsorbed H_2O or of the dissociation product OH, but not as a subject in itself.

The results obtained on kinetic aspects of adsorption and desorption as well as surface diffusion and reaction are summarized in Table 3.

Si (100) and its reconstructions

The kinetics of adsorption has been investigated in detail in the temperature range from below 140 K, where multilayer adsorption becomes possible, to above 400 K, where OH radicals begin to react further eventually forming atomically adsorbed oxygen [96R2, 97W].

STM work [93A, 93C2] shows that the reconstruction dimers of the substrate are not broken, during dissociative adsorption of H_2O with the formation of Si-OH and Si-H surface molecules (Fig. 1 [97K]). Correspondingly, LEED experiments show that the (2×1) periodicity is conserved [82I2, 84S1, 85C, 87L2]. The coverage dependence on dosing as well as the detailed analysis of Si 2p core-level shifts [85R3] indicate a saturation coverage θ_{sat} of 1/2 monolayer (ML). However, a small fraction of dangling bonds always remains unoccupied [93A] since water dissociation needs two adjacent empty dangling bonds, which do not always belong to one dimer. When approaching saturation, some isolated single dangling bonds remain unsaturated, which are unable to dissociate water. Thus, the highest coverage achieved is below 0.5 ML (0.48 ML [93A], 0.41 ML [96F]).

All studies agree that the initial sticking coefficient S_0 is high (near unity). It is reported to be almost constant up to saturation [85R3, 90S] leading to the assumption that a mobile precursor state exists which allows to model the coverage vs exposure time dependence as in Fig. 3 [96R2].

Si (111) and its reconstructions

The RT adsorption of H_2O on Si(111)7×7 can be divided into three adsorption regimes. The values given for the sticking coefficients and the transition coverage or saturation coverage vary in different reports (see Table 3) depending evidently on sample preparation and experimental parameters (e.g. temperature, dosing, applied experimental technique). The first fast regime is attributed to a fast, precursor mediated, dissociative adsorption probably on rest-atom/adatom pairs forming OH and H radicals, which saturate two neighboring dangling bonds (Figs. 4, 5) [91P3, 96F]. This dissociation is also observed at low temperature (180 K). The second regime corresponds to the complete saturation of all Si(111) surface dangling bonds forming a two-dimensional hydrosilicate phase (Si-OH + Si-H). This process is eventually accompanied by complete dissociation of adsorbed H_2O in minor amounts (Si-O-Si + 2SiH). Both processes involve the surface diffusion of Si atoms and of the adsorbed species e.g. OH_{ads}. The last very slow regime at coverage above approximately $\theta = 0.6$ is related to Si-oxide formation and reactive attack of back bonds.

Ge in different surface orientations

There are only very few studies on the kinetics of H_2O adsorption on Ge surfaces and no final conclusion can be drawn. The sticking coefficient is lower compared to Si surfaces being highest for the Ge (100) ([87K3], Fig. 6). A physisorbed precursor state is assumed [92C]. On Ge(111) adsorption of one H_2O molecule induces structural rearrangements of 50 to 80 atoms on the substrate surface [73H, 75S]. Heating to elevated temperatures (T > 600 K) leads to a complete dissociation of H_2O with the formation of Ge-O-Ge groups in analogy to Si(100) [91P1].

3-5 semiconductors in different surface orientations

The experimentally found adsorption rate of H_2O is very low at RT for all surface orientations [84M, 89S, 96H, 00H]. Desorption spectra are characterized by a molecular desorption peak at low sample temperatures (150 - 180 K) due to desorption of physisorbed H_2O including multiple ice layers [93C1, 97M1, 97M2, 98C]. Another well defined desorption peak occurs at 350 K due to desorption of strongly interacting H_2O (dissociative or molecularly?) and broad ill defined desorption peaks extend up to 750 K depending on surface orientation and conditions, which are related to desorption from surface hydroxyls. H_2O desorption and dissociation is induced by annealing (needed temperatures depend on the system) and can also be induced by irradiation with 50 eV electrons [96S2]. At elevated temperatures complete dissociation and formation of oxides sets in. On GaAs(110) the differential sticking coefficient shows a pronounced discontinuity, which has been related to an adsorbate induced loss of surface relaxation ([84M], Fig. 8).

Miscellaneous semiconductors

No systematic kinetic studies on the desorption of H_2O from layered semiconductors have been performed. Only qualitative results are given on the desorption temperatures of the adsorbed ice layer at substrate temperatures of about 150 K [92M, 93M].

3.8.2.9 Local structure

Detailed information on the local structure of the adsorbed species is only available for the Si(100)2×1 surface. Here a number of different experimental techniques have been applied and have been complemented with theoretical calculations. As a result, the electron rich O atom is placed close to the electrophilic dangling bond (downward shifted Si atoms of the dimer) and the hydrogen towards the nucleophilic dangling bond (upward shifted Si atom of the dimer, i.e. the outer dimer atom ODA). The reaction mechanism may be described as simultaneous weakening of an O-H bond and formation of Si-O and Si-H bonds on the electrophilic and nucleophilic sites of the dimer, respectively (Fig. 1). Also information on the orientation, bonding distances and bonding angles of the dissociation products OH and H are given (see Table 4). ESDIAD results clearly indicate that the O-H bond direction is off-normal (Fig. 9a, 9b) [87L2, 94G] and that the Si-OH bond direction is normal to the dimer bond direction. Detailed numbers on bond angles are given from photoelectron diffraction data [98F](Fig. 12) and theoretical calculations [89O, 95V, 97K].

On “clean” Si(100)2×1 surfaces three defects are usually observed in STM images, which were interpreted as missing dimers (A), pairs of missing dimers (B) and pairs of half dimers with two Si atoms missing on the same side of a dimer row (C). Also cluster defects CD composed of the defects A, B, C are found [89H, 92W]. The number of sites appearing like C and A defects increases with exposure to 0.05 L H_2O and are termed W and M in Fig. 10 [93C2]. The occupied state image obtained with H_2O saturated surfaces shows that the dimers bound to the dissociation products H and OH are atomically resolved. In addition, the density of missing dimers is reduced after water adsorption [93A]. Thus the dark features M

and W induced by low H_2O dosage are attributed to nondissociated H_2O molecules. Also the C defects are attributed to two water molecules on the same side of adjacent dimers in a row and A defects to two water molecules on each side of one dimer. The water molecules are assumed to be stabilized by hydrogen bonds. Since single water molecules are not found in STM, they are assumed to be rather mobile. The formation of chains of molecular H_2O appears to be an important precursor for dissociative chemisorption [93C2]. With increasing exposure to H_2O the growth of islands of dimers saturated with H and OH is observed while the number of islands is constant. At saturation a few single dangling bonds remain uncovered due to the fact that two dangling bonds are necessary for dissociation, which also may belong to different (neighboring) dimers (Fig. 11) [93A]. Both STM studies have noticed that adsorbed water appears identical to features previously assigned to intrinsic defects of the Si surface, suggesting that at least some of those apparent defects are actually due to water adsorbed from the background pressure (see above).

For all other semiconductor surfaces there is only rudimentary information on the structural arrangement of adsorbed H_2O/OH available in the literature. On Si(111)7×7 OH_{ads} is considered to be adsorbed on top sites with an Si-O bond orientation normal to the surface [85N, 86N]. STM data indicate dissociative adsorption of adatom-restatom pairs and adsorbate islands due to H-bond formation (Fig. 13) [91A, 97S1]. On FeS_2 and $CuInSe_2$ a preferential occupation of molecularly adsorbed H_2O on Fe and Cu sites has been deduced (Fig. 14) [91P2, 92S]. This selective bonding to only one kind of the available surface atoms has been explained by the atomic orbital character of the conduction band state involved in the donor like coordination bonding of the H_2O lone pair orbitals. Based on the limited information available it can be concluded that the adsorption of H_2O is governed by a coordination type bonding of its lone pair orbitals with the nucleophylic sites (conduction band forming orbitals) of the semiconductor substrate. In addition, interadsorbate interactions due to H-bond formation have to be taken into account. After dissociation the bonding geometry of OH_{ads} to the surface is governed by the orientation of the σ bonds formed with the semiconductor dangling bonds.

3.8.2.10 Long range order

No detailed quantitative investigations of the surface structure of adsorbed H_2O and its dissociation products on semiconductors are given in the literature. LEED has mostly been used as qualitative argument for the discussion of adsorption modes and bonding sites. In addition, a few STM experiments are available, giving information on the long range order of substrate and adsorbates (see Table 5). If the coverage is kept at about one monolayer (for molecular adsorption at low temperatures) the LEED superstructure spots of the substrates remain unchanged indicating that the surface reconstruction is retained. Also in the regime where OH_{ads} and H_{ads} are formed by dissociative adsorption the LEED superstructures are usually conserved as e.g. for Si(100)2×1 [87L2, 93L] or Si(111)7×7 [86N, 91P3, 92D, 97Z]. This indicates that the adsorbates only saturate the available danglings bonds on the surface and do not destruct the stabilizing surface back bonds. But there are also cases known, where the superstructure is lost and a (1×1) structure is formed as for Si(111)2×1 [85S] or Ge(111)2×1 [73H, 75S, 79G] indicating a change in substrate surface bonding. The detailed analysis of LEED data shows that the adsorption of one H_2O molecule converts the superstructure in an area of 50 - 300 surface atoms around the adsorption site [73H, 75S]. On GaAs(110) a qualitative interpretation of I(V) curves in LEED indicates the loss of surface relaxation with H_2O adsorption [84M]. The LEED reflections and thus the long range order are completely lost, when the surface conditions favor surface oxidation by complete dissociation of adsorbed H_2O, which already starts at RT for high exposures.

STM studies show that adsorbed water is not uniformly distributed over the Si(100)2×1 surface at low coverages. Instead the water fragments form small islands, consistent with adsorption through a mobile precursor state (Fig. 10, 11) [93A, 93C2]. Simultaneous changes in both dangling bonds of a single dimer were observed, so that there is a preference for adsorbed fragments to remain paired. Anderson and Köhler [93A] observed a strong correlation among occupied dimers, with adsorption much more likely to occur at a dimer adjacent to an already occupied dimer. Adsorbate islands grow preferentially in the direction along and perpendicular to dimer rows. Also on Si(111)7×7 the 7×7 superstructure is conserved and adsorbate islands are formed [91A, 97S1] (Fig. 13).

3.8.2.11 Electronic properties

The investigation of the electronic structure of adsorbed H_2O by photoelectron valence band spectra (UPS) has mostly contributed to the controversy about dissociative vs. molecular adsorption (Table 1 and 6). Adsorbed H_2O in its molecular state should lead to three typical main emission lines in the upper valence band (see Fig. 17, 19, 23, 24, 25, 26) corresponding to the $1b_1$ molecular orbital (MO) (non bonding, O lone pair, gas phase ionization potential I_p = 12.6 eV), $3a_1$ MO (partly bonding, partly non-bonding, O lone pair, I_p = 14.7 eV) and the $1b_2$ MO (OH-bonding, I_p = 18.5 eV). The gas phase spectra and the spectra of condensed molecules are given e.g. in [87T] and in LANDOLT-BÖRNSTEIN III 23A, chapter 2.3. After adsorption these states may broaden, split or shift in energy depending on interadsorbate interaction and on the interaction with the substrate [83S1, 87K3]. The $3a_1$ state of H_2O will split into two levels by the formation of dimers and will lead to a broad feature by ice layer formation due to hydrogen bonding. The characteristic emission pattern of molecular H_2O adsorption is given in Fig. 19 for H_2O monomers, H_2O dimers and ice on Ge(100) [87K3]. Typical ice spectra are found in Fig. 26 for layered chalcogenide substrates [92M, 93M]. When the binding energy values measured for the gas phase spectra are compared to the measurements of the adsorbates different contributions of binding energy shifts must be considered. One important contribution is the unknown decrease of the measured binding energy value due to extraatomic relaxation effects (final state hole screening), which depends on the spatial distance of the adsorbate to the substrate. If the measured binding energy values of adsorbates are referred to the Fermi level of the substrate, a further reduction of the binding energy by the value of the work function must be taken into account which may further depend on band bending effects (see also section 3.8.2.4). For the valence band maximum as reference level the ionisation potential must be taken into account. Its value may change with adsorbate coverage. The experimentally determined values of the adsorbate induced additional emission lines and reference value used in the experiments are given in Table 6. However, as in many cases the position of E_F in the bandgap and the value of the work function was not reported, the different binding energy values are not compared to each other. However, a typical value for referring the gas phase ionisation potentials to E_F is $\Delta E_B \approx 7$ eV which is composed of a typical value of 5 eV for ϕ and 2 eV for the extraatomic relaxation term.

For dissociated H_2O the molecular orbitals of OH_{ads} and H_{ads} should be found. For OH_{ads} assuming a negative charge, e.g. OH^-_{ads} gas phase MOs are often derived from the isoelectronic HF molecule which leads to a degenerate 1π MO (nonbonding, F lone pairs, I_p = 16.0 eV) and the 3σ MO (FH-bonding, I_p = 19.9 eV) in the upper valence band region [82G]. The ionization potentials of OH^- as measured for solid NaOH are at ~ 8.2 eV (1π) and ~ 12.5 eV (3σ) (vs. E_{vac}) [87T]. However, if the orientation of the adsorbed OH will not be exactly perpendicular to the substrate surface the degeneracy of the 1π MO is lifted and a bonding and non-bonding state with respect to substrate-bonding interaction may be formed. The assignment of the OH_{ads} emission lines is still done in a controversial way. The experimentalists tend to assign the strong emission and the often observed shoulder line at low binding energy to the 1π MO of adsorbed OH, which has lost its degeneracy due to interaction with the substrate [87K3, 88M, 89L, 91L1, 91L2]. The high binding energy line is due to the 3σ MO OH-bonding state. However, based on theoretical calculations the assignments of the lines are given as (from low to high binding energies): O 2p non-bonding lone pair (deduced from 1π MO), the 3σ MO OH-bonding state energetically shifted to lower binding energies due to reduced OH bond strength, and the Si-O σ bonding state (MO formed by the overlap of the second 1π MO and Si s orbitals) [83C1, 83C2, 87K1, 89F, 94S1]. Which assignment is correct cannot be decided, yet, and therefore both are used in Table 6. Furthermore, the contributions of H_{ads} should lead to additional adsorbate induced states in the upper valence band region, which, however, are generally believed to be of low intensity. Again the binding energy position of the adsorbate states may depend on the given energy scale and interatomic relaxation effects.

Thus, depending on the assumptions used for spectral interpretations experimentally found adsorbate induced emissions may be related to different energy states of adsorbate species and substrate bonds. Furthermore, if the binding energy scale is referred to the Fermi level, band bending effects induced by the adsorbate or differences in the doping level, which shift the position of the Fermi level in the bandgap, may lead to additional problems in assigning the UPS valence band emission lines. Finally, for most semiconductors the adsorption of H_2O does not lead to a stable adsorbate state, but depending on the conditions, e.g. the substrate temperature, chemical reactions with the semiconductor back bonds may occur in parallel. Therefore, the adsorbate state depends very much on the specific parameters used in the adsorption sequence and a not well defined state of the surface may be analyzed.

As already discussed before the electronic surface potentials, as surface position of the Fermi level, respectively band bending and work function, may change considerably during the adsorption process. But in many cases published in literature the authors were evidently not specifically interested in these effects and therefore no systematic data are available. For this reason we did not include the scarce data in our review. The reported changes of work function due to adsorption are given by Jacobi in LANDOLT-BÖRNSTEIN III/42A2, chapter 4.2

Si(100)2×1

On Si(100)2×1 after saturation of H_2O adsorption at RT the photoemission spectrum shows two strong adsorbate induced lines at about 6.5 and 11.5 eV, the former one indicating a shoulder at about 7.5 eV (see Figs. 15, 16) [84O, 85R1, 85R3, 87L1, 88M, 89F, 90S, 91L1, 94S1, 96R2]. These lines are now assigned to adsorbed OH formed after dissociation; the corresponding H_{ads} does not give prominent structures. The surface states contribution of the Si(100)2×1 surface close to the Fermi edge is quenched during the adsorption process indicating the loss of the corresponding dangling bonds [85R3]. These typical emission lines are already found at lowest coverage even at low sample temperatures (Fig. 16) [85R1], which excludes a stable initial molecular adsorption state.

Molecular adsorption of H_2O showing the typical emission features is obtained for multilayer condensation at low temperatures (Fig. 16) [85R1]. After annealing such low temperature adsorbate phases to RT first a spectrum typical for OH_{ads} is obtained and later the substrate oxidation sets in. The UP spectra, which originally have been interpreted to be due to chemisorbed molecular H_2O [81F1], has not been reproduced by other authors besides in difference spectra [85R1]. They are probably due to a mixed adsorption state composed of surface oxides with OH and H-bonded H_2O.

The given assignments are supported by a number of theoretical calculations performed for different orientations of molecular and dissociatively adsorbed H_2O (see Table 6). The energetic order of the OH states and H_2O molecular states depends on the assumed orientation of the adsorbates to the surface.

Si(111)7×7

Also on Si(111)7×7 after low temperature H_2O adsorption and annealing to RT or after quasi-saturation coverage at RT a valence band photoemission spectrum is obtained, which is dominated by two strong lines with the low binding energy feature evidently composed of two overlapping emission lines (see Fig. 17) [85R1, 85R2, 86S2, 89F]. As for Si(100) this spectrum can be assigned to dissociatively adsorbed H_2O in the form of OH_{ads} and H_{ads}. The adsorbed H leads to very weak emission lines at even lower binding energy and thus is not discriminated in the experimental data.

At low sample temperature H_2O is adsorbed as ice layer showing the typical three emission line spectrum [85R1, 85R2, 85R3, 86S2]. The three line emission spectrum as obtained by Fujiwara [79F, 81F1, 81F2] assigned to chemisorbed H_2O was obtained later on only in difference spectra (RT saturation coverage- RT low coverage regime, Fig. 17) [85R1, 85R2]. It is clear now that the originally given interpretation as due to molecular adsorption does not hold. Based on the given spectral features it also does not fit to coadsorbed H_2O stabilized by OH_{ads} and H_{ads}. Therefore, in agreement to the vibrational data the best interpretation may be to assume a mixture of OH_{ads}, H_{ads}, and a certain concentration of Si-O due to complete dissociation of H_2O.

The expected electron states of molecularly adsorbed H_2O on Si(111) dangling bonds have also been calculated and compared to the experimental data (Table 6). The electron states found depend on the assumptions on binding geometry: for H_2O adsorbed normal to the surface (O pointing downwards) the original $3a_1$ MO state of H_2O is strongly shifted in energy close to the $1b_2$ state due to overlap with the Si 3s states. The $1b_2$ state is hardly affected. For H_2O tilted 90° the original $1b_1$ state is shifted close to the $1b_2$ state and the $3a_1$ state is hardly affected. For an intermediate bonding angle also an intermediate situation with remnants of all H_2O based MOs is found [87K1].

Si in other orientations

Also on Si(110) [85R1] and typical stepped surfaces (e.g. Si (113) [97R]) H_2O is dissociatively adsorbed at RT showing the typical spectral features of OH_{ads} and H_{ads}, which saturate the existing dangling bond states.

Ge in different surface orientations

On Ge(100) or (111) surfaces at low sample temperature (110 K) molecular adsorption has been observed showing the transition of physisorbed isolated H_2O molecules, to H_2O dimers, and finally to H_2O clusters (ice) in the UP spectra (Fig. 19, 20, 23) [87K3]. The spectral features are very similar to each other besides a splitting of the $3a_1$ level and finally the broadening of this level as expected for interadsorbate interaction mediated by H-bonding. After annealing to RT dissociatively adsorbed H_2O is found with spectral features in close correspondence to the above given data on Si. The dispersion found for these adsorbate states is small (Fig. 21, 22) [91L2].

3-5 semiconductors in different surface orientations

The spectral features as obtained for different surfaces of 3-5 semiconductors after H_2O adsorption so far do not allow a final conclusion on the adsorbate species formed and an unambiguous assignment of the valence band features. Only the spectra, which are obtained as condensed ice layers at low temperatures (Fig. 24, 25) can be clearly assigned [97H, 00H]. It seems reasonable to assume dissociative adsorption on the (110) plane for certain conditions, as the surface arrangement of dangling bonds are similar as for Si(100)2×1. The spectral features obtained may be interpreted in this way but the given assignment to the possibly formed group 3-OH and group 5-H surface molecules is not completely clear yet, as the intensity pattern does not agree to the expectations (strong -OH and weak -H emissions) (Fig. 24, 25) [97H, 00H].

Miscellaneous semiconductors

The adsorption of H_2O on different chalcogenide surfaces (layered chalcogenide (0001), FeS_2(100), $CuInSe_2$(011) is only possible at low temperatures with spectral features in UPS which can well be assigned to molecularly adsorbed H_2O in the form of ice (Fig. 26) [75Y, 87J, 88J, 91P2, 92M, 92S, 93M, 96M].

3.8.2.12 Core level lines

The core level photoelectron spectra found for H_2O adsorption on semiconductors are mostly related to substrate binding energy shifts. We therefore present these data as they are good indications for the mode of adsorption. In some cases it is not clear whether the use of high brilliance light as e.g. synchrotron light enhances the surface oxidation after dissociative adsorption due to electron impact of the secondary electrons (see e.g. [95P]). Alternatively, the data may suggest partial oxidation to occur already in parallel to the adsorption process by thermal activation of surface diffusion. All semiconductor surfaces show additional emissions in their photoelectron core level spectra besides the bulk emission lines (surface core level shifts) which are due to surface reconstructions/relaxation [92B, 94S2, 95L, 95M]. On the clean Si(100)2×1 surface three surface components of the Si 2p core level are discriminated. Their binding energy shift relative to the bulk component and assignment are given as: -0.49 eV (outer dimer atoms ODA), +0.06 eV (inner dimer atoms) and +0.22 eV (second layer atoms) [92L]. The accepted model of the 7×7 reconstruction of Si(111) surface as proposed by Takayanagy et al. [85T] leads to complex Si 2p core level spectra [94K, 94L, 97P] which have been assigned differently by different authors. We follow

here the assignment as suggested by [94K] as it was used for the discussion of H_2O adsorption [95P] consisting of surface components at S_1: -0.698 eV (rest atom), S_3: 0.530 eV (adatom), S_4 : -0.183 eV and S_5: 0.930 eV with respect to the bulk component. Also Ge(100)2×1 [89L, 91L1, 93R1] and the surfaces of compounds with Zinkblende structure show surface core level shifts [94S2, 95M, 97H] which must be considered in the interpretation of adsorbate induced binding energy shifts. For all investigated semiconductors dissociative adsorption leads to the loss of surface core level shifts in the substrate emissions. These core level shifts indicate a different charging of different surface atoms (in addition to different final state screening), which is immediately lost when the surface dangling bonds become saturated indicating adsorption on the corresponding sites. Nearly no high quality core level photoemission data do exist for the O core lines as the O 1s level was beyond the high resolution limit for second generation synchrotrons and the O 2s line has a very low photoionization cross section.

3.8.2.13 Vibrational properties

Vibrational data of adsorbed H_2O (OH) species on semiconductor surfaces have been obtained either from electron energy loss spectra (HREELS) or infrared absorption spectroscopy (IRAS). In order to separate adsorption from the residual background in the vacuum chamber in many cases the deuterated analogs D_2O (OD) have been studied (in addition). It was suggested to account for different interpretations of adsorption modes from UPS and HREELS data that the formation of OH from the molecular precursor H_2O was induced by the electron beam in HREELS. But later studies also with IRAS indicate no strong disturbance of the adsorbate phase by these low energy electrons. Different adsorption modes can be discriminated depending on adsorption conditions (see Table 8): molecular adsorption of H_2O (ice) is characterized by the typical broad features due to the hindered rotational and translational modes (around 100 meV or 800 cm^{-1} and 25 meV or 200 cm^{-1}), the scissor mode (at around 200 meV or 1600 cm^{-1}), which is the most significant mode for molecular adsorption, and the stretching modes (in the range of 410-460 meV or 3300-3700 cm^{-1}). The determined values and the widths of spectral features depend strongly on interadsorbate interactions due to hydrogen bonding and also on the bonding to the substrate. The dissociation of H_2O forming OH_{ads} and H_{ads} leads to the loss of H_2O modes especially the scissor mode and to the occurrence of sharp stretching modes of O-H (around 460 meV or 3700 cm^{-1}) and S-H (S substrate adsorption site, around 260 meV or 2100 cm^{-1}). The S-H stretching mode is more significant as the O-H stretching mode, which may also be broadened by coadsorbed H_2O. The S-O stretching modes, and the S-OH and S-H bending modes of dissociatively adsorbed H_2O are all found in the spectral range of 80 to 120 meV or 650 to 950 cm^{-1} and are also not very specific. At elevated temperatures H_2O is completely dissociated and the beginning oxidation of the substrate leads to the transformation of spectra. The resulting spectra may now be rather complex as depending on the oxidation mechanism differing bonding geometries, numbers of substrate atoms, and intermediately formed surface molecular species will be involved.

Si(100)2×1

On Si(100)2×1 the vibrational data obtained by EELS and IRAS (see Fig. 34, 35, 36) have unambiguously established that dissociation of H_2O into H_{ads} and OH_{ads} takes place on the clean surface even at low sample temperatures [82I2, 84C1, 84C2, 84S3, 85C, 97S2]. The spectral assignments were confirmed by isotope shifts (H-D and O^{16}-O^{18}). The observed isotope frequency shifts have been confirmed by cluster calculations assuming different coupling constants of the stretching and bending modes [83B, 95V, 96R1, 97K]. Additional information on the local site and orientation of the adsorbates have been deduced from the vibrational spectra, which already have been given in Table 4. Not included in the data collection are detailed information on the technically important initial oxidation which were drawn from vibrational measurements on annealed surfaces and respective cluster calculations [82I1, 82I2, 97W]. The temperature dependence of ESDIAD patterns have been attributed to a low frequency (200 cm^{-1}) Si-OH torsion mode, which is already thermally activated at substrate temperatures below RT (Fig. 9) [94G].

Si(111) and its reconstructions

On Si(111)7×7 vibrational spectra typical for the different adsorption modes (molecular and dissociative) have been obtained depending on the adsorption conditions (Table 8). A comparison of spectra of molecularly adsorbed H_2O (D_2O) and dissociatively adsorbed H_2O clearly show the formation of Si-OH and Si-H in the latter case [82I2, 83K1, 85N, 86N, 86S2]. The spectral changes related to complete dissociation and Si-oxide formation are presented in [85N, 86N]. By changing the angle and primary electron energy in HREELS the variation in vibrational loss intensities were determined and used to estimate the relative contribution of the dipole, impact and resonance mechanism to vibrational excitation [86N].

On Si(111)2×1 the coexistence of molecular and dissociative adsorption has been found and related to interadsorbate stabilization of H_2O by Si-OH groups due to H-bonding (Fig. 39) [84S2, 85S, 86S1]. Besides monohydrides also dihydrides are found indicating a reorganisation (diffusion) of adsorbate species. For such surface conditions extremely high resolution in the HREEL spectra were obtained [85S].

Ge in different surface orientations

At low sample temperature the adsorption of H_2O on Ge(100)2×1 is characterized by spectral features in HREELS, which are attributed to the simultaneous existence of dissociatively and molecularly adsorbed H_2O in contrast to Si(100)2×1 [89P]. Annealing to RT leads to the loss of the vibrational features of adsorbed H_2O with the formation of OH_{ads} and H_{ads}. In mixed GeSi alloys a surface segregation of Ge is discussed, which indicates a pronounced surface mobility of substrate atoms and adsorbate species [86B, 89P].

3-5 semiconductors in different surface orientations

No vibrational spectra have been reported, yet, for H_2O adsorption on the well defined (110) cleavage plane of 3-5 semiconductors. Most of the presented studies deal with the (100) surfaces also because of the interest in the subsequent thermally induced oxidation process after adsorption [96S2, 97M1, 98C]. The different dimer reconstructions of the (100) surfaces are not well defined and depend strongly on the preparation method used. As the dissociation of H_2O is preferred, when group 3 and group 5 sites exist in close neighborhood to each other, the experimentally observed dissociative adsorption at RT may involve some rearrangement of the initially present surfaces. Furthermore, the starting conditions of the surface for adsorption was not completely free of preadsorbed H_2O from the background pressure.

3.8.2.14 Data as given in Tables

The data are organized in relation to the different adsorbate properties as given in the introductory section of this volume by Bonzel (LANDOLT-BÖRNSTEIN III 42A1) whenever possible, which means, if data are available. We do not subdivide the data according to the different semiconductor substrates, as it would impede the direct comparison of typical adsorbate properties. Thus, the data are summarized in the following tables:

Table1. Mode of adsorption on different semiconductor surfaces: Molecular or dissociative in dependence on experimental conditions.
In this table the mode of adsorption - molecular or dissociative - as suggested by the authors are presented. In cases, where there is now general agreement of the mode of adsorption, we have added a respective comment on deviating conclusions. In other cases, where the mode of adsorption is still not clarified, only the opinion of the authors is presented.

Crystal surface	Technique	Conditions[a]	Adsorption mode[b]	Conclusions and remarks[c]	Ref.
Si(100)	Ellipsometry	RT, θ_{sat}	dissociative	H-Si-O-Si-H formation assumed	71M
	UPS	RT, θ_{sat}	molecular	Si-OH_2 molecular chemisorption assumed	81F1
Si(100)2×1	HREELS	RT, θ_{sat}	dissociative	physisorbed H_2O can be excluded	82I2
	UPS, SXPS	RT, θ_{sat}	molecular	Si-OH_2 molecular chemisorption assumed (spectra to be assigned to dissociative adsorption?)	83S2
	IR polarised	80-500 K, ~1L	dissociative	only Si-H and SiO-H modes detected	84C2
	LEED, AES, UPS	160, 300, 600 K, θ_{sat}	dissociative	H-Si-Si-OH bond formation assumed	84O
	UPS	100 K, 0.25L	molecular	Si···OH_2 physisorption of H_2O molecules assumed	84S2
	UPS, SXPS, LEED	RT, θ_{sat}	dissociative	Si-OH and Si-H bond formation assumed	87L1
	UPS, SXPS	RT, θ_{sat}	dissociative	Si-OH and Si-H bond formation assumed	91L1
	STM	RT, 0.05L 0.1L	molecular dissociative	-Si-Si-OH_2 formation assumed for very low coverages on conserved Si-dimers.	93C2
	UPS, XPS, static SIMS	RT, θ_{sat} heating to 400°C	dissociative	H-Si-Si-OH formation assumed H-Si-O-Si-H formation assumed	94S1
	SXPS	90 K, 1-80L and RT, 1-80L	dissociative	Si-O-Si and oxide formation assumed even at 90K (oxidation reaction enhanced by SXPS radiation ?)	95P
	UPS	137 - 412 K, 0.03 ML - θ_{sat}	dissociative	H-Si-Si-OH formation assumed also at low coverage and low temperature	96R2

Crystal surface	Technique	Conditions[a]	Adsorption mode[b]	Conclusions and remarks[c]	Ref.
Si(100)2×1 vicinal	IR polarised	RT, θ_{sat}	dissociative	dissociation takes place at terrace dimers, not at step dimers	85C
	ARUPS, SXPS, LEED	RT, θ_{sat}	dissociative	Si-OH and Si-H bond formation assumed	88M
	ARUPS	RT, θ_{sat}	dissociative	Si-OH and H-Si bond formation assumed	89F
Si(111)7×7	Ellipsometry	RT	dissociative	Si-O-Si and Si-H bond formation assumed	71M
	EELS	RT, < 100 L	molecular/ dissociative	molecular adsorption assumed; electron beam induced oxidation with time	75F, 77F
	UPS	RT, >100 L	molecular	$Si-OH_2$ molecular adsorption assumed; (spectra probably due to the onset of oxidation?)	79F, 81F1, 81F2
	HREELS	≤ 100 K, 2 L	molecular	condensed ice layer	82I2, 86S2
	HREELS	100 K, 2 L → 300 K RT, 60 - 10^3 L	dissociative	Si-OH and Si-H bond formation	82I2, 83K2, 85N, 86N, 86S2
	UPS	80 K, 2.5 L → 300 K RT, 8 - 1200 L	molecular	$Si-OH_2$ molecular adsorption assumed; (spectra to be assigned to dissociative adsorption?)	85R1, 85R2, 86S2
	UPS	RT, θ_{sat}	dissociative	Si-OH species assumed	89F
	UPS	≤ 100 K,< 0.5 L > 0.5 L	molecular	physisorbed H_2O condensed ice layer	85R1, 85R2 86S2
	STM	RT, < 25 L	dissociative	dissociative adsorption on adatom-restatom pair	91A, 97S1
	XPS, EELS	150 K 150 – 900 K	dissociative	Si-OH and Si-H bond formation assumed; reaction to oxide at T >175 K	92D
	SXPS	90 K, 5 - 95 L 300 K, 5 - 95 L	dissociative	initial formation of OH bonds to Si adatoms, further reaction to SiO_X $x \leq 4$ even at 90K; (oxidation reaction enhanced by SXPS radiation ?)	95P
	EELS, Auger, PYS, LEED	RT, < 100 L RT, > 100 L	dissociative and some oxidation	some Si-O-Si formation, no influence of electron beam reported SiO_X formation	97Z
Si(111)2×1	LEED, HREELS, XPS	100 K, < 0.3 L 100 K 0.3 - 2 L 100 K > 2 L RT	dissociative dissociative and molecular molecular dissociative	 intermediate coverage region disruption of π-bonded chains of 2×1 reconstruction	84S1

Crystal surface	Technique	Conditions[a]	Adsorption mode[b]	Conclusions and remarks[c]	Ref.
Si(113)3×1	HREELS	RT, 1 L	dissociative	adsorption at dimer dangling bonds	96I
Si(113)3×2	HREELS, UPS, SXPS	RT, θ_{sat}	dissociative	3×2 is transformed to 3×1 by a fraction of a monolayer of H_2O adsorbed	93J, 96S1, 97R
Ge(100)2×8 transforms to Ge(100)2×1	UPS	110K, 0.4 L 1.1 L 3.7 L →300 K	molecular dissociative	monomeric H_2O dimerized, H-bridged H_2O ice clusters Ge-OH and Ge-H bond formation assumed	87K2, 87K3
Ge(100)2×1	IR	80 K RT	molecular dissociative	 no adsorption at RT for exposure of 10L	84C2
	UPS, SXPS LEED	160 K, 0.5 -10^2 L → 300K	molecular and some dissociative dissociative	ice layer Ge-OH and Ge-H bond formation assumed	89L, 91L1, 91L2
	HREELS	100 K 345 K	dissociative and molecular dissociative	Ge-OH and Ge-H bond formation assumed	89P, 91P1
	UPS, SXPS	110 K, 10 L → 300 K	dissociative	Ge-OH and Ge-H bond formation assumed	93R1, 93R2
	TDS	170 K, 30 ML	dissociative	no adsorption at RT	92C
Ge(111)2×8	UPS	110 K, 0.3 - 3 L → 300 K	molecular dissociative and molecular	ice clusters Ge-OH and Ge-H bond formation assumed, some remaining rests of molecular H_2O	87K2, 87K3
Ge_xSi_{1-x} (100)2×1	HREELS	RT, 1L	dissociative	mostly Ge-OH and Ge-H due to Ge surface segregation	86B
GaAs(100)	UPS, XPS, SIMS	RT, 7×10^{12} L	dissociative	Ga-OH bond formation assumed	82W
GaAs(100)2×4	HREELS, TDS	100 K, 0.2 L > 200 K, 0.2 L	molecular dissociative	chemisorbed H_2O As-H and Ga-OH bond formation after annealing	98C

Crystal surface	Technique	Conditions[a]	Adsorption mode[b]	Conclusions and remarks[c]	Ref.
GaAs(100)4×6	Photo-reflectance	RT, <100 L	molecular	physisorbed and chemisorbed H_2O assumed	93C1
	XPS, TPD, HREELS	100 K, 3 ML	molecular	chemisorbed H_2O; H_2O ice layer on top; dissociative after electron beam irradiation	96S2
GaAs(110)	UPS	180K, 0.1 - 600 L 300 K, 10^2 - 10^6 L	molecular	chemisorbed H_2O assumed chemisorbed H_2O assumed for low coverage physisorbed H_2O assumed for high coverage (origin of spectral features unclear)	79B
	PSID	RT, 400 L	dissociative	As-OH and Ga-OH bond formation assumed	81T
	SXPS	100 K, < 0.5 L > 0.5 L	dissociative molecular	As-H and Ga-OH bond formation assumed ice formation	96H
	SXPS	RT, 10^6 L RT, 2×10^9 L RT, 4×10^{10} L	dissociative dissociative and molecular oxidation	As-H and Ga-OH bond formation assumed mixture of As-H and Ga-OH and H_2O Ga-suboxide	97H
InP (110)	SXPS	100 K, < 0.5 L 100 K, > 0.5 L	dissociative molecular	In-OH and P-H bond formation assumed condensed ice layer	00H
InP($\bar{1}\,\bar{1}\,\bar{1}$)	UPS, HREELS	RT, 2×10^3 L	no adsorption	partial dissociative adsorption induced by Na codeposition	88D
AlAs(100)1×1	TPD, Auger, HREELS	100 K, 2 L	molecular	thermal induced desorption and reaction	97M1, 97M2
FeS_2(100)	XPS,UPS, LEIS	100 K, 0.5 - 1.5 L	molecular	preferential adsorption on Fe sites	91P2
GaSe(0001)	UPS,SXPS	100 K, 0.5 - 7 L	molecular	condensation of ice clusters	92M, 93M
InSe(0001)	UPS,SXPS	100 K, 0.3 - 10 L	molecular	condensation of ice clusters	92M, 93M
$MoSe_2$(0001)	UPS	80 K, 0.5 - 5 ML	molecular	condensation of ice clusters	75Y
MoS_2(0001)	UPS	100 K	molecular	condensation of ice clusters	87J, 88J
WSe_2(0001)	UPS,SXPS	100 K, 1-10.5L	molecular	condensation of ice clusters	92M, 93M, 96M
$CuInSe_2$	UPS,LEIS,XPS	80 K, 0.01 - 10 L	molecular	preferential adsorption on Cu sites	92S

[a] Experimental conditions as given in the references [b] Proposed adsorption mode as suggested by the authors of the given papers [c] Additional information as given by the authors of the given papers; remarks by the authors of this data collection are given in parenthesis

Table 2. Thermodynamic data on adsorption energies of H_2O and its dissociation products OH and H on different semiconductor surfaces
Thermodynamic data obtained by experiments approaching thermodynamic equilibrium do not exist for well defined semiconductor surfaces. In this table we will therefore summarize data on adsorption energies as obtained by kinetic experiments and by theoretical calculations.

Crystal surface	Technique	Conditions[a]	Adsorption energy [eV]	Model[b]	Conclusions and remarks	Fig.	Ref.
Si(100)2×1	adsorption kinetics by UPS	180-300K, 0-θ_{sat}	0.062	$Si^{\cdots}OH_2$	binding energy of mobile molecular precursor as derived from adsorption kinetics measured at different temperatures		96R2
	adsorption kinetics by UPS	around 400K, 0-θ_{sat}	0.311	$Si^{\cdots}OH_2$	binding energy of mobile molecular precursor as derived from adsorption kinetics		96F, 96R2
Si(100)	THEORY MNDO		1.19 1.7 5.1 4.2 2.0 2.0 2.6	Si-OH_2 Si-H_2O-Si Si-OH-Si Si-OH Si-H Si-H-Si H-Si and Si-OH-Si on one Si cluster	ideal, unreconstructed clusters of 12-16 Si atoms; most stable: OH bridge bonded and H on top; dissociation barrier of 2.51eV		87B, 87R
	THEORY Empirical Pair Potential [1)]		1.07 2.21 2.05 0.20	Si-OH_2 Si-H_2O-Si Si-OH-Si and Si-Si-H H-Si-Si-OH	difference between molecular and dissociative adsorption is small; dissociation barrier of 2.61eV		90E
	THEORY DFT/LDA[2)]		3.9 0.1	H-Si-Si-OH OH-OH interadsorbate hydrogen bond	dissociative adsorption, calculation for a repeatable slab geometry		95V
	THEORY DFT [3)]		0.31 - 0.61 2.13 - 2.73 0.1	$Si^{\cdots}OH_2$ H-Si-Si-OH OH-OH interadsorbate hydrogen bond	no net activation barrier to dissociation	1	97K
Si(111)7×7	THEORY EHT[4)]	low coverage regime	-1.26 4.38 4.27 11.52	$Si_{ad}{}^{\cdots}OH_2$ Si_{ad}-OH and Si_{ad}-H Si_{ad}-OH and Si_{rest}-H Si_{ad}=O and 2Si_{ad}-H	comparison of adsorption energies depending on adsorption sites: molecular adsorption endothermic; best sites Si adatoms (Si_{ad}); dissociative adsorption on two adatoms exothermic; dissociative adsorption on adatom-restatom pair exothermic; complete dissociation on three adatoms strongly exothermic		97E

Crystal surface	Technique	Conditions[a]	Adsorption energy [eV]	Model[b]	Conclusions and remarks	Fig.	Ref.
Si(111)1×1	THEORY Empirical Pair Potential [1)]		1.49 1.13	Si-OH_2 Si-OH and Si-H	difference between molecular and dissociative adsorption is small		90E
Si(110) stepped	THEORY ETB[6)]			Si-OH_2 on different Si sites, Si-OH and Si-H	total electronic energy calculation leads to dissociative adsorption, core-core repulsion neglected		96K
Ge(111)2×1[7)]	TDS	RT	1.1	molecular or dissociative adsorption in close neighbourhood	metastable adsorption state		75S
Ge(111)1×1[8)] (8×2)	TDS	RT	1.4	probably dissociative adsorption	normal adsorption state		75S
GaAs(100) 4×6	Isothermal desorption	RT	0.56	molecular	local surface rearrangement assumed		93C1
GaAs(110)	TDS	250 K, 0.9ML	0.7	As-OH_2	molecular adsorption, formation of As-OH_2 bonds assumed		84M
	THEORY LCAO / LDA[5)]		0.5 3.5 2.5	As-OH_2 Ga-OH_2 Ga-OH and As-H	preferential molecular adsorption on Ga-sites, dissociation possible after adsorption on As-sites.		96R3
GaAs(110) 4×6 Ga rich	TPD	23 ML, 100 K	0.49 0.55	ice layer chemisorbed molecular H_2O	high coverage regime studied.		96S2

[a] Experimental conditions as given in the references

[b] Proposed adsorption model as suggested by the authors of the given papers

[1)] Values are given as calculated for the symmetric dimer geometry

[2)] Density functional theory in the local density approach

[3)] Density functional theory with different basis sets and functionals

[4)] Extended Hückel theory; values are given for the best adsorption site

[5)] Selfconsistent LCAO approach with local density approximation

[6)] Empirical tight binding method

[7)] Freshly cleaved surface

[8)] Annealed surface to 130°C or H_2O exposed surface ($3x10^{-6}$ Torr)

Table 3. Kinetics of adsorption/desorption, surface diffusion, and surface reactions on different semiconductor surfaces
In this table the results on saturation coverage and sticking coefficients are summarized. Conclusions on surface diffusion and reactions, which follow from the investigations of adsorption kinetics, are also given. Data on desorption are only available from physisorbed H_2O (ice layer) as chemisorbed species tend to react with the substrate forming oxides, when the sample temperature is increased.

Crystal surface	Technique	Conditions[a]	Results and conclusions	Fig.	Ref.
Si(100)2×1	HREELS, IR, UPS, Auger, TPD	RT and below, 0 - θ_{sat}, different pressure ranges around 5×10^{-9}mbar	$S_0 \sim 1$; abrupt saturation;		93C2
			$\theta_{sat} \sim 0.5 \rightarrow$ one H_2O molecule saturates two dangling bonds		84C2, 85R3, 96F, 96R2
			$S(\theta)$ is constant nearly up to saturation $\rightarrow$ mobile physisorbed molecular precursor on occupied and unoccupied sites		85R3, 90S, 96F, 96R2
	UPS, IR	80 K, 0 - θ_{sat}, different pressures	dissociation occurs even at 80 K $\rightarrow$ activation energy is small or zero		84C2, 85R3, 96R2
	UPS	180 - 300 K, 0 - θ_{sat}, pressure ranges around 5×10^{-9}mbar	S/S_0 versus θ/θ_{sat} modeled by two reaction channels: chemisorption of H and OH on two dangling bonds of one dimer or on two randomly adjacent dangling bonds; binding energy of mobile molecular precursor around 0.062 eV/molecule at RT and below	3	96R2
	TPD	RT, 0 - θ_{sat}, 1×10^{-8}mbar	$\theta_{sat} = 0.41$		96F
	STM	RT, θ_{sat}	some single dangling bonds always remain unsaturated		93A
	STM	RT, 0.005 ML	the formation of chains of several H_2O molecules along the dimer rows is assumed to be a precursor for dissociation		93C2
	UPS	~ 400 K, 0 - θ_{sat}, 1×10^{-8} mbar resp. 5×10^{-9} mbar	first order Langmuir like adsorption isotherm; binding energy of mobile molecular precursor around 0.311 eV/molecule at 400 K		96F, 96R2
	TPD	423 K, 0 - θ_{sat}, 1×10^{-8} mbar	adsorption modeled by Langmuir isotherm; 0.291 eV/molecule difference between activation energies for adsorption and desorption		96F

Crystal surface	Technique	Conditions[a]	Results and conclusions	Fig.	Ref.
Si(111)7×7	UPS	RT, 2 L	fast adsorption up to θ_{sat} ~ 0.1 ML		84S1
	LITD[1)], TPD, AES	140 K, ~10 - 180 L; →700 K	dissociative adsorption followed by ice layer; ice layer desorption at 160 K; coadsorbed H blocks dissociation sites		89K
	TPD	RT	dissociative adsorption with 3 regimes; in the 2. regime θ_{sat} ~ 0.6 ML and the sticking coefficient S is depending on the pressure: S = 0.08 at 10^{-11}-10^{-9} torr; S = 0.016 at 2×10^{-8} torr; S = 0.009 at 4×10^{-8} torr	4	91P3, 91P4, 91U
	STM	RT, < 25 L	initial dissociative adsorption on adatom-restatom pairs followed by slow reaction with back bonds		91A, 97S1
	LITD[1)] TPD	180 - 800 K, 0 - 800 L	precursor-mediated dissociative adsorption; $S_0 = 1.9\times10^{-2}$ at 180 K; $S_0 = 9.6\times10^{-3}$ at 300 K; constant adsorption rate up to θ = 0.15 - 0.2 ML and θ_{sat} ~ 0.35 ML at 300 - 700 K		95W2
	TPD	D_2O exposure 373 K, 1×10^{-6} - 1×10^{-7} mbar	dissociative adsorption on all dangling bonds; Si-OD, Si-D formation; initial fast adsorption up to θ ~ 0.12 ML on adatom-restatom pairs; S_0 = 0.23±0.08; θ_{sat} = 0.22±0.02ML	5	96F
	EELS, Auger, PTS, LEED	RT, 0.6 - 15000 L	dissociative adsorption for exposure < 100 L; oxidation reaction for exposure > 100 L		97Z
Si(111)1×1	LITD[1)], TPD	180 - 800 K, 0 - 800 L laser heated modified surface	precursor-mediated dissociative adsorption $S_0 = 6.9\times10^{-1}$ at 180 K		95W2
Si(111)2×1	XPS	100 K, 0 - 10 L	dissociative adsorption followed by ice layer; 3 adsorption regimes		85S

Crystal surface	Technique	Conditions[a]	Results and conclusions	Fig.	Ref.
Ge(100)2×1	LEED, Auger	RT, 10^2 - 10^5 L; 110 K, 1L → 300 K	dissociative adsorption, θ_{sat}= 0.2ML θ_{sat} = 0.5 ML	6	87K2
	TPD	173 K, 20 L 273 K	physisorbed precursor, θ_{sat} = 0.5 ML assumed S_0 = 0.28 S_0 = 0.02		92C
Ge(111)2×1 → 8×2	LEED, Auger	RT 10^{-9} - 10^{-1} torr.min	dissociative adsorption, θ_{sat} = 0.25 - 0.3 ML	7	73H
GaAs(100)4×6	photo-reflectance	200 K, 100 - 3×10^6 L	molecular adsorption, *S* strongly depending on exposure: $S \sim 10^{-2}$ at 100 L $S \sim 5\times10^{-7}$ at 3×10^6 L		89S
		180 K - 320 K, 0 - 3000 L	molecular chemisorption via physisorbed precursor, 4 surface sites involved per H_2O molecule; estimate of kinetic quantities by model calculation		93C1
	TPD	D_2O exposure 100 K, < 23 L; →700 K	molecular adsorption; D_2O ice layer desorption at 170 K; D_2O desorption tail up to 600 K of molecular D_2O formed by thermally activated association of dissociatively adsorbed D_2O		96S2
GaAs(100)2×4	TDS	100 K, < 2.5 L; → 850 K	chemisorbed molecular H_2O; H_2O desorption at 180 K; H_2O desorption tail up to 750 K of molecular H_2O formed by thermally activated association of dissociatively adsorbed H_2O		98C
GaAs(110)	TDS	250 K, 10 - 2×10^4 L; → 670 K	chemisorbed H_2O, θ_{sat} = 1 ML *S* strongly depending on exposure: $S \sim 1.3\times10^{-3}$ at 6 L $S \sim 7\times10^{-5}$ at 200 L $S > 6\times10^{-4}$ at 4800 L: singularity due to loss of relaxation; desorption of chemisorbed H_2O at 350 K, desorption tail up to 630 K	8	84M

Crystal surface	Technique	Conditions[a]	Results and conclusions	Fig.	Ref.
GaAs(110)	Auger $M_1M_{15}V$	RT, 10 - 10^6 L	*S* is 2-3 orders larger than for O_2 adsorption		84C3
	UPS	100 K, 0.1 - 8 L; → RT	dissociatively adsorbed H_2O, θ_{sat}= 0.5 ML; ice layer on top; ice layer desorbs at ~155 K; thermally activated formation of GaO_x and desorption of AsH_3 at ~250K		96H
AlAs(100)1×1	TDS	D_2O exposure 100 K, 0.1 - 3 L; → 750 K	molecular adsorption of D_2O; desorption of D_2O and thermally activated dissociation at 150 K - 180 K and recombinative desorption of D_2O from Al-OD and As-H at 550 - 750 K		97M1, 97M2
InP (110)	UPS	100 K, 0.1 - 5 L; → RT	dissociatively adsorbed H_2O, θ_{sat} ~ 0.5 ML; ice layer on top desorbs at ~ 150 K; thermally activated formation of InO_x and desorption of PH_3 at ~250 K		00H

[a] Experimental conditions as given in the references

Table 4. Local stucture of adsorbed H_2O and OH on semiconductor surfaces.
Information on the bonding site and the orientation of the adsorbed species is given. Detailed investigations only exist for the Si(100) surface.

Crystal Surface	Technique	Conditions[a]	Results and Conclusions	Fig.	Ref.
Si(100)2×1	IR, polarisation dependent	RT, θ_{sat}	bond angle Si-Si-H 130°		84C1
	ESDIAD H^+-desorption	130 - 145 K, 0.5 L, two domain 2×1 LEED RT , 0 - 2 L	O-H bond direction off-normal; azimuthal orientation of O-H bond in [011], [$0\bar{1}1$], [$01\bar{1}$], [$0\bar{1}\bar{1}$] direction; essentially no structure in H^+ desorption pattern	9a	87L2 94G
	differential ESDIAD	130 K, θ_{sat}, RT, θ_{sat}, two domain 2×1 LEED	OH vibration anisotropic, additional information given on thermal activation of vibrational modes.	9b	94G
	ESDIAD	160 K, 0.5 L, (100) vicinal, one domain 2×1 LEED	O-H bond direction nearly perpendicular to dimer bond		87L2
	ARUPS polarzation dependent	RT, θ_{sat} one domain 2×1 LEED	OH–σ-orbital not perpendicular to the surface and not constrained to lie in the dimer plane		88M
	STM	RT, 0.05 ML	non dissociative adsorption assumed; H_2O molecule assumed to adsorb on lower atom of buckled dimer; adsorbed molecule assumed to induce static buckling on neighboring dimers of the same row; two H_2O molecules on one dimer appear as A defects of "clean" surface, two H_2O molecules on the same side of two dimers appear like C defects of "clean" surface;	10a	93C2
	STM	RT, 0.1 ML - θ_{sat}	dissociative adsorption; growing patches of dissociatively adsorbed H_2O indicate adsorbate-adsorbate interaction; single Si atoms of occupied dimers atomically resolved	10b,c	93C2
	STM	RT, 0.1 L - θ_{sat}, (100) vicinal, one domain 2×1	growing patches of dissociatively adsorbed H_2O on terraces; chemisorbed H_2O molecules appear like A defects of "clean" surface	11	93A

Crystal Surface	Technique	Conditions[a]	Results and Conclusions	Fig.	Ref.
Si(100)2×1	TOF-SARS 4 keV Ar^+ H, O, Si recoil	RT, θ_{sat}, 5×10^{-9} Torr H_2O during experiment	H and OH bound to dangling bonds of 1st-layer Si atoms; Si-H bond shorter than Si-OH; Si-O and Si-H aligned with dimer bond axis		94B
	scanned-energy mode PED, O1s emission	RT, θ_{sat}	bond angle Si-OH: 22±5° from surface normal; bond length Si-OH: 1.7±0.1Å; additional information given for Si bonding geometry of Si-OH	12	98F
	THEORY CNDO cluster calculation	geometry according to ESDIAD results	bond length [Å] Si-OH 1.93 O-H 1.04 Si-H 1.54		89O
	THEORY LDFT/LDA		bond length [Å] Si-OH 1.65 O-H 0.98 Si-H 1.53 Si-Si 2.38 bond angle buckling 2° Si-Si-O 111° Si-Si-H 109° Si-O-H 117° O-H perpendicular to dimer	12	95V
	THEORY DFT cluster calculation, single dimer		bond length [Å] Si-Si 2.458 Si-OH 1.757 O-H 0.974 Si-H 1.499 bond angle buckling 0.0° Si-Si-O 116.7° Si-O-H 116.4° O-H 62.2° to dimer	12	97K
	THEORY DFT, two dimers		similar values as for single dimer but O-H bond angle 85.3° to dimer		97K
Si(100)2×1 vicinal	UPS, HeI, cut off 6°, 9° and 12.5°	RT, θ_{sat}	dissociative adsorption on dimer dangling bond and on adatom like dangling bond since the intensity of OH related features follows the total density of dangling bonds		90S, 97R
Si(111)7×7	HREELS	RT, 2000 L	OH and H at on-top sites, normal to surface; O-H tilted away from surface normal by 75°		85N, 86N

Crystal Surface	Technique	Conditions[a]	Results and Conclusions	Fig.	Ref.
Si(111)7×7	STM	RT, ~5 L; RT, ~25 L	dissociative adsorption on adatom restatom pairs, center adatoms react twice as often as corner adatom as they have twice the number of neighboring restatoms; island formation of adsorbates due to H-bond interaction; at high coverages a statistical distribution of covered adatom sites is reached	13	91A, 97S1
	THEORY Ext. Hückel		dissociative adsorption, bond length Si-OH: 1.74Å		97E
Si(113)3×1	HREELS	RT, 1 L	dissociative adsorption at dimer dangling bonds only; intensity ratio of saturated (113) to saturated (100) is similar to the ratio of the respective number of dimers		96I
Ge(100)2×1	comparison of UPS and THEORY	160 K RT, 0.5 - 100 L	molecular adsorption of H_2O on top site, bond length Ge-OH_2: 2.5Å two adsorption modes assumed: OH and H on-top sites bond length Ge-OH: 1.6Å, OH at bridge sites bond length Ge-OH: 1.7Å		91L1, 91S
FeS_2(100)	LEISS	100 K, 0 - 1L	site selective molecular adsorption of H_2O on Fe sites	14	91P2
$CuInSe_2$(011)	LEISS	80 K, 0.01 - 10 L	site selective molecular adsorption of H_2O on Cu sites		92S

[a] Experimental conditions as given in the references, e.g. Si(100)

Table 5. Long-range order of the substrate/adsorbate interface for different semiconductor surfaces.
The results obtained by LEED and STM on the long-range order of the adsorbate and/or the substrate/adsorbate complex are given. These data mostly give information on the persistence of substrate reconstructions. No quantitative results on the geometry of the adsorbate layer are available.

Crystal surface	Technique	Conditions[a]	Results	Conclusion and remarks[b)]	Fig.	Ref.
Si(100)2×1	LEED	RT, θ_{sat}	2×1 reconstruction conserved	dimer bond not broken by dissociative chemisorption		93L
	STM	RT, θ_{sat}	2×1 reconstruction conserved	dimer bond not broken by dissociative chemisorption	10, 11	93A, 93C2
	TOF-SARS 4 keV Ar^+ H, O, Si ion recoil	RT, θ_{sat}, 5×10^{-9} mbar	2×1 reconstruction conserved	dimer bond not broken by dissociative chemisorption, H and OH bound to Si dangling bonds		94B
vicinal (100)	LEED, one domain 2×1	RT, θ_{sat}	2×1 reconstruction conserved	dimer bond not broken by dissociative chemisorption		87L2
	STM	RT, θ_{sat}	2×1 reconstruction conserved	dimer bond not broken by dissociative chemisorption; no change of step structure		93A
Si(111)7×7	LEED	RT, 2000 L	7×7 is conserved but fading of diffraction spots induced	dissociative adsorption forming disordered structures		85N, 86N
	LEED	RT, 0 - 450 L	7×7 is transformed to 1×1 at high coverage	dissociative adsorption on dangling bonds involving diffusion of Si adatoms		91P2, 91P3, 91U
	STM	RT, < 25 L	7×7 conserved	dissociative adsorption on Si adatoms; formation of adsorbate islands	13	91A, 97S
	LEED	150 K, 0 - 5 L; →RT	7×7 conserved fading of diffraction spots	dissociative adsorption on unchanged Si adatom-restatom pairs formation of disordered SiO_x surface layer		92D
	LEED	RT, < 150 L RT, 800-1000 L	7×7 conserved, fading of diffraction spots loss of diffraction spots	dissociative adsorption on Si adatoms formation of disordered SiO_x surface layer		97Z

Crystal surface	Technique	Conditions[a]	Results	Conclusion and remarks[b)]	Fig.	Ref.
Si(111)2×1	LEED	LT, 2L → RT	2×1 lost 1×1 reconstruction formed	π-bonded chains broken by dissociative adsorption		85S
Si(113)(3×2)	LEED	RT, 10% of θ_{sat}	transformation 3×2 → 3×1	transformation of reconstruction induced by dissociative adsorption		93J
Ge(100) c(4×2)/2×1	LEED	160 K, 0 - 5 L →RT	c(4×2) → 2×1 weak 2×1 weak → 2×1 sharp	molecular adsorption at LT dissociative adsorption on Ge dimers		89L, 91L1, 91L2
Ge(100)2×1	LEED	100 K, 1 L	2×1 is conserved	molecular and dissociative adsorption on Ge dimers		91P1
Ge(111)2×1	LEED	RT, < 10 L > 10 L	2×1→ 1×1 or 8×2 loss of diffraction spots	dissociative adsorption on 2 adsorption sites; area of 50-300 surface atoms involved/per adsorbed water molecule. formation of disordered surface oxide layer	7	73H, 75S, 79G
GaAs(100)1×1	LEED	RT, < 4×10^3 L	1×1 reconstruction conserved			81T
GaAs(110)1×1	LEED	RT, < 10^5 L, $\theta \leq 1$ ML	1×1 reconstruction conserved	I(V) curves indicate loss of relaxation		84M
		100K, < 0.5L → RT	1×1 reconstruction conserved, fading of diffraction spots	dissociative adsorption on Ga-As surface pairs onset of surface oxidation		97H
InP(100)1×1	LEED	RT, 10^4-10^5 L RT, >10^9 L	partial loss of 1×1 spots loss of diffraction spots	molecular adsorption oxide formation		82M
InP(110)1×1	LEED	100 K, < 0.5 L → RT	1×1 reconstruction conserved fading of diffraction spots	dissociative adsorption on In-P surface pairs onset of surface oxidation		00H

[a] Experimental conditions as given in the references

Table 6. Valence band electron states, binding energies, and assignments for different semiconductor surfaces and adsorption conditions.
Only for physisorbed H_2O the measured electron states are strictly adsorbate molecular orbital states. For chemisorbed species the measured electron states result from adsorbate states which strongly hybridize with substrate states (semiconductor dangling bonds) in covalent bond formation. The states as measured on different semiconductor surfaces and for different adsorption conditions are given together with their assignments. Also results from theoretical calculations for different adsorption geometries are presented here.

Crystal surface	Technique	Conditions[a]	Refe-rence level[b]	Binding energies [eV]	Molecular orbital assignment[c] as given in Ref.	Additional information or assignment by authors of data collection	Remarks[d]	Fig	Ref
Si(100)2×1	UPS, HeI	300 K, 1 L - 100 L	E_F	6.1 8.0 10.6	$1b_1$ of H_2O $3a_1$ of H_2O $1b_2$ of H_2O	assignment questionable	(spectra unclear, probably due to beginning oxidation?)		81F1
	SXPS, $h\nu$=51eV	300K, θ_{sat}	E_{VBM}	6.2 7.2 11.5	$1b_1$ of H_2O $3a_1$ of H_2O $1b_2$ of H_2O	OH-1π OH-1π OH-3σ	molecular adsorption assumed (spectra due to dissociation ?)	15	83S2
	UPS, HeII	160 K, 1.5 L annealed 300 K	E_{vac}	10.9 11.7 16.2	O lone pair SiO-H Si-OH				84O
	UPS, HeI	300 K, 0.7-1000 L	E_F	6.6 7.6 11.9	assignments left open	OH-1π OH-1π OH-3σ	cylindrical Si crystal; difference spectra 1000 L - 0.7 L are similar to the spectra presented by [81F1]		85R1
		100 K, < 0.3 L	E_F	6.6 7.6 11.9	assignments left open	OH-1π OH-1π OH-3σ	spectra identical to RT spectra	16	85R1
		100 K, 0.3 - 0.7 L	E_F	6.8 9.2 12.9	molecular H_2O	$1b_1$ $3a_1$ $1b_2$	physisorbed H_2O	16	
		100 K, > 0.7 L	E_F	7.2 10.2 13.3	molecular H_2O	$1b_1$ $3a_1$ $1b_2$	condensed ice layer	16	

Crystal surface	Technique	Conditions[a]	Refe-rence level[b]	Binding energies [eV]	Molecular orbital assignment[c] as given in Ref.	Additional information or assignment by authors of data collection	Remarks[d]	Fig	Ref
Si(100)2×1	UPS, HeI SXPS, $h\nu$=73eV	300 K, 0.06 ML - θ_{sat}; 233 K, θ_{sat}	E_{VBM}	6.2 7.2 11.5 24.5	O-2p of OH O-2p of OH O-2p of OH O-2s of OH	OH-1π OH-1π OH-3σ O-2s of OH	OH adsorbed on dimer dangling bonds; E_{VBM} is taken at the Fermi edge of the surface state of clean Si(100)2×1		85R3, 90S, 96R2
	SXPS, $h\nu$=30 eV	300 K, 10 L - θ_{sat}	E_{VBM}	6.3 11.2	Si-OH SiO-H		OH adsorbed on dimer dangling bonds;		87L1
	ARUPS, $h\nu$=50 eV p-polarized	RT, θ_{sat}	E_{VBM}	6.1 7.1 11.4	OH-1π OH-σ		vicinal (100) one domain (2×1); no dispersion observed on changing the emission angle		88M
	SXPS, $h\nu$=36 eV	RT, θ_{sat}	E_F	6.5 7.5 11.9	O-2p SiO-H Si-OH		OH adsorbed on dimer dangling bonds; vicinal (100) one domain (2×1)		89F
	SXPS, $h\nu$=30eV	300 K, θ_{sat}	E_{VBM}	6.3 7.4 11.2	OH-1π OH-1π OH-3σ	Oπ nonbonding Si-OH weak bonding	OH adsorbed on dimer dangling bonds		91L1
	UPS, HeII	295 K, θ_{sat}	E_F	5 6.4 7.6 11.9	Si-H OH SiO-H Si-OH	Si-sp^3 + H-1s O-2p lone pair O-2p + H-1s Si-sp^3 + O-2p	OH adsorbed on dimer dangling bonds		94S1
	THEORY extended Hückel		E_{vac}	12.1 14.8 18.5	OH-1π OH-3σ Si-OH	O-π nonbonding O-p + H-s Si-s + O-p, σ bonding	OH adsorbed on dimer dangling bonds		83C1, 83C2
	THEORY tight binding approach		E_{vac}	12.2 16.0 18.8	OH OH-3σ Si-OH	O-p, O-π nonbonding O-p + H-s Si-s + O-p, σ bonding	OH adsorbed on dimer dangling bonds;		87K1

Crystal surface	Technique	Conditions[a]	Refe-rence level[b]	Binding energies [eV]	Molecular orbital assignment[c] as given in Ref.	Additional information or assignment by authors of data collection	Remarks[d]	Fig	Ref
Si(100)2×1	THEORY tight binding approach		E_{vac}	12.2 18.4 20.0 35.8	$1b_1$ of H_2O $1b_2$ of H_2O σ of Si-OH_2 $2a_1$ of H_2O	O-p + Si-s, σ bonding	molecular H_2O adsorption; values given for 180° orientation; also different orientations of the bond direction calculated		87K1
	THEORY fully self-consistent calculation		E_{vac}	14.38 15.58 19.99	OH OH Si-OH	O-p Si-s + O-p	OH adsorbed on dimer dangling bonds		89F
Si(110)	UPS, HeI	300 K, 2 - 170 L	E_F	6.6 7.6 11.9	assignments left open	OH-1π OH-1π OH-3σ	for low exposures same spectral features as on Si(100) RT, θ_{sat}	17	85R1
		100K, 0.45L	E_F	6.8 9.2 12.9	molecular H_2O	$1b_1$ $3a_1$ $1b_2$	physisorbed H_2O	16	
		100K, > 0.45L	E_F	7.2 10.2 13.3	molecular H_2O	$1b_1$ $3a_1$ $1b_2$	condensed ice layer		
Si(111)7×7	EELS	RT, 10 - 100 L; 150 K, 0.25 - 5 L		3.7 4.7 8.7	no assignment given	transitions from occupied to unoccupied states	extrinsic surface states induced by H_2O, molecular adsorption assumed	9b	75F, 77F, 92D
	UPS, HeI	RT, < 135 L; 100 K, 2.5 L →RT	E_F	6.5 7.5 11	H_2O-orbitals	OH-1π OH-1π Si-3σ	molecular adsorption assumed (spectra due to dissociation ?)	17	85R1, 85R2, 86S2

Crystal surface	Technique	Conditions[a]	Refe-rence level[b]	Binding energies [eV]	Molecular orbital assignment[c] as given in Ref.	Additional information or assignment by authors of data collection	Remarks[d]	Fig	Ref
Si(111)7×7	UPS, HeI	RT, < 10^3 L	E_F	~ 6 ~ 8 ~ 11	$1b_1$ of H_2O $3a_1$ of H_2O $1b_2$ of H_2O	assignment questionable	molecular adsorption assumed (spectra due to onset of oxidation?)	17	79F, 81F1, 81F2, 85R1, 85R2
	UPS SXPS, $h\nu$ = 36 eV	RT	E_F	6.2 7.2 11.6	OH SiO-H Si-OH	O-2p lone pair O-2p +H-1s Si-sp^3+O-2p	dissociative adsorption of H_2O; emission dominated by Si-OH groups		89F
	UPS, HeI	< 100 K	E_F	~ 7 ~ 9-10 ~ 13	$1b_1$ of H_2O $3a_1$ of H_2O $1b_2$ of H_2O		for low exposures physisorbed H_2O, then condensed ice layer; spectra as on Si(110), see Fig. 23		85R1, 85R2, 85R3, 86S2
Si(111)	THEORY Ext. Hückel	molecular	E_{vac}	12.0 18.8 19.4 36.6	$1b_1$ of H_2O $3a_1$ of $Si-OH_2$ $1b_2$ of H_2O $2a_1$ of H_2O	$O-p_x$, nonbonding $O-p_z$ + Si-s, bonding	H_2O on top of Si dangling bond		83C1
	THEORY Ext. Hückel	dissociative	E_{vac}	9.9 12.1 14.8 18.5 33.8	Si-H OH-$1\pi_x$ OH-3σ Si-OH OH-2σ	H-1s + Si-sp, σ bonding $O-p_x$, O-π nonbonding $O-p_z$ + Si-s, σ bonding	Si-OH and Si-H on top of Si dangling bond		83C2
	THEORY tight binding	molecular	E_{vac}	12.2 18.4 19.2 35.8	$1b_1$ of H_2O $1b_2$ of H_2O $3a_1$ of $Si-OH_2$ $2a_1$ of H_2O		H_2O on top of Si dangling bond perpendicular to surface		87K1
		molecular	E_{vac}	14.6 19.2 35.8	$3a_1$ of H_2O $1b_2$ of H_2O $2a_1$ of H_2O	and $O-p_y$+Si-s, O-σ bonding	H_2O on top of Si dangling bond , parallel to surface		87K1

Crystal surface	Technique	Conditions[a]	Refe-rence level[b]	Binding energies [eV]	Molecular orbital assignment[c] as given in Ref.	Additional information or assignment by authors of data collection	Remarks[d]	Fig	Ref
Si(111)	THEORY tight binding	dissociative	E_{vac}	10 12.2 16 18.8 33.2	Si-H OH-1π OH-3σ Si-OH OH-2σ	Si-p_z + H-1s, σ-bonding O-p_x lone pair, π non bonding O-p_z + Si-s, O-σ bond.	Si-OH and Si-H on top of Si dangling bond		87K1
Si(113), Si(115), Si(5,5,12), Si(112)	UPS, HeII	RT, θ_{sat}	E_F	6.2 7.2 11.5	emission shape characteristic for OH +H	OH-1π OH-1π Si-3σ	dissociative adsorption of H_2O; orientation dependent saturation coverages derived and related to the number of dimers and adatom-like rebonded atoms at steps	18	97R
Ge(100)2×1	UPS, HeI	110 K, 0.4 L	E_{VBM}	5.9 9.8 12.9	$1b_1$ of H_2O $3a_1$ of H_2O $1b_2$ of H_2O		H_2O monomers	19	87K3
		110K, 1.1 L	E_{VBM}	6.1 8.5 10.0 12.9	$1b_1$ of H_2O $3a_1$ of H_2O $3a_1$ of H_2O $1b_2$ of H_2O		H_2O dimers with H-bonding; $3a_1$ MO is split by dimer bond		
		110K, 3.7 L	E_{VBM}	6.3 8.8 9.9 12.9	$1b_1$ of H_2O $3a_1$ of H_2O $3a_1$ of H_2O $1b_2$ of H_2O		H_2O ice cluster; $3a_1$ MO is broadened		
		110 K, 3.7 L → 300 K	E_{VBM}	5.6 7.5 9.2 10.0	OH-π OH-π OH-σ_p	nonbonding Ge-OH bonding assignment unclear	thermally induced dissociation	20	

Crystal surface	Technique	Conditions[a]	Refe-rence level[b]	Binding energies [eV]	Molecular orbital assignment[c] as given in Ref.	Additional information or assignment by authors of data collection	Remarks[d]	Fig	Ref
Ge(100)2×1	SXPS, $h\nu$ = 60 eV	160 K, 0.5 - 100 L → 300 K	E_{VBM}	5.5 7.3 9.3 10.4	OH-π OH-π Ge-H OH-σ_p	nonbonding lifting of degeneracy	thermally induced dissociation		89L, 91L1
		160 K, 0.5 - 100 L	E_{VBM}	5.9-6.5 8.1-8.4 12.4-12.7	$1b_1$ of H_2O $3a_1$ of H_2O $1b_2$ of H_2O		H_2O ice layer		
	SXPS, $h\nu$=17,20,24 eV	160 K, 2 L →300 K	E_F	~ 4.8 ~ 5.8 ~ 7.8 ~ 9.5 ~10.6	Ge-H OH-π Ge-OH-π Ge-H OH-σ	nonbonding weak bonding	dispersion investigated, only weak dispersion observed	21, 22	91L2
	THEORY LCAO x_α	dissociative	E_{vac}	12 16.9	Ge-OH-π Ge-OH-σ_p		OH on top site		91S
			E_{vac}	12 16.8 15.8	Ge-OH-π_a Ge-OH-π_b Ge-OH-σ		OH on bridge site between two Ge		
		molecular	E_{vac}	12.2 14.5 19	$1b_1$ of H_2O $3a_1$ of H_2O $1b_2$ of H_2O		H_2O on top site		
Ge(111)2×8	UPS	110 K, 0.3 - 3 L	E_{VBM}	6.4-6.6 8.9 9.9 13.0	$1b_1$ of H_2O $3a_1$ of H_2O $3a_1$ of H_2O $1b_2$ of H_2O		H_2O ice cluster, $3a_1$ splitting due to H-bonding	23	87K3
		110 K, 3 L →300 K	E_{VBM}	5.2 7.6 10.2	OH-π OH-π Ge-OH-σ_p	nonbonding Ge-OH bonding	thermally induced dissociation; additional emissions (due to coadsorbed molecular H_2O?)	20	

Crystal surface	Technique	Conditions[a]	Refe-rence level[b]	Binding energies [eV]	Molecular orbital assignment[c] as given in Ref.	Additional information or assignment by authors of data collection	Remarks[d]	Fig	Ref
GaAs (110)	UPS, HeI	180 K	E_{VBM}	3.2 5 9.4	H_2O orbitals	$1b_1$ $3a_1$ $1b_2$	physisorbed H_2O assumed (origin of spectral features unclear ?)		79B
		300 K, 10^4 L	E_{VBM}	3.2 4.4 8.4	H_2O orbitals	$1b_1$ $3a_1$ $1b_2$	chemisorbed H_2O assumed (origin of spectral features unclear ?)		
	SXPS, $h\nu$ = 41eV	~100 K, 0.5 L	E_{VBM}	5 7 9.1 12.1	Ga-OH As-H Ga-OH As-H		dissociatively adsorbed H_2O (given assignment unclear?)	24	96H, 97H
		~100 K, > 2L	E_{VBM}	5.5 8 12	$1b_1$ of H_2O $3a_1$ of H_2O $1b_2$ of H_2O		physisorbed H_2O, ice layer	24	
GaAs (100)	UPS	RT, 7×10^{12} L		6.1 10.9	OH orbitals		dissociatively adsorbed H_2O (origin of emissions unclear?)		82W
InP(110)	SXPS, $h\nu$ = 41 eV	100 K, 0.5 L	E_{VBM}	4.2 6 8.4 11.1	In-OH P-H In-OH P-H		dissociatively adsorbed H_2O (given assignment unclear?)	25	00H
		100 K, > 1.3 L	E_{VBM}	5.7 8.1 11.6	$1b_1$ of H_2O $3a_1$ of H_2O $1b_2$ of H_2O		physisorbed H_2O, ice layer		
FeS_2(100)	UPS, HeI	100 K, 0.5 - 1.5 L	E_F	~7 ~10 ~13	$1b_1$ of H_2O $3a_1$ of H_2O $1b_2$ of H_2O		molecular adsorption preferentially on Fe-sites		91P2
GaSe(0001)	SXPS, $h\nu$ = 21 eV	100 K, 0.5 L - 7 L		6.5-7.3 9.5-10 12.7-13.2	$1b_1$ of H_2O $3a_1$ of H_2O $1b_2$ of H_2O		condensed ice layer; E_B^F depending on coverage;		92M, 93M

Crystal surface	Technique	Conditions[a]	Refe-rence level[b]	Binding energies [eV]	Molecular orbital assignment[c] as given in Ref.	Additional information or assignment by authors of data collection	Remarks[d]	Fig	Ref
InSe(0001)	SXPS $h\nu$ = 21 eV $h\nu$ = 30 eV	100 K, 0.1 L - 10 L	E_F	6.8-7.7 9.5-10.3 13.0-13.9	$1b_1$ of H_2O $3a_1$ of H_2O $1b_2$ of H_2O		condensed ice layer; E_B^F strongly depending on coverage and substrate doping; ionisation energies E_B^{vac} weakly depending on coverage	26	92M, 93M
			E_{vac}	11.4 14 17.6	$1b_1$ of H_2O $3a_1$ of H_2O $1b_2$ of H_2O				
$MoSe_2$ (0001)	UPS	80 K, 0.5 - 5 ML	E_{vac}	~11.2 ~13.5 ~17	$1b_1$ of H_2O $3a_1$ of H_2O $1b_2$ of H_2O		condensed H_2O; ionisation energies E_B^{vac} nearly constant; dipole between substrate and adsorbate assumed		75Y
MoS_2 (0001)	UPS	100 K	E_F	~7 ~10 ~13	$1b_1$ of H_2O $3a_1$ of H_2O $1b_2$ of H_2O		condensed ice layer		87J, 88J
WSe_2 (0001)	UPS SXPS $h\nu$ = 21 eV $h\nu$ = 30 eV	100 K, 1 - 10.5 L	E_F	6.4-8.0 9.2-10.9 12.3-14.3 25.9-27.9	$1b_1$ of H_2O $3a_1$ of H_2O $1b_2$ of H_2O $2a_1$ of H_2O		condensed ice layer; E_B^F depending on coverage and substrate doping; ionisation energies E_B^{vac} nearly independent on coverage; dipole between substrate and adsorbate assumed		92M, 93M, 96M
			E_{vac}	11.0-11.4 ~ 14 16.9-17.5 30.4-31.3	$1b_1$ of H_2O $3a_1$ of H_2O $1b_2$ of H_2O $2a_1$ of H_2O				
$CuInSe_2$ (001)	UPS	80 K, 0.01 - 10 L	E_F	~7.3 ~9.9 ~13	$1b_1$ of H_2O $3a_1$ of H_2O $1b_2$ of H_2O		molecularly adsorbed H_2O		92S

[a] Experimental conditions as given in the references

[b] E_F: Fermi level; E_{vac}: vacuum level; E_{VBM}: valence band maximum

[c] For a detailed presentation of the orbital assignment see text of section 3.8.2.11; Si-OH indicates Si-OH bonding state, SiO-H indicates O-H bonding state.

[d] Remarks in parenthesis like e.g. (spectra due to dissociation ?) are given by the authors of this data collection

Table 7. Core level electron binding energies E_B of H_2O adsorbate species and binding energy shifts ΔE_B of substrate emissions obtained for different semiconductor surfaces and adsorption conditions.
Core level binding energy shifts measured for the substrate lines as well as the binding energies of the adsorbate lines are presented here, as they have been used for the determination of adsorption mode and adsorbate properties.

Crystal/ surface	Technique $h\nu$ [eV]	Conditions[a]	Core level	E_B [eV]	ΔE_B [eV]	Assignment[b,c]	Remarks[c]	Fig.	Ref.
Si(100)2×1	SXPS $h\nu$ = 120	300 K, θ_{sat}	Si $2p_{3/2}$		+0.9	Si-OH_2 (Si-OH?)	molecular adsorption assumed (shift due to Si-OH?)		83S2
	SXPS $h\nu$ =138.5	350 K, 2 L, θ_{sat}	Si $2p_{3/2}$	98.74	 –0.46 +0.80	bulk ODA(clean) Si-OH	ODA disappeared after saturation; Si-OH intensity equal to original ODA intensity		85R3
		→ 640 K	Si $2p_{3/2}$		+1.0 +1.8	Si^+ Si^{2+}	after annealing to 640 K $Si^+$and Si^{2+} oxidation states formed		
		→ 870 K	Si $2p_{3/2}$		+2.6 +3.5	Si^{3+} Si^{4+}	after annealing to 870 K aditional Si^{3+} and Si $^{4+}$ emissions and ODA intensity restored		
	SXPS $h\nu$ = 130	300 K, 10L, θ_{sat}	Si $2p_{3/2}$		–0.43 +0.25 +1.00	ODA(clean) Si-H Si-OH	ODA intensity strongly decreased after saturation; no oxidation observed		87L1
Si(100)	SXPS $h\nu$ = 130	RT, 2 L, θ_{sat}, (100) vicinal, one domain 2×1 LEED	Si $2p_{3/2}$		–0.52 +0.31 +1.00	ODA(clean) Si-H Si-OH	ODA intensity strongly decreased after saturation; no oxidation observed	27	88M
		300 K, 5 L, θ_{sat}	Si $2p_{3/2}$		–0.43 +0.24 +1.04	ODA(clean) Si-H Si-OH	ODA intensity strongly decreased after saturation; no oxidation observed		91L1
	XPS	RT, θ_{sat}; → 670 K; → 920 K;	O 1s referred to Si $2p_{3/2}$	432.8 432.2 433.2		Si-OH Si-O-Si Si-oxide sub-stoichiometric	O1s binding energy monitored in the temperature range 0 - 650 °C		94S1

Crystal/ surface	Technique $h\nu$ [eV]	Conditions[a]	Core level	E_B [eV]	ΔE_B [eV]	Assignment[b,c]	Remarks[c]	Fig.	Ref.
Si(100)	SXPS $h\nu$ = 145	90 K, 1 - 80 L	Si $2p_{3/2}$		–0.55 +0.30 +0.85 +1.65 +2.45 +3.35	ODA(clean) Si-H Si-OH/Si^{+} Si^{2+} Si^{3+} Si^{4+}	ODA intensity slowly decreased with exposure; Si^{2+} already observed at 5 L; with higher exposures (80L) also Si^{3+} and Si^{4+} observed; (source induced enhancement of oxidation?)	28	95P
	SXPS $h\nu$=145	300 K, 1 - 40 L	Si $2p_{3/2}$	99.6	 –0.55 +0.85 +1.65	bulk ODA(clean) Si-OH/Si^{+} Si^{2+}	ODA intensity slowly decreased with exposure; (source induced enhancement of oxidation?)	29	95P
Si(111)7×7	XPS	150 K,<0.25 L; 150 K, 0.25 - 5 L; →RT	O1s	530.0 531.7 530.2		Si-O Si-OH Si-O	preadsorbed state (origin of spectral features unclear?) H_2O dissociation assumed surface oxide		92D
	SXPS $h\nu$=145	300 K, ≤ 90 L; 90 K, 40 L; → RT	Si $2p_{3/2}$		+0.89	Si_{ad}-OH	OH bonding to Si adatom; slow attenuation of restatom intensity to 50%; oxidation states up to Si^{4+}at RT and 90 K observed (source induced enhancement of oxidation?)	30	95P
Si(111)2×1	XPS	100 K, 0.2 - 2 L; 100 K, > 2 L; RT, θ_{sat};	O1s	534.0 532.6 534.6 532.6		H_2O Si-OH H_2O ice Si-OH	no chemically shifted component in Si 2p line evident	31	85S
Si(113)	SXPS $h\nu$=135	RT, 0.01 - 2 L	Si $2p_{3/2}$		+0.22 +0.90	Si-H Si-OH	dissociation at dimers assumed		96S1

Crystal/ surface	Technique $h\nu$ [eV]	Conditions[a]	Core level	E_B [eV]	ΔE_B [eV]	Assignment[b,c]	Remarks[c]	Fig.	Ref.
Ge(100)2×1	SXPS $h\nu = 70$	160 K, 1 L 300 K, 1 L	Ge $3d_{5/2}$		–0.43 +0.75 +0.43	Ge dimer (clean) Ge-OH Ge-H	loss of emission of Ge dimer due to adsorbed H_2O	32	89L, 91L1
	SXPS $h\nu = 64$	110 K, 10 L → 360 K	Ge $3d_{5/2}$		–0.45 +0.56 0 ±0.1	Ge dimer (clean) Ge-OH Ge-H	loss of emission of Ge dimer due to adsorbed H_2O		93R1
GaAs(100) 4×6	XPS	100 K, 3 ML	O 1s	533.2		H_2O	ice layer		96S2
		100 K, 3 ML addtional 50 eV electron beam	O 1s	531.0-531.6 529.4-530.4		OH Ga-oxide	electron induced dissociation of H_2O		96S2
GaAs(110)	SXPS $h\nu = 60$ $h\nu = 80$	100 K, < 0.5 L	Ga $3d_{5/2}$ As $3d_{5/2}$		+0.60 +0.60 –0.65	Ga-OH As-H As*	 As* due to Ga-OH formation		97H
		RT, 10^6 L 2×10^9 L- 4×10^{10} L	Ga $3d_{5/2}$ As $3d_{5/2}$ Ga $3d_{5/2}$		+0.6 +0.6 +1.0	Ga-OH As-H Ga-suboxide			
GaAs	XPS	RT, 7×10^{12} L	Ga 3d Ga 2p O1s	 530.8	+1.6 +1.7	Ga-OH Ga-OH Ga-OH	dissociative adsorption assumed; no binding energy shift of As resolved; (onset of surface oxidation?)		82W
GaSe(0001) InSe(0001) MoS(0001) WSe_2(0001)	SXPS	120 K, 0.5 - 3.5 L	O2s		26.0	H_2O	molecular adsorption, no chemically shifted substrate components observed; adsorbate binding energy shifts assumed to be due to surface dipols	33 a,b	87J, 88J, 92M, 93M, 96M

[a] Experimental conditions as given in the references
[b] Assignment as given by the authors of the original paper
[c] Remarks in parenthesis are given by the authors of this data collection

Table 8. Vibrational properties of adsorbed H_2O or its dissociation products for different adsorption conditions on different semiconductor surfaces
Vibrational frequencies of adsorbate/substrate bonding: In this table the vibrational modes and their assignments obtained after adsorption on different semiconductors and for varying adsorption conditions are given. For chemisorbed and dissociatively adsorbed species the measured eigenmodes and frequencies depend on the specific surface molecule formed thus being strongly influenced by substrate atoms and bonding geometry.

Crystal surface Adsorbate	Technique	Conditions[a]	Vibrational energy[b] [meV]	Vibrational frequency[b] [cm^{-1}]	Vibrational mode	Conclusion and remarks	Fig.	Ref.
Si(100)2×1 H_2O	HREELS E_0 = 14 eV	165 - 420 K, 0.1 - 1 L	78.1 101.7 259.1 459.0	630 820 2090 3700	Si-H bend Si-OH stretch/ Si-OH bend Si-H stretch SiO-H stretch	dissociative adsorption; Si-OH stretch also observed as double loss at 1600 cm^{-1}	34	82I2
	IRAS p-pol.	80 K, 10 L	207.1 ~409.0	1670 ~3300	H_2O scissor H_2O stretch	condensed molecular H_2O; the H_2O stretching mode is a broad feature due to H-bonding	35	84C2
	IRAS s-pol. p-pol. p-pol.	80 K, 0.5 L 300 K, 10 L 80 K,10 L →RT	257.9 258.1 453.7	2080 2082 3660	Si-H stretch Si-H stretch SiO-H stretch	dissociative adsorption; for the given temperatures and exposures identical spectra are found	35	84C1, 84C2
	HREELS E_0 = 1.5 eV	RT, 10 L	78 103 260 458	629 830 2097 3694	Si-H bend Si-OH stretch Si-H stretch SiO-H stretch	dissociative adsorption		84S3
	IRAS s-pol. p-pol.	RT, 2 L	257.6 257.9	2078 2080	Si-H stretch Si-H stretch	dissociative adsorption; 9° cut off vicinal surface		85C
	IRAS internal mirror	RT, 2 L	102.3 111.3 258.5	825 898 2085	Si-OH stretch Si-OH bend Si-H stretch	dissociative adsorption; calculated frequencies show unusual isotope shift Si-OH(D)	36	97S2
	THEORY cluster calculation	dissociative adsorption	78.9-80.6 102-104 101-102 259.0 458.4	637-650 823-840 816-824 2089 3697	Si-H bend Si-OH stretch Si-OH bend Si-H stretch SiO-H stretch	calculation with different coupling constants between different modes lead to wave numbers in the given range		83B

Crystal surface Adsorbate	Technique	Conditions[a]	Vibrational energy[b] [meV]	Vibrational frequency[b] [cm^{-1}]	Vibrational mode	Conclusion and remarks	Fig.	Ref.
Si(100)2×1 H_2O	THEORY $Si_9H_{13}OH$ DFT cluster calculation	dissociative adsorption	101.7 112.7	821 909	Si-OH stretch Si-OH bend	67% stretching + 33% bending; 33% stretching + 67% bending; coupling of stretching and bending modes; intensity bend/stretch = 16%		96R1
	THEORY LDA/MD Car-Parrinello	dissociative adsorption	108.6 445.8	876 3596	Si-OH stretch/ Si-OH bend SiO-H stretch	only the Si-OH group was allowed to move in the MD calculation		95V
	THEORY DFT cluster calculation	dissociative adsorption	8.6 86.8 114.3 261.4 455.3	69 700 922 2108 3672	Si-O-H torsion Si-OH stretch Si-OH bend Si-H stretch SiO-H stretch	unconstrained cluster model underestimates Si-OH stretch frequency, calculated frequencies show unusual isotope shift Si-OH(D)		97K
Si(100)2×1 D_2O	HREELS E_0 = 14 eV	165 - 420 K, 0.1 - 1 L	59.5 80.6 104.1 188.5 334.8	480 650 840 1520 2700	Si-D bend Si-OD bend Si-OD stretch Si-D stretch SiO-D stretch	dissociative adsorption	34	82I2
	HREELS E_0 = 1.5 eV	RT, 10 L	60 80 190 335	484 645 1532 2702	Si-D bend Si-OD stretch Si-D stretch SiO-D stretch	dissociative adsorption; (assignment to Si-OD bend ?) also sum frequencies observed		84S3
	IRAS internal mirror	RT, 2 L	81.6 104.1 188.1	658 840 1517	Si-OD bend Si-OD stretch Si-D stretch	dissociative adsorption; intensity of Si-OD stretching mode decreased by 55% versus Si-OH	36	97S2
	THEORY cluster calculation	dissociative adsorption	62.1-62.7 75.8-78.6 101-103 186.5 333.9	501-506 611-634 815-828 1504 2693	Si-D bend Si-OD bend Si-OD stretch Si-D stretch SiO-D stretch	calculations with different coupling constants between different modes lead to wave numbers in the given range; stretching mode intensity Si-OD/Si-OH = 50%		83B

Crystal surface Adsorbate	Technique	Conditions[a]	Vibrational energy[b] [meV]	Vibrational frequency[b] [cm^{-1}]	Vibrational mode	Conclusion and remarks	Fig.	Ref.
Si(100)2×1 D_2O	THEORY DFT cluster calculation	dissociative adsorption	82.6 103.5	666 835	Si-OD bend Si-OD stretch	coupling of stretching and bending modes leads to unusual isotope shift		96R1
Si(100)2×1 $H_2{}^{18}O$	HREELS		~99.2	~800	Si-^{18}OH stretch	dissociative adsorption; unpublished results by Ibach,Wagner,Bruchman cited by [83B]		83B
	IRAS; internal mirror	RT, 2 L	99.8 110.5	805 891	Si-^{18}OH stretch Si-^{18}OH bend	stretching mode intensity Si-^{18}OH/Si-^{16}OH = 97%		97S2
	THEORY cluster calculation	dissociative adsorption	98.3 106.0	793 855	Si-^{18}OH stretch Si-^{18}OH bend	calculated for H-O-Si/O-Si-Si bend-bend interaction force constant = -0.1 mdyn Å		83B
	THEORY $Si_9H_{13}OH$ cluster calculation	dissociative adsorption	98.6 102.1	795 904	Si-^{18}OH stretch Si-^{18}OH bend	stretching mode intensity Si-^{18}OH/Si-^{16}OH = 90%		96R1
Si(111)7×7 H_2O	HREELS	100 K, 2 L	~ 95 ~ 210 ~ 435	765 1610 3510	H_2O trans/rot H_2O scissor H_2O stretch	molecular H_2O adsorbed; combined translation and rotation; H_2O stretching mode is a broad feature due to H-bonding	37	82I2, 86S2
	HREELS	300 K, θ_{sat}, 60 L; 80 K, condensed H_2O →RT	95 258 460	766 2081 3710	Si-OH bend Si-H stretch SiO-H stretch	different adsorption procedures used for obtaining dissociative H_2O		86S2

Crystal surface Adsorbate	Technique	Conditions[a]	Vibrational energy[b] [meV]	Vibrational frequency[b] [cm^{-1}]	Vibrational mode	Conclusion and remarks	Fig.	Ref.
Si(111)7×7 H_2O	HREELS	100K, 2L→RT	78 100 118 259 424 456	630 807 950 2090 3420 3680	Si-H bend Si-OH stretch Si-OH bend Si-H stretch SiO-H stretch/ H bonded SiO-H stretch	dissociative adsorption	37	82I2
	HREELS E_0 = 2.5- 11 eV	RT, θ_{sat}, 200 - 2000 L	95-98 258-260 456-460	766-790 2081-2097 3678-3710	Si-OH stretch/ Si-OH bend Si-H stretch SiO-H stretch	dissociative adsorption; additional overtone losses observed; angle and energy dependent measurements of scattering intensities		83K2, 85N, 86N
Si(111)7×7 D_2O	HREELS E_0 = 2.5 - 11 eV	RT, θ_{sat}, 200 - 1000 L	73 104 188 332-334	589 839 1516 2678-2694	Si-OD bend Si-OD stretch Si-D stretch SiO-D stretch	dissociative adsorption; additional overtone losses observed; angle and energy dependent measurements of scattering intensities	38	83K2, 86N
Si(111)2×1 H_2O	HREELS E_0 = 2 - 15 eV	100 K, < 2 L	100-102 255-257 450 195 420	807-823 2057-2073 3630 1573 3388	Si-OH bend Si-H stretch SiO-H stretch H_2O scissor H_2O stretch	dissociatively and molecularly adsorbed H_2O present		84S1, 85S
	HREELS	100 K, 5 - 100 L	25 96-103 195-205 420-425	202 774-823 1573-1614 3388-3428	H_2O frust-trans. H_2O rotation H_2O scissor H_2O stretch	ice layer at coverage > 2 L; additional overtone losses observed		84S1, 85S

Crystal surface Adsorbate	Technique	Conditions[a]	Vibrational energy[b] [meV]	Vibrational frequency[b] [cm^{-1}]	Vibrational mode	Conclusion and remarks	Fig.	Ref.
Si(111)2×1 H_2O	HREELS	RT, < 20 L 100 K, 2 L →RT 100 K,100 L→RT	24 195-205 100-103 255-257 450-453 60 78 111	194 1573-1654 807-830 2057-2073 3630-3654 484 629 895	H_2O frust-trans. H_2O scissor Si-OH bend and stretch Si-H stretch SiO-H stretch Si-H_2 rocking Si-H_2 wagging Si-H_2 scissor	molecularly and dissociatively adsorbed H_2O present; additional lines due to Si-H_2 formation; additional overtone losses observed	39	84S1, 85S, 86S1
Si(113)3×1	HREELS	RT, 1 L	76 100 256	613 807 2065	Si-H bend Si-OH stretch Si-H stretch	dissociatively adsorbed H_2O on dangling bonds; additional overtone observed at 200 meV		96I
Ge(100)2×1 H_2O	HREELS E_0 = 6.5 eV	100 K 0.32 - 1 L	83 110-115 243 450 65-75 200	670 887-928 1960 3630 524-605 1613	Ge-OH stretch Ge-OH bend Ge-H stretch GeO-H stretch H_2O libration H_2O scissor	dissociatively and molecularly adsorbed H_2O present		91P1
		100 K, 1 L → 345 K	83 115 247 450	670 928 1992 3630	Ge-OH stretch Ge-OH bend Ge-H stretch GeO-H stretch	dissociative adsorption		89P, 91P1
Ge(100)2×1 D_2O	HREELS E_0 = 6.5 eV	100 K, 5 L → 345 K	85 170 330	686 1371 2662	Ge-OD stretch Ge-D stretch GeO-D stretch	dissociative adsorption		89P, 91P1
Ge_xSi_{1-x} (100)2×1 H_2O	HREELS E_0 = 5 - 6.5 eV	RT, 1 L	98 245 257 460	790 1976 2073 3710	Ge-OH and Si-OH stretch Ge-H stretch Si-H stretch Ge-OH and Si-OH stretch	additional overtones observed; surface segregation of substrate atoms and mobility of adsorbed species discussed		86B, 89P

Crystal surface Adsorbate	Technique	Conditions[a]	Vibrational energy[b] [meV]	Vibrational frequency[b] [cm^{-1}]	Vibrational mode	Conclusion and remarks	Fig.	Ref.
GaAs(100) 4×6 H_2O	HREELS	100 K, 3 ML D_2O	147.3 179.3 330.3 357.7	1188 1446 2664 2885	D_2O scissor overtone O-D stretch overtone	D_2O ice layer		96S2
GaAs(100) 4×2 H_2O	HREELS	100 K, 0.2 L > 200 K, 0.2 L	202.1 455.0 261.6 455.0	1630 3670 2110 3670	H_2O bend H_2O stretch As-H stretch GaO-H stretch	Ga stabilized surface; molecular adsorption dissociative adsorption		98C
AlAs(100) 1×1 D_2O	HREELS	100 K, 0.5 L D_2O > 200 K	145.1 337.2 298.8 186.6 262.8 337.2 463.7	1170 2720 2410 1505 2120 2720 3740	D_2O scissor D_2O stretch D_2O stretch As-D stretch As-H stretch AlO-D stretch AlO-H stretch	isolated D_2O D-bonded D_2O (ice) dissociation of D_2O; contamination by dissociatively adsorbed background H_2O in all spectra		97M1

[a] Experimental conditions as given in the references

[b] For comparison the data of the original papers are given in vibrational energy [meV] as well as wavenumbers [cm^{-1}] (1 cm^{-1} = 0.123981 meV)

3.8.2.14 Figures for 3.8.2

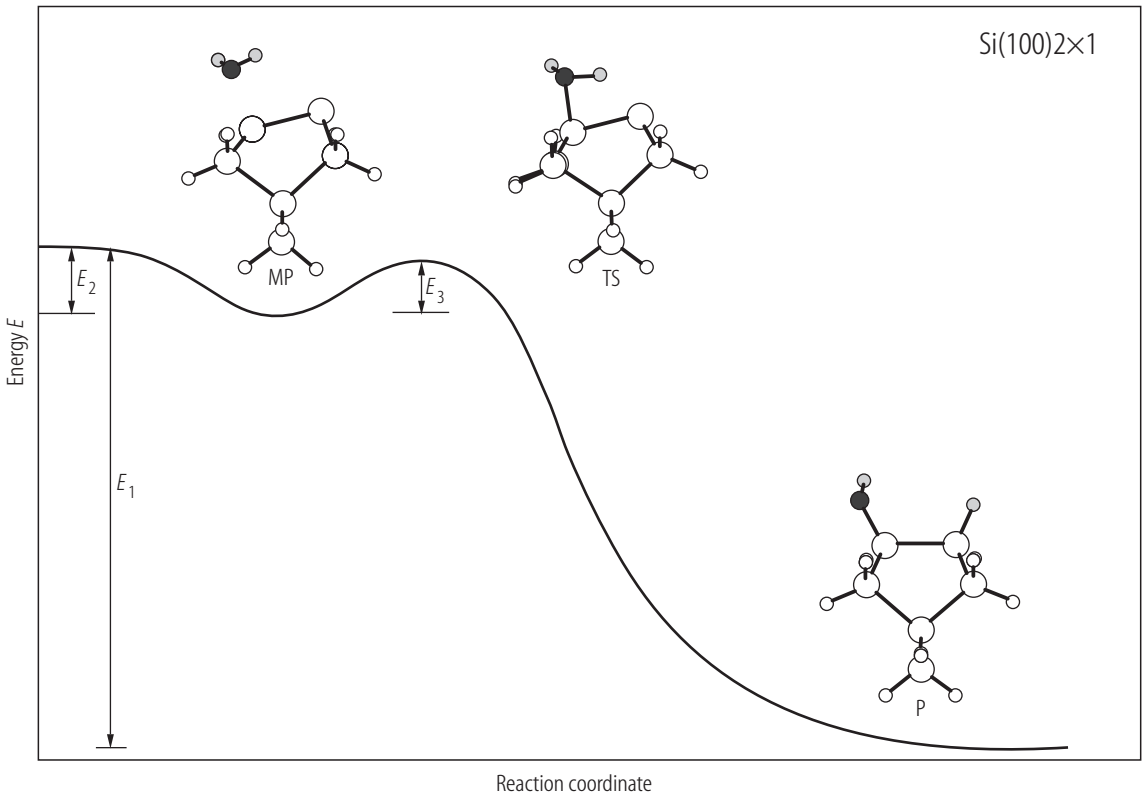

Fig. 1. Energy profile of the reaction of water with the Si(100) surface as calculated by DFT. At a certain level of the calculation (BLYP/TZ94P) the calculated values are: Total adsorption energy E_1 = 2.13 eV, molecular precursor adsorption energy E_2 = 0.31 eV activation energy for dissociation E_3 = 0.23 eV [97K].

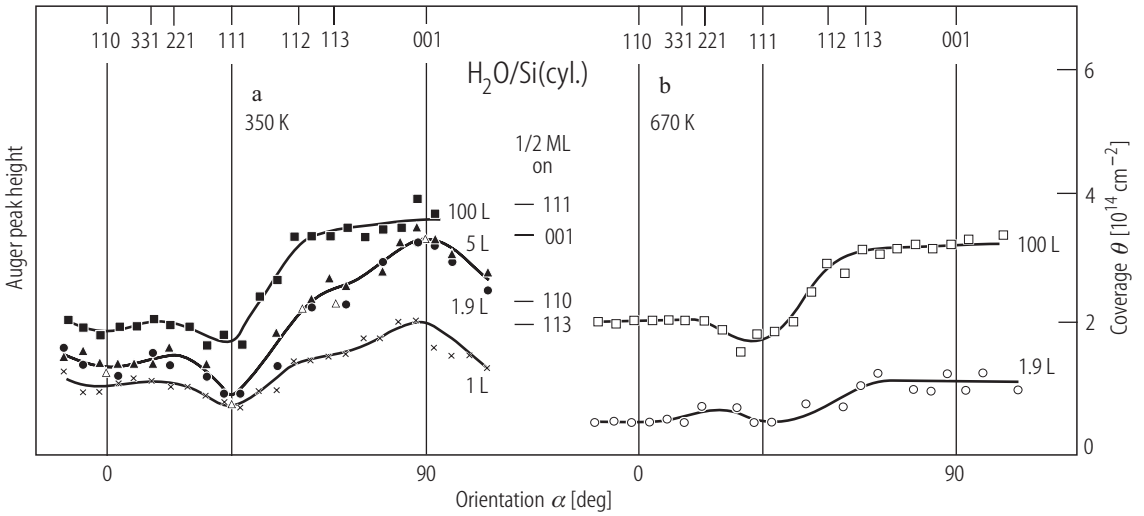

Fig. 2a. Orientation dependence of the oxygen KLL Auger peak intensity on a cylindrical Si crystal after exposure to the indicated amounts of water: (a) exposure at 350 K, (b) exposure at 670 K. The intensity corresponding to 1/2 ML (oxygen atoms per surface unit cell) for the main orientations is indicated. The calibration of the coverages is given in the right hand scale [85R3].

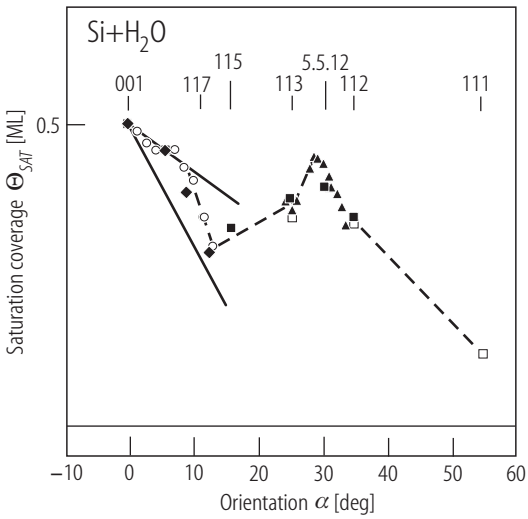

Fig. 2b. Dependence of the OH + H saturation coverage on orientation of a disk shaped Si crystal as derived from photoelectron spectra for exposures between 300 and 350 K. The respective surface orientations are indicated by Miller Indices. Solid triangles: $h\nu$ = 50 eV; solid squares: $h\nu$ = 40.8 eV; solid diamonds: $h\nu$ = 21.2 eV; open squares: $h\nu$ = 73 eV; open circles: $h\nu$ = 21.2 eV . Measurements normalized to 0.5 ML at (001) [97R].

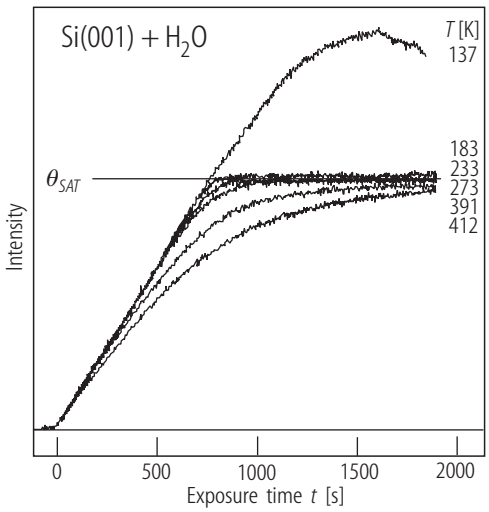

Fig. 3. OH+H photoelectron intensity versus exposure time to water for different sample temperatures as indicated. θ_{sat} refers to saturation at T > 220 K (corresponding to 0.5 ML)[96R2]. The linear range of the plot (constant adsorption rate) indicates a mobile molecular precursor state.

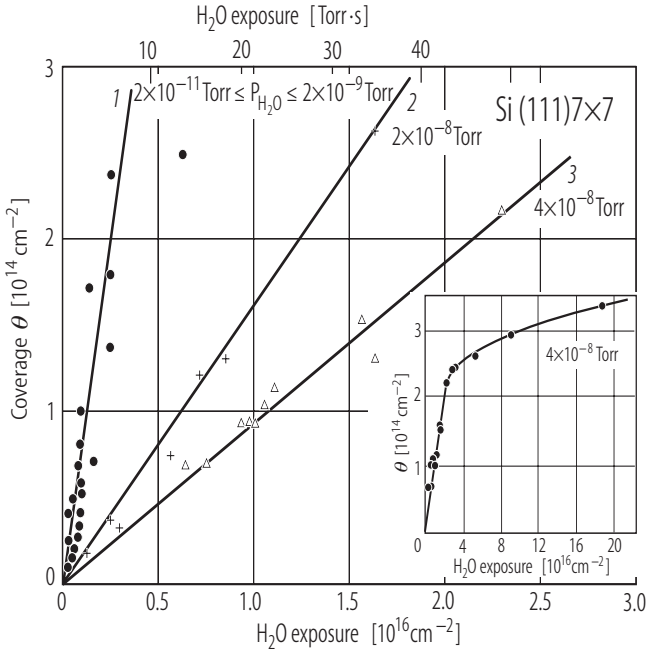

Fig. 4. Coverage of (dissociated) H_2O molecules on the Si(111)7×7 surface as a fun-ction of exposure to water vapor with various pressures P: solid circles, line 1: 2×10^{-11} Torr < P < 2×10^{-9} Torr; crosses, line 2: $P = 2\times10^{-8}$ Torr; open triangles, line 3: $P = 4\times10^{-8}$ Torr. The inset presents the same dependence for water vapor pressure $P = 4\times10^{-8}$ Torr at longer exposures. (The same units are used for coordinate axes both in the main figure and in the insert) [91P3]. The graph covers the second and third adsorption regime above θ > 0.2 ML. The transition between the second and third regime occurs at $\theta \approx$ 0.6 ML.

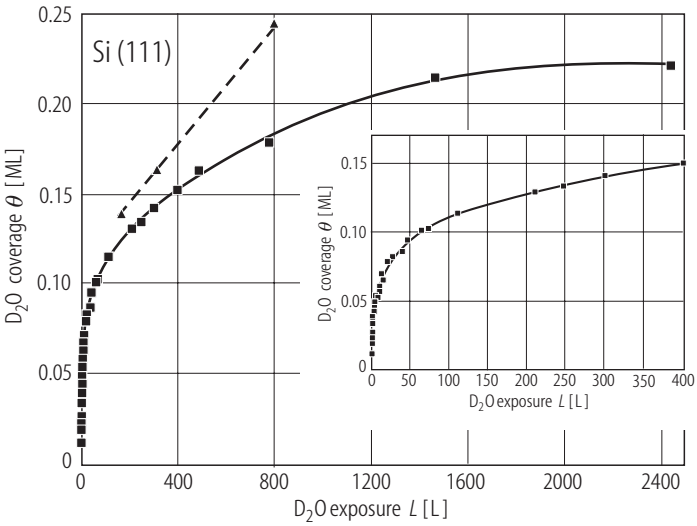

Fig. 5. D_2O coverage on Si(111) at 373 K as a function of exposure. Solid squares: ion gauge off. Solid triangles: ion gauge on. Line: spline through data [96F]. The graph covers the first and second adsorption regime.

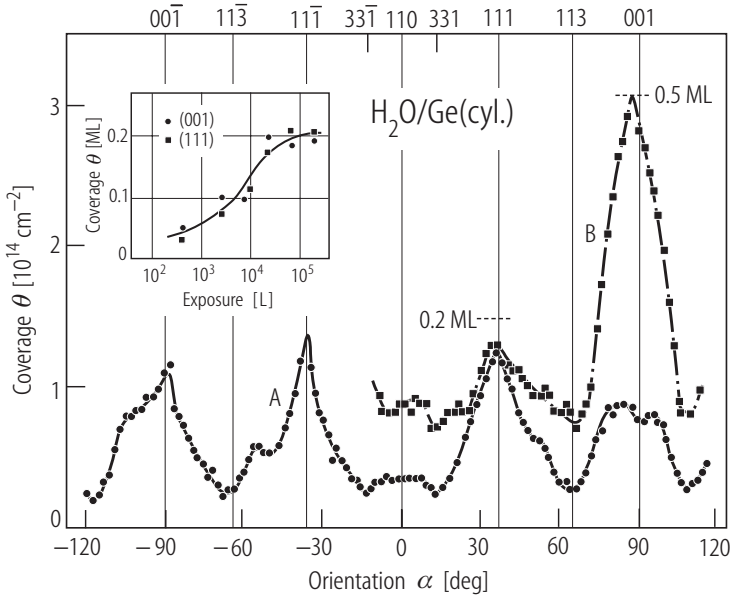

Fig. 6. Orientation-dependent coverage as derived from the intensity of the O_{KLL} Auger Signal after water adsorption on a cylindrical Ge crystal. The respective surface orientations are indicated by Miller Indices. The intensity is scaled to the number of oxygen atoms per cm^2. (A) 10^4 L H_2O exposed at 300 K. (B) 1 L H_2O exposed at 110 K and warmed up to 300 K. Insert: H_2O coverage in monolayers (ML) on Ge(001) and Ge(111) at 300 K [87K3].

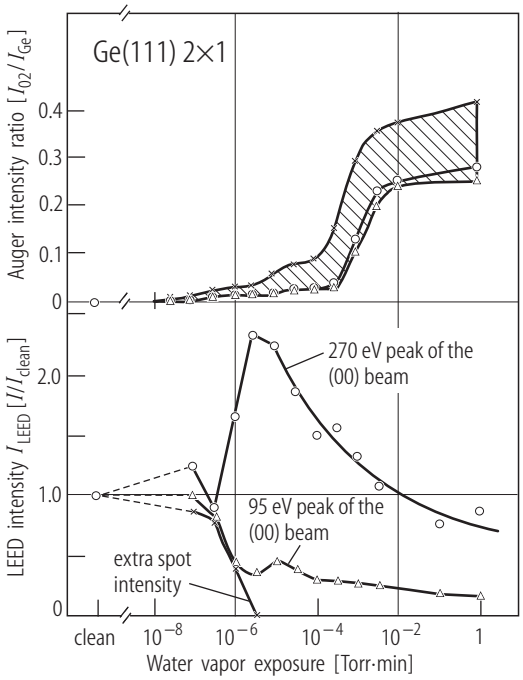

Fig. 7. Upper part: Adsorbed amount of water vapor on Ge(111)2×1 (as ratio of oxygen to germanium Auger signal) versus water vapor exposure to a freshly cleaved germanium surface. Each spot has been used only once to avoid effects of the electron beam. Lower part: LEED intensities of the (00) beam and of a half order beam of the freshly cleaved germanium surface. The two chosen voltages are typical for all voltages of the complete $I - V$ plots [75S].

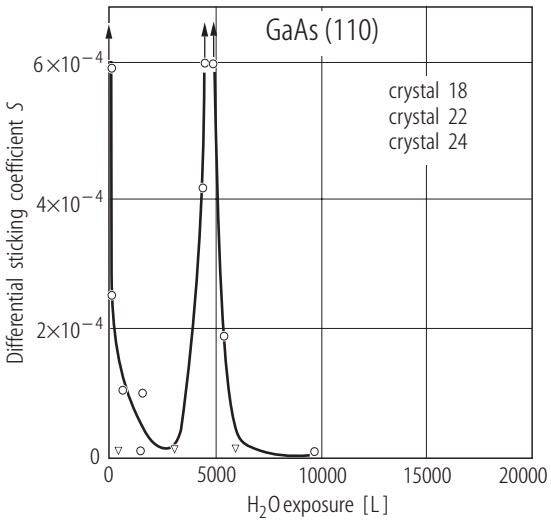

Fig. 8. Differential sticking coefficient of H_2O adsorption on GaAs(110) as a function of H_2O exposure. The relative sticking coefficient was obtained by dividing the difference between two consecutive values of the integrated H_2O desorption flux by the difference of the corresponding H_2O exposures. A sticking coefficient of 0.003 is obtained at exposures below 20 L [84M].

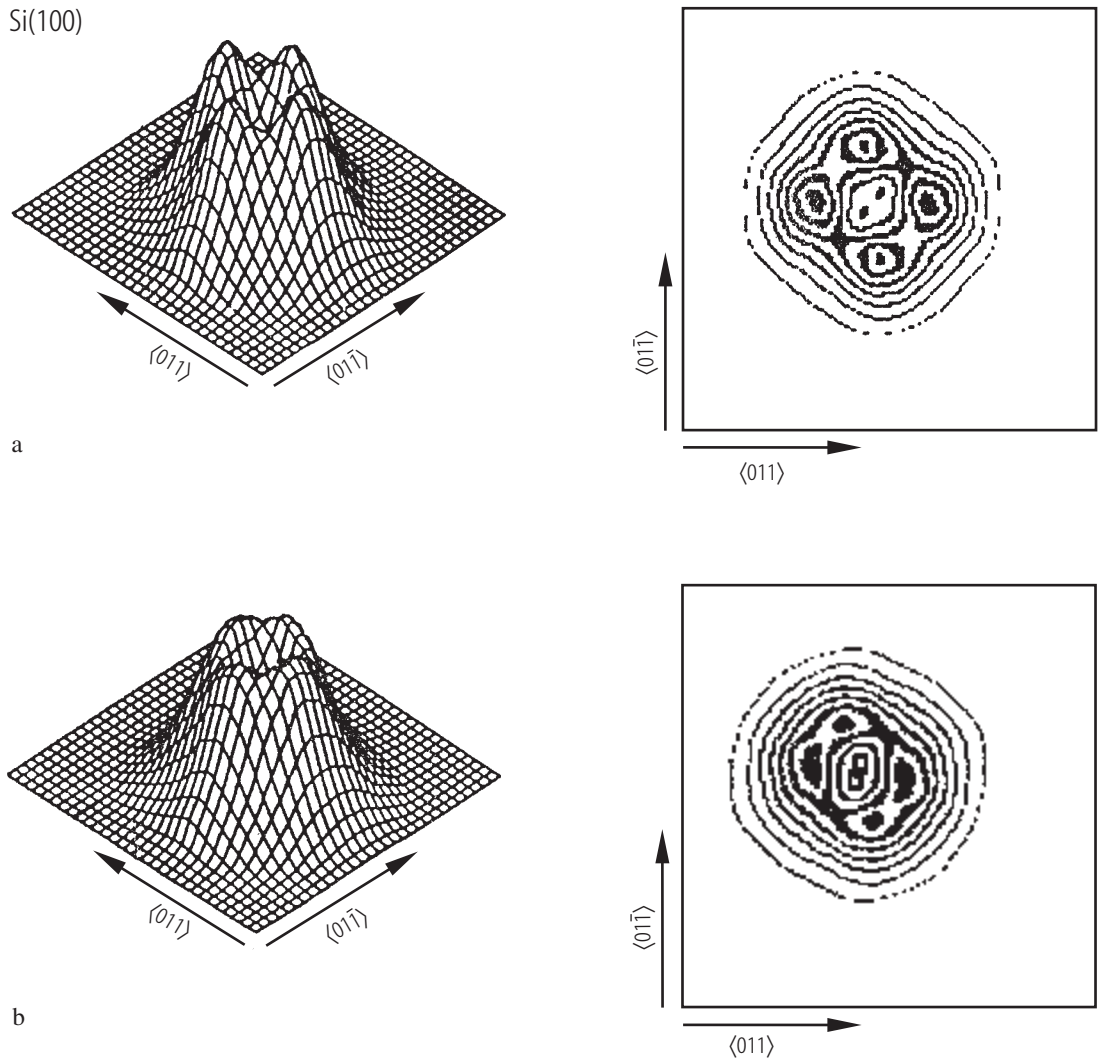

Fig. 9a. Reversible temperature-dependent ESDIAD patterns of OH/Si(100). (a) 130 K Si substrate temperature; (b) 305 K Si substrate temperature. H_2O was adsorbed at 305 K to saturation. The figures on the left are perspective plots; they are generated by mapping the counts of H^+ ion of the adsorbed OH group in the z direction as a function of the (x, y) coordinates on the detector. The figures on the right are contour plots. Each contour line in each individual plot represents an increment of 1/7 of the maximum count rate at a peak, with a width of ±5% of the median value of that contour [94G]. For a vicinal surface a two fold symmetry is observed (see [87L2]).

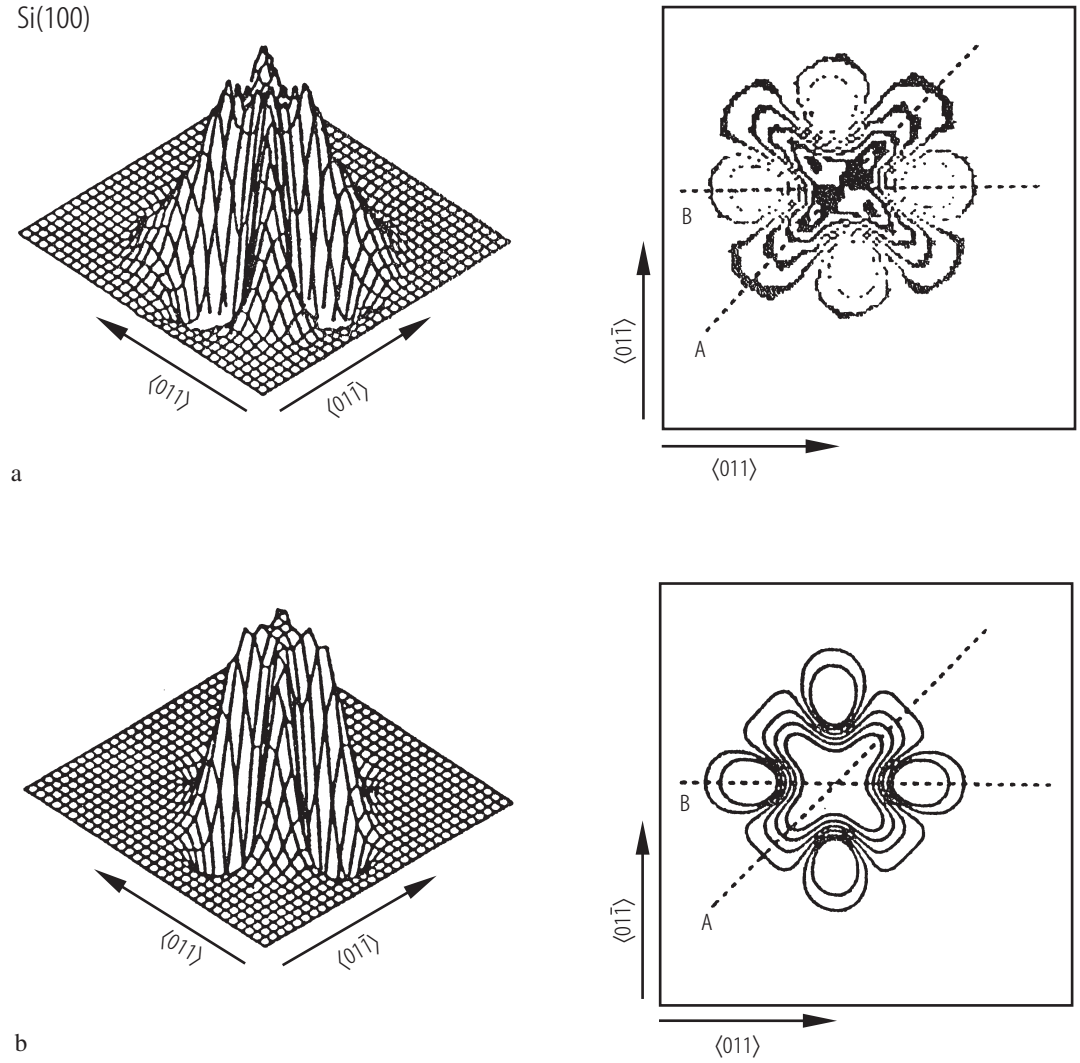

Fig. 9b. The difference ESDIAD patterns for OH/Si(100). (a) Experimental difference pattern obtained by digital subtraction of the 130 K ESDIAD pattern from the 305 K ESDIAD pattern (see Fig. 9a). (b) Modeled difference ESDIAD pattern with Gaussian distribution peak profiles [94G].

Si(100) 2×1

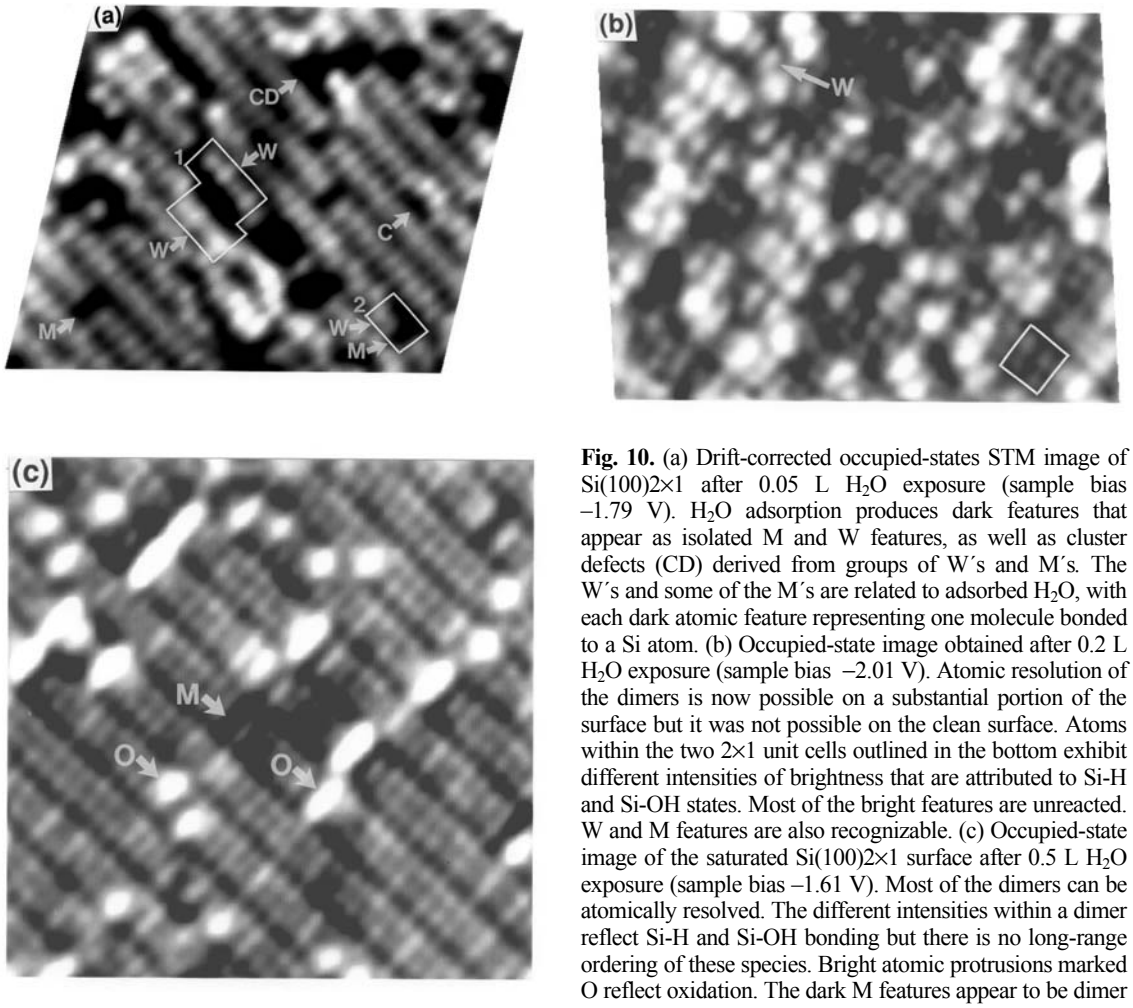

Fig. 10. (a) Drift-corrected occupied-states STM image of Si(100)2×1 after 0.05 L H_2O exposure (sample bias –1.79 V). H_2O adsorption produces dark features that appear as isolated M and W features, as well as cluster defects (CD) derived from groups of W′s and M′s. The W′s and some of the M′s are related to adsorbed H_2O, with each dark atomic feature representing one molecule bonded to a Si atom. (b) Occupied-state image obtained after 0.2 L H_2O exposure (sample bias –2.01 V). Atomic resolution of the dimers is now possible on a substantial portion of the surface but it was not possible on the clean surface. Atoms within the two 2×1 unit cells outlined in the bottom exhibit different intensities of brightness that are attributed to Si-H and Si-OH states. Most of the bright features are unreacted. W and M features are also recognizable. (c) Occupied-state image of the saturated Si(100)2×1 surface after 0.5 L H_2O exposure (sample bias –1.61 V). Most of the dimers can be atomically resolved. The different intensities within a dimer reflect Si-H and Si-OH bonding but there is no long-range ordering of these species. Bright atomic protrusions marked O reflect oxidation. The dark M features appear to be dimer vacancies that remain unreacted [93C2].

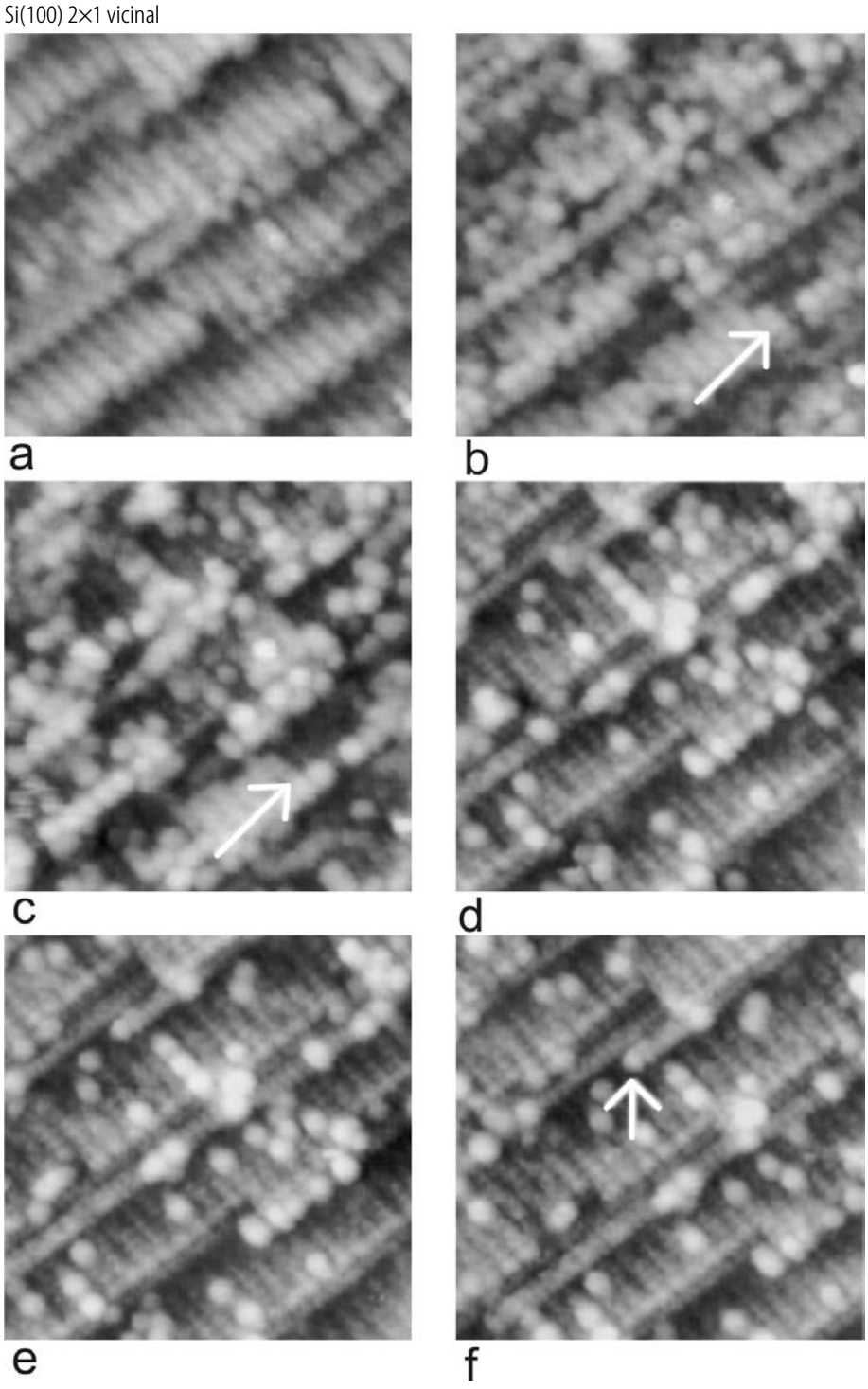

Fig. 11. H_2O adsorption sequence measured by STM on vicinal Si(100) tilted 4° towards [011]. Exposure is increased from 0 to 1.0 L in steps of 0.25 L. The surface shown in (f) was additionally exposed to 1 L. The images show the same area of 150 x 150 $Å^2$ with only small displacements due to thermal drift. The step structure is not altered during adsorption. In (b) and (c) a growing island is marked [93A].

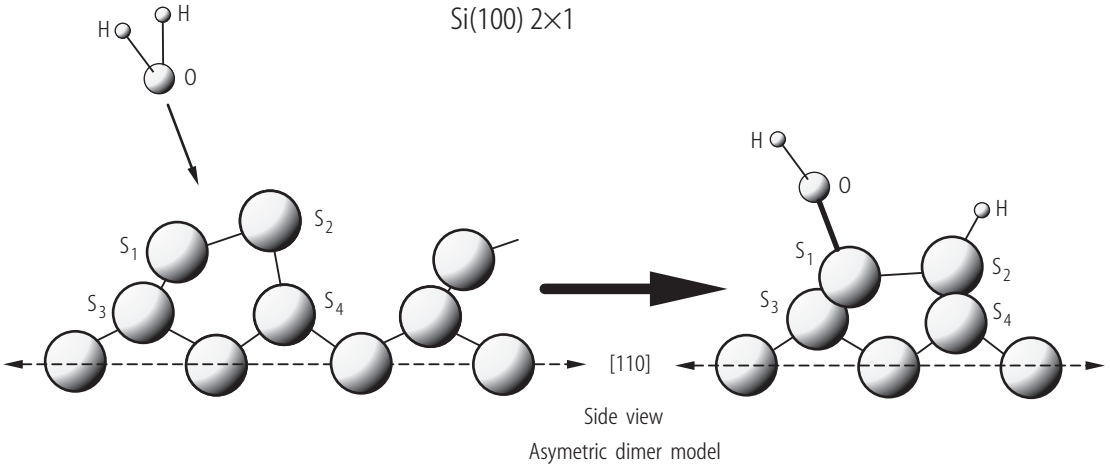

Fig. 12. Schmematic sectional view showing the structural parameter labels for the O atom in the Si(100)2×1-OH system, which have been optimised by a fitting procedure between the O 1s photoelectron diffraction data and multiple scattering simulations. In the plot the configuration of the H_2O molecules, OH fragments and Si dimers before and after the surface reaction have been schematically indicated [98F]. The values of distances and angles are given in table 4.

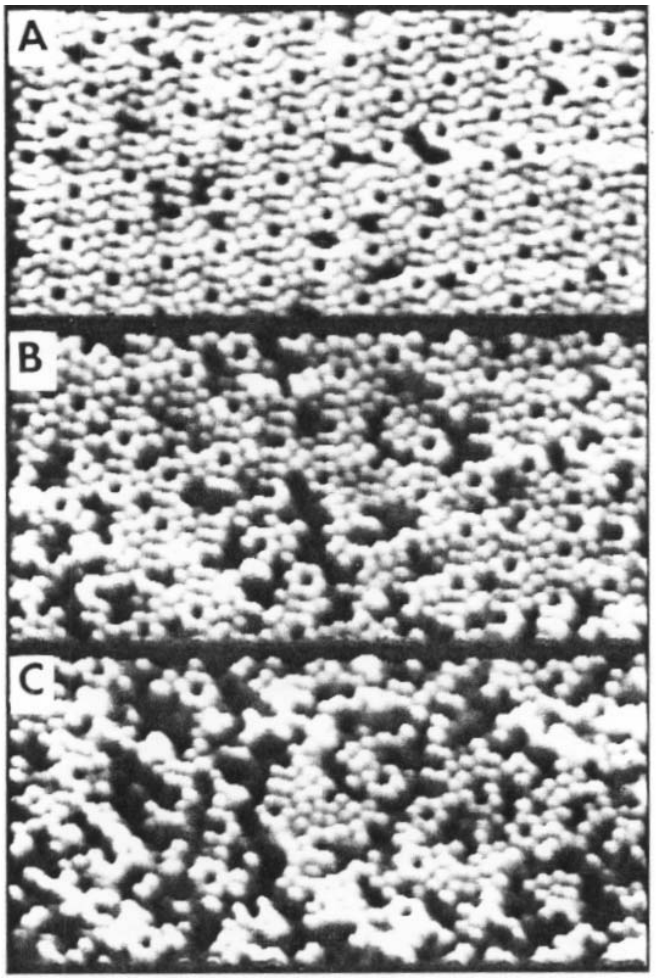

Si(111)7×7

Fig. 13. (A) STM topograph of a clean Si(111)7×7 surface. (B) after exposure to 5 L of H_2O and (C) after exposure to 25 L of H_2O at RT [91A].

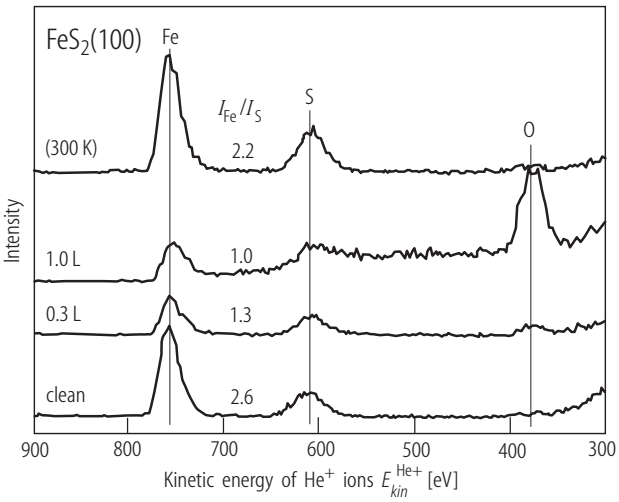

Fig. 14. He^+ LEIS-spectra (1 keV) for different H_2O coverages on FeS_2 (100). The S/Fe intensity ratio is shown in the spectra, indicating preferential adsorption on Fe-sites [91P2].

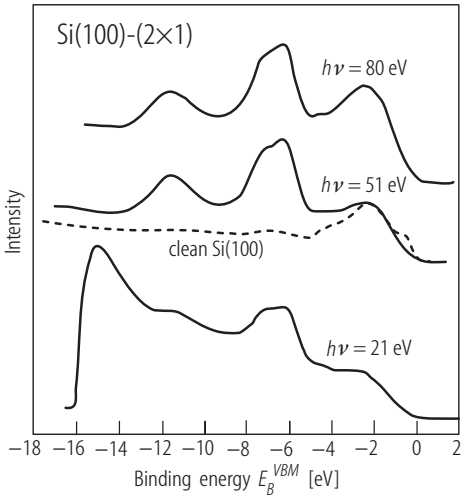

Fig. 15. Angle-integrated photoelectron valence band spectra for saturation coverage of H_2O Si(100)2×1 taken at room temperature with different photon energies. The Fermi level is 0.4 eV above the valence-band maximum [83S2].

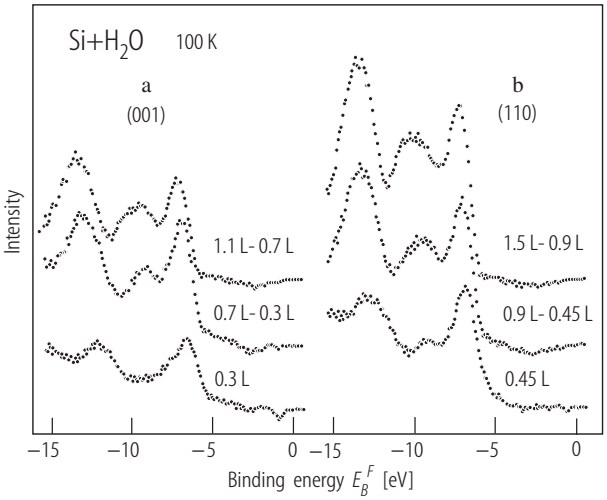

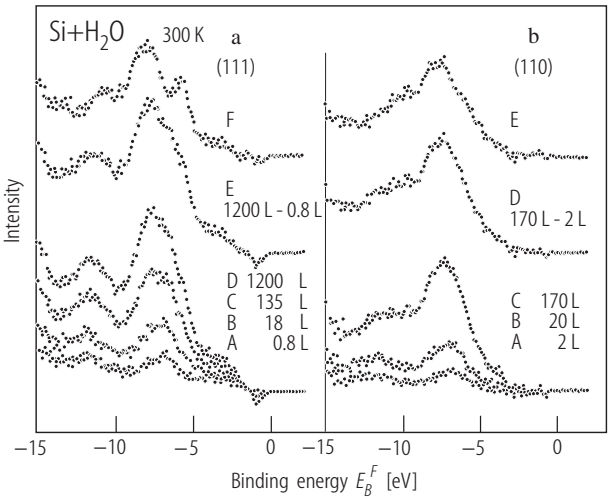

Fig. 16. HeI UP spectra of H_2O adsorption at 100 K for the Si (001) surface a) and the (110) surface b). Displayed are the difference spectra between subsequent exposure steps as indicated [85R1].

Fig. 17. HeI UP spectra of H_2O adsorption on Si (111) and Si (110) at room temperature. (a) Curves A-D: exposure dependence on (111) (difference spectra); curve E: difference between 0.8 and 1200 L spectra; curve F: same as curve E, but reduced by 35% of the difference curve of 0.7L on Si(100). (b) Curves A-C: exposure dependence on (110) (difference spectra); curve D: difference between 2 and 170 L spectra; curve E: same as curve D, but reduced by 15% of the difference curve of 0.7L on Si(100) [85R1].

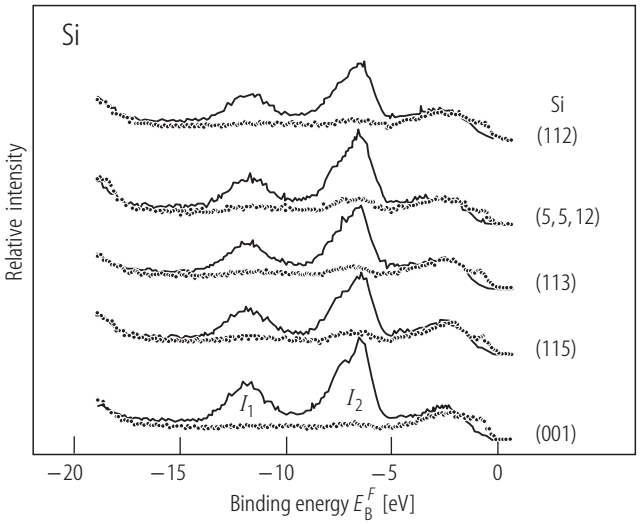

Fig. 18. Angle integrated valence band photoelectron spectra ($h\nu = 40.8$ eV) from five flat Si samples of the indicated orientations on one sample holder, taken in one run before and after exposure. Dots: clean surfaces; lines: after exposure to water equivalent to the number of 2.4 ML of Si (100) leading to saturation with OH + H [97R].

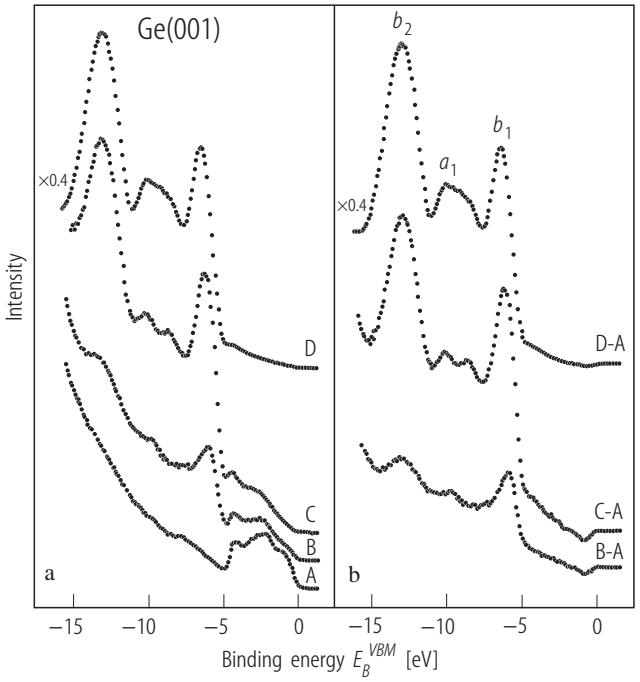

Fig. 19. HeI photoelectron spectra on Ge(001) at 110 K. (a) Original spectra of the clean surface (A), exposed to 0.4 L (B), 1.1 L (C) and 3.7 L water (D). The intensities are scaled relative to the intensity of the clean surface spectrum (A). (b) Difference curves (covered minus clean surface spectra) [87K3].

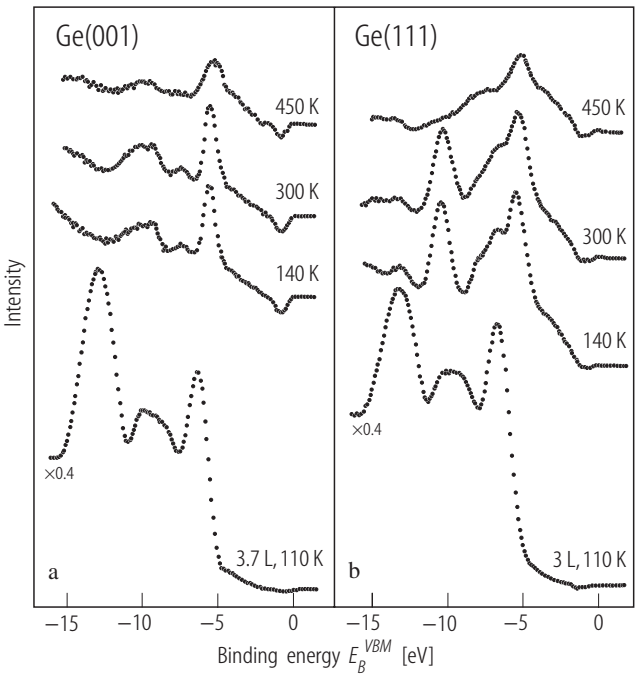

Fig. 20. HeI difference spectra of H_2O on Ge(001) (a) and Ge(111) (b). The surface was first covered with a condensed H_2O layer at 110 K and then warmed up to the indicated temperatures [87K3].

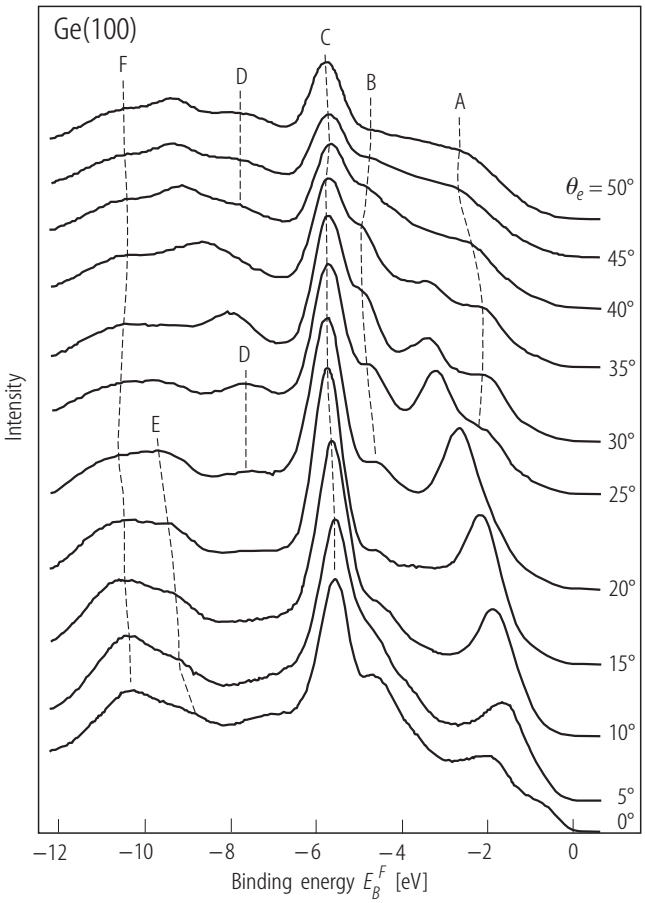

Fig. 21. Angle-resolved photoelectron spectra of Ge(100) + H_2O recorded at $h\nu$ = 24 eV. The analyzer was rotated in the incident photon ionization plane and the sample was oriented such that the [010] direction was probed. The photon incident angle was θ_i = 60°. The surface was exposed to 2 L H_2O at 160 K and annealed to 300 K. The spectra were recorded with the surface at 300 K [91L2].

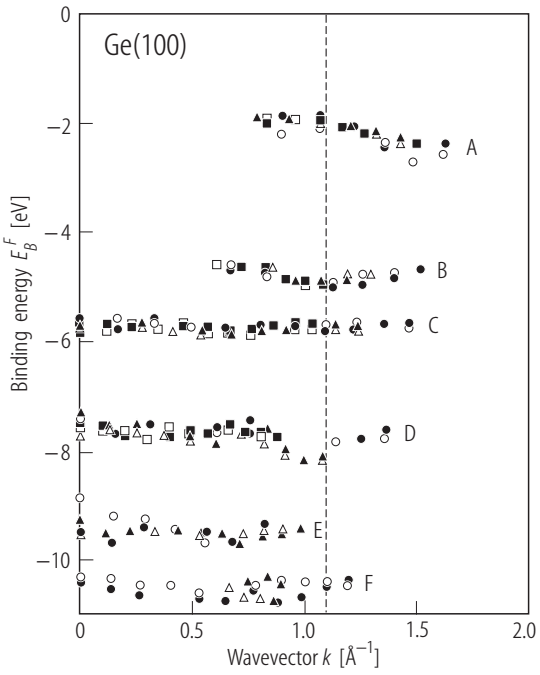

Fig. 22. Energy dispersions for the states related with dissociated H_2O adsorbed on the Ge(100) surface. The open symbols indicate dispersions in the spectra recorded with an incident photon angle θ_i = 60° and the solid symbols indicate dispersions in the spectra recorded with an incident photon angle θ_i = 15° [91L2]. (See also Fig. 21; A: Ge-Ge bond, B: Ge-H bond, C: OH π (nonbonding), D: Ge-OH π (weak bonding), E: Ge-H bond, F: OH σ)

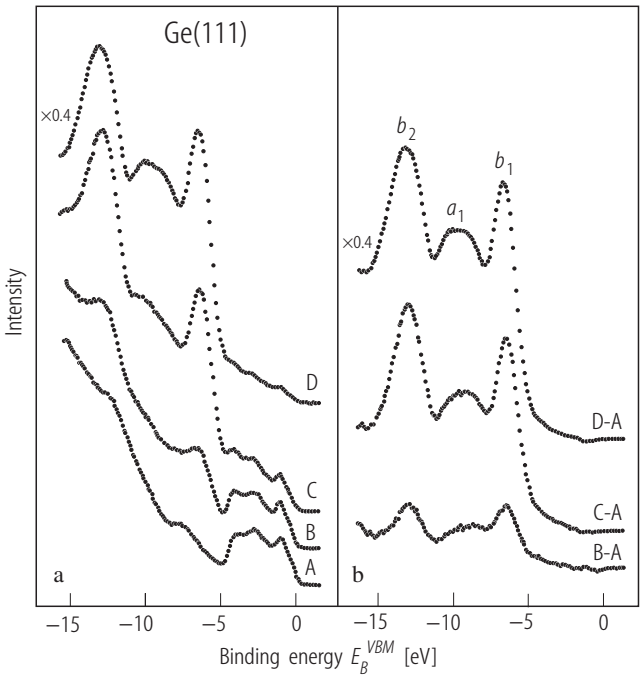

Fig. 23. HeI photoelectron spectra of H_2O on Ge(111) at 110 K. a: Original spectra of the clean surface (A), exposed to 0.3 L (B), 1 L (C) and 3 L water (D). The intensities are scaled relative to the intensity of the clean surface spectrum (A). (b) Difference curves (covered minus clean surface spectra) [87K3].

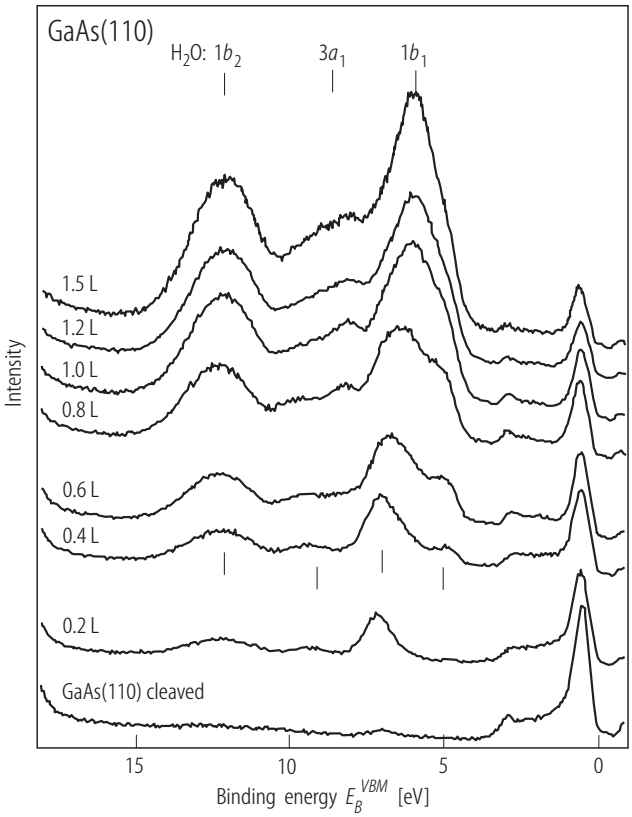

Fig. 24. SXP valence band spectra of H_2O adsorbed onto GaAs(110) surface at 100 K, excitation energy $h\nu$ = 41 eV. The marks at 0.4 L H_2O indicate As-H and Ga-OH bonds [97H].

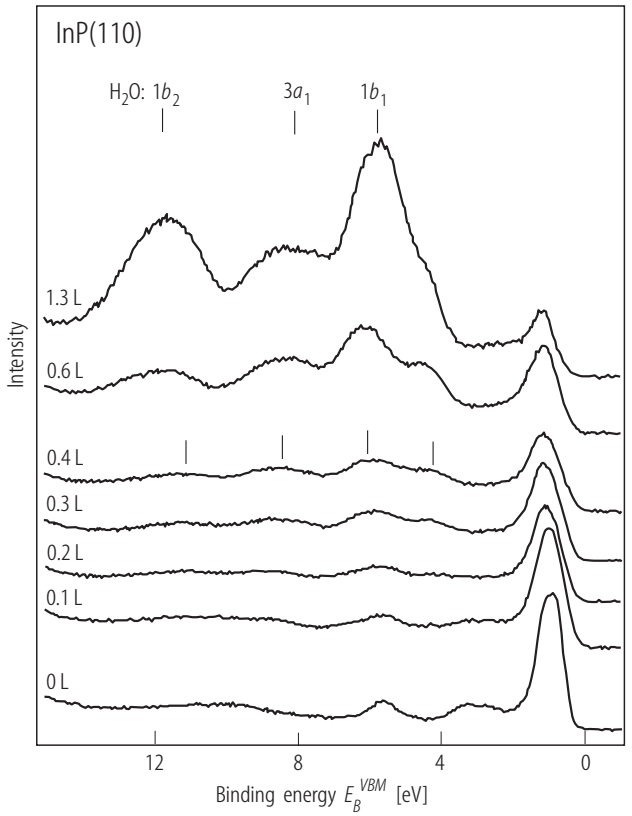

Fig. 25. SXP valence band spectra of cleaved InP(110) with increasing H_2O dosage at 100 K. Excitation energy $h\nu$ = 41 eV. The marks at 0.4 L H_2O indicate In-OH and P-H bonds [00H].

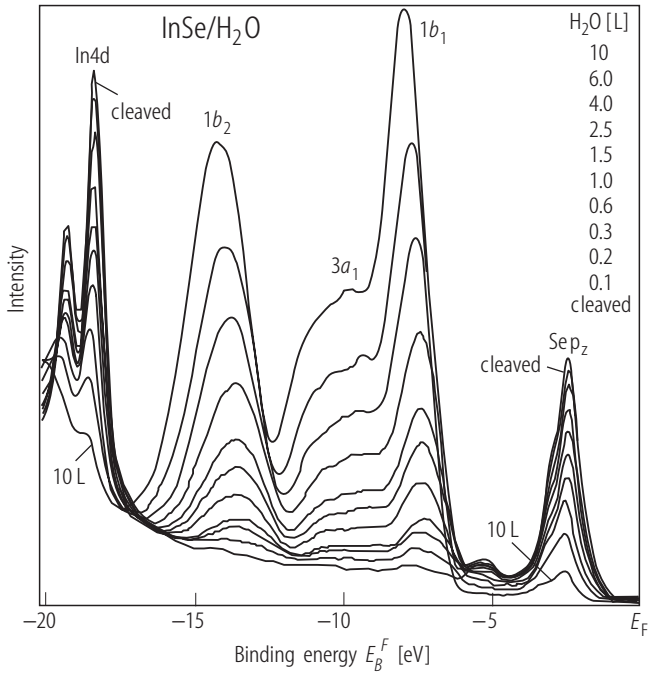

Fig. 26. SXP valence band spectra of water adsorbed onto InSe(0001) surface at 100 K, excitation energy $h\nu = 30$eV [93M].

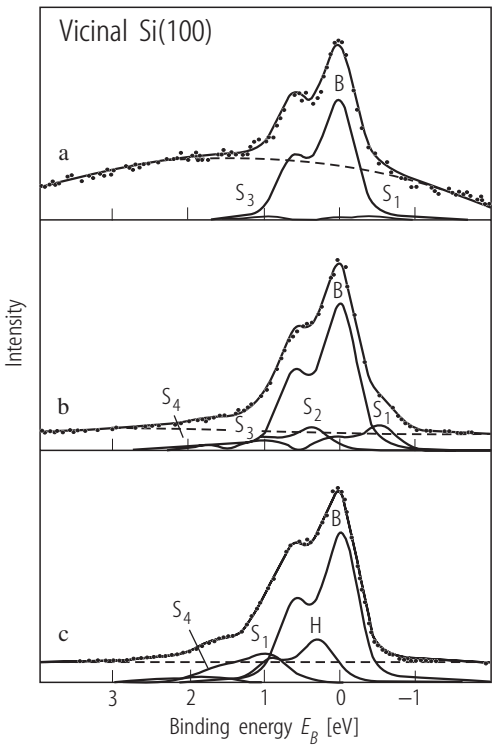

Fig. 27. (a) Si 2p core level photoemission spectrum recorded at a bulk-sensitive photon energy of $h\nu = 112$ eV for the clean Si(100) surface. The energy scale is in binding energy referenced to the bulk Si $2p_{3/2}$ component. The solid lines denote a fit with five spin-orbit doublets S_1, B, S_2, S_3 and S_4. (b) As in (a), but at a surface-sensitive photon energy $h\nu = 130$ eV. (c) Si 2p spectrum as in (b) after exposure to saturation coverage of 2 L of H_2O. The new peak labelled H is attributed to emission from Si atoms bonded to H [88M].

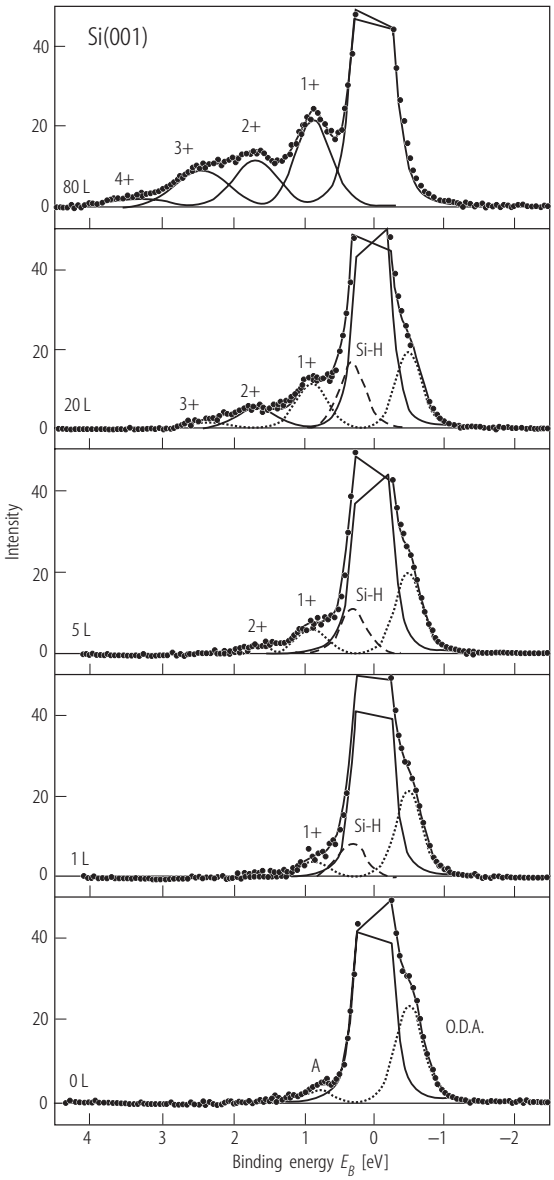

Fig. 28. Si $2p_{3/2}$ spectra (peak maxima normalized to 100) of the Si(001) surface exposed at 90 K to increasing water exposures. Excitation energy hv = 145 eV. The vapor pressure was 2×10^{-8} Torr for the first two exposures and 5×10^{-8} Torr for the last three ones. Curve reconstructions are also given, a SiH contribution (dashed line) at about +0.3 eV is introduced for the best resolved spectra [95P]. (1+, 2+ etc. denote the different oxidation states of Si; ODA contribution, dotted line, of outer dimer atoms, A not defined by authors).

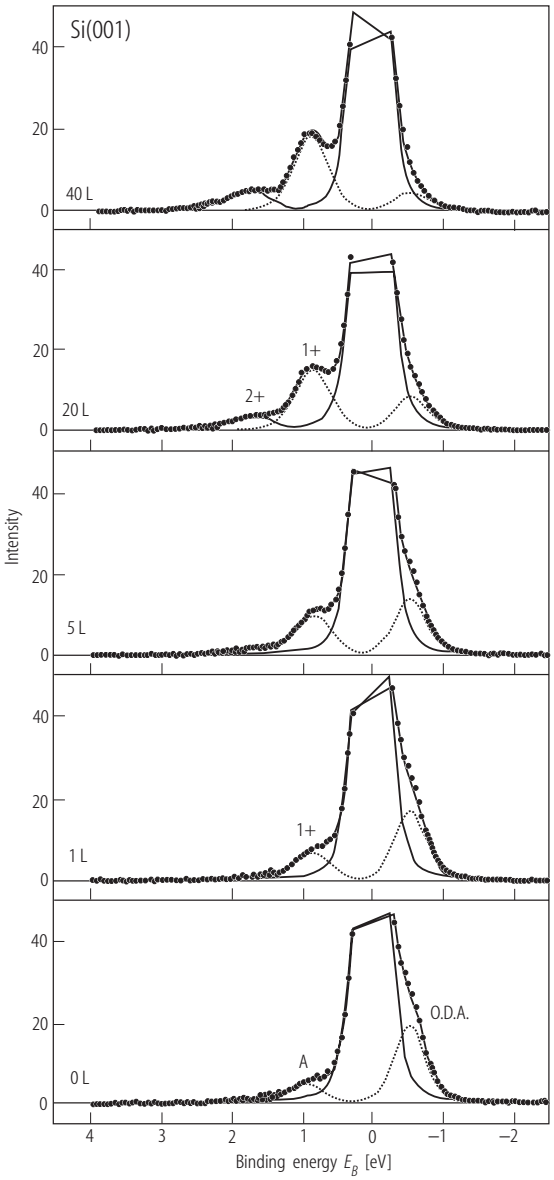

Fig. 29. Si $2p_{3/2}$ spectra (peak maxima normalized to 100, E_B is given relative to bulk Si $2p_{3/2}$) of the Si(001)2×1 surface exposed at 300 K to increasing water exposures (under 2×10^{-8} Torr). Excitation energy hv = 145 eV. Curve reconstructions are also given [95P]. (1+, 2+ denote the different oxidation states of Si; ODA contribution, dotted curve, of outer dimer atoms, A not defined by authors).

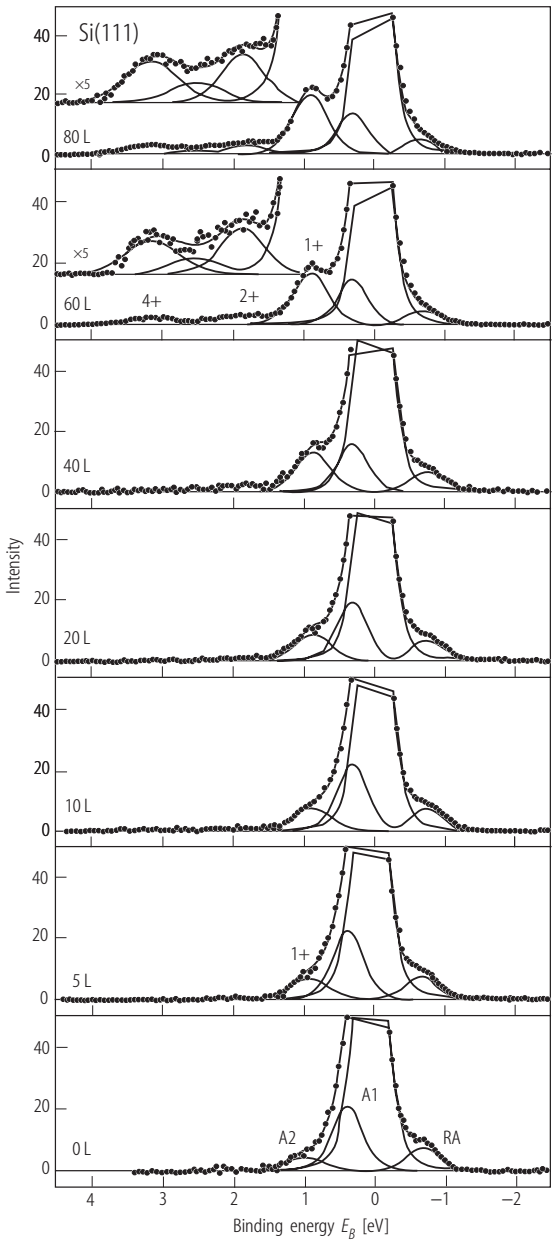

Fig. 30. Si $2p_{3/2}$ spectra (peak maxima normalized to 100, E_B is given relative to bulk Si $2p_{3/2}$) of the Si(111)7×7 surface exposed at 300 K to increasing water exposures (under 5×10^{-8} Torr). Excitation energy $h\nu$ = 145 eV Curve reconstructions are also given [95P]. (RA: rest atom, A1: Si-adatoms, A2: not defined by authors, +1, +2, etc. denote the different oxidation states of Si).

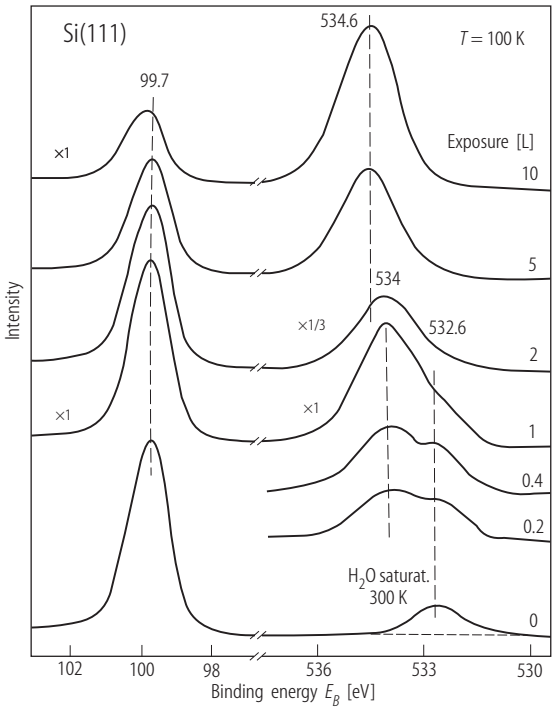

Fig. 31. Si 2p (left) and O 1s (right) Mg K_α photoelectron spectra for water adsorbed on Si(111)2×1 [85S].

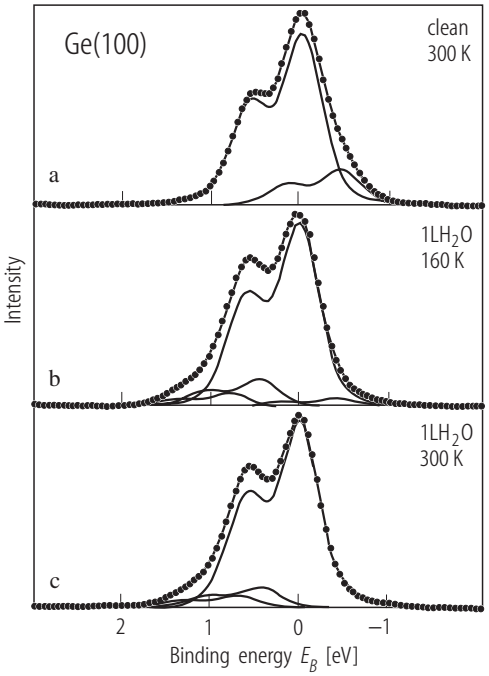

Fig. 32. Ge(100) 3d core-level spectra recorded at 70 eV photon energy. The filled circles show the raw data after background subtraction and the lines show the calculated fits to the data: (a) the spectrum from the clean surface recorded at 300 K, (b) the spectrum from the surface after a 1 L H_2O exposure at 160 K, and (c) the spectrum from the surface after a 1 L H_2O exposure at 160 K and heating to 300 K. The binding energy is referred to the bulk Ge $3d_{5/2}$ components [89L].

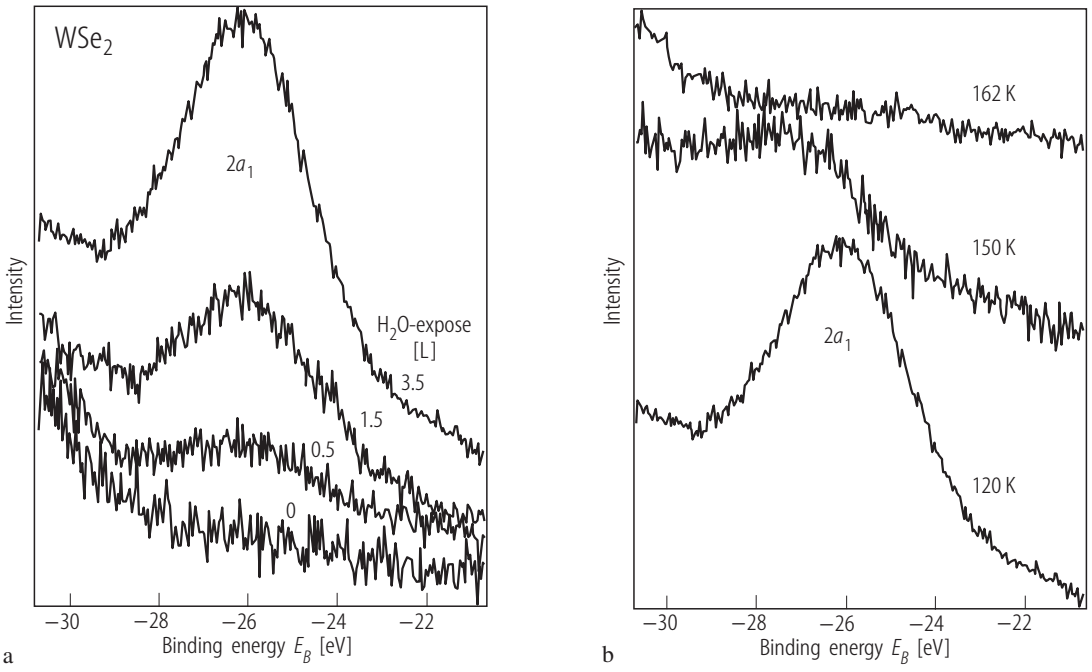

Fig. 33. H_2O adsorption on WSe_2 (0001) at 120 K. SXP spectra of the O 2s level as function of coverage during adsorption (a) and during desorption, after 3.5 L H_2O-exposure (b), excitation energy $h\nu$ = 80 eV [93M].

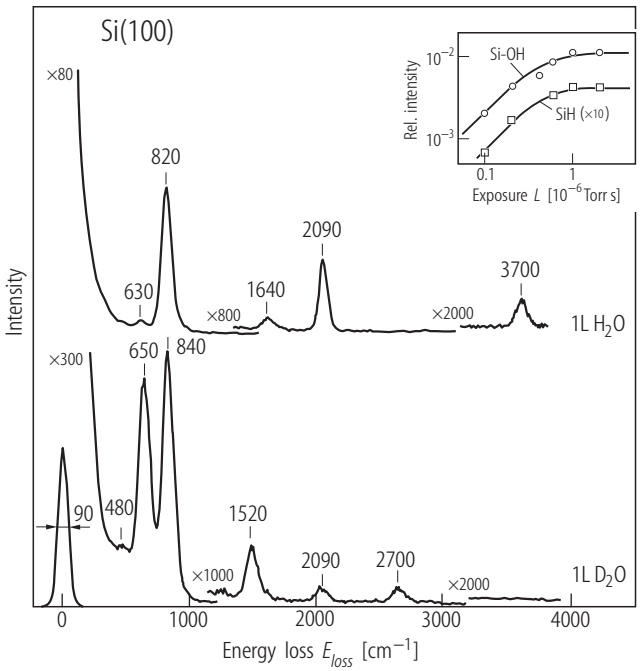

Fig. 34. Electron energy loss spectra of 1 L of H_2O and D_2O, respectively, on a Si(100) surface at 300 K. The loss at 1640 cm^{-1} in the upper spectrum is a double loss of 820 cm^{-1}. The 2090 cm^{-1} loss on the D_2O exposed surface is produced through some H-D-exchange or H_2O contamination. The electron impact energy was 14 eV. The insert displays the intensities of the 820 cm^{-1} loss and the 2090 cm^{-1} (SiH) loss vs coverage [82I2].

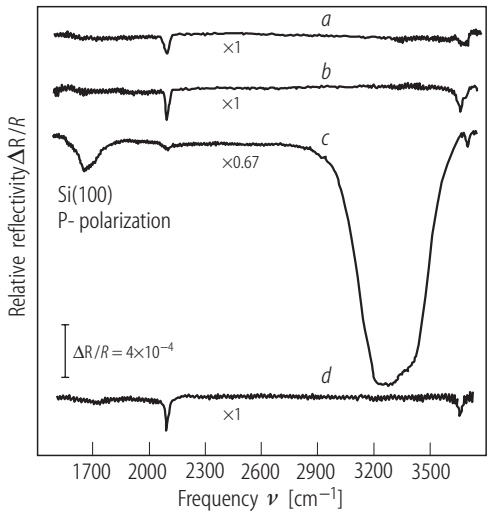

Fig. 35. Water-induced infrared reflection spectra, $\Delta R/R$, upon water exposure on clean Si(100)2×1 at 80 K: a, 0.5 L with T_S = 80 K; b, 0.5 L with T_S = 80 K and after annealing to 285 K for 1 min with no additional water exposure; c, 10 L with T_S = 80 K; and d, 10 L with T_S = 80 K and after annealing to 280 K for 1 min [84C2].

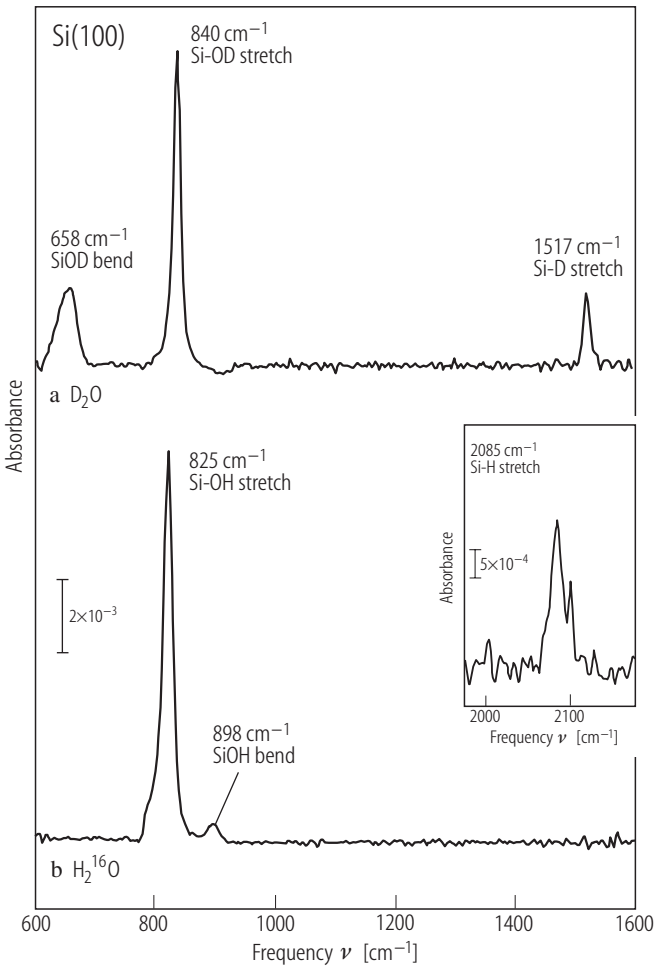

Fig. 36. Infrared absorption spectra of Si(100) surfaces after 2 L exposures to (a) D_2O and (b) $H_2^{16}O$ at ~300 K [97S2].

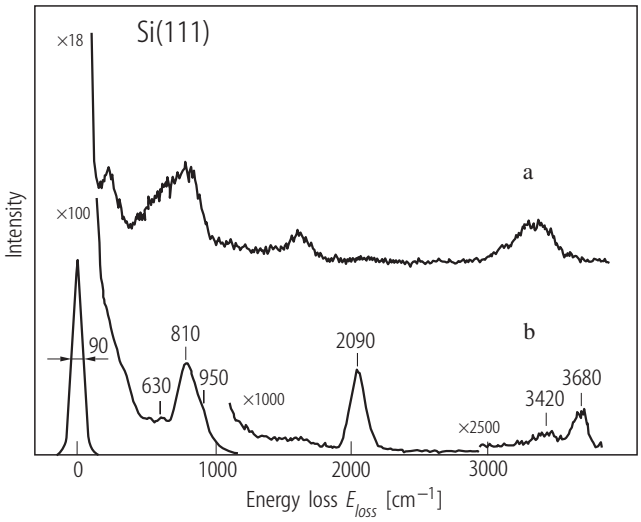

Fig. 37. Electron energy loss spectra of (a) 2L of H_2O condensed on a Si(111)7×7 surface held at 100 K. (b) The same surface after annealing briefly to 300 K [82I2].

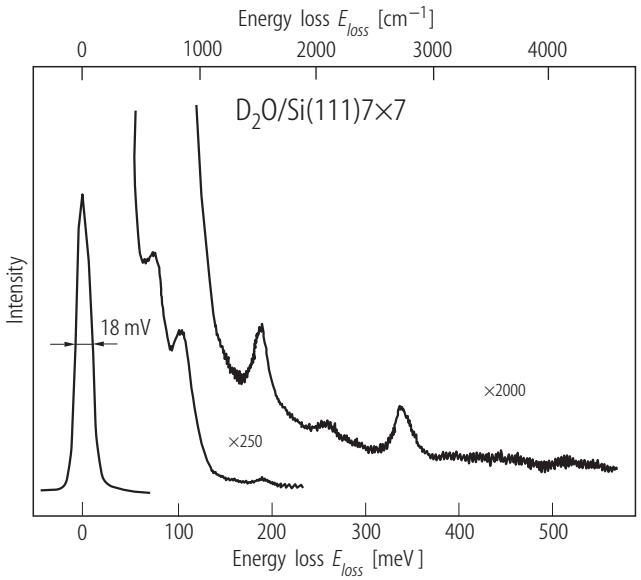

Fig. 38. Electron energy loss spectrum for heavy water adsorbed on Si(111)7×7 surface at saturation coverage (300 K), E_0 = 7.98 eV [83K2].

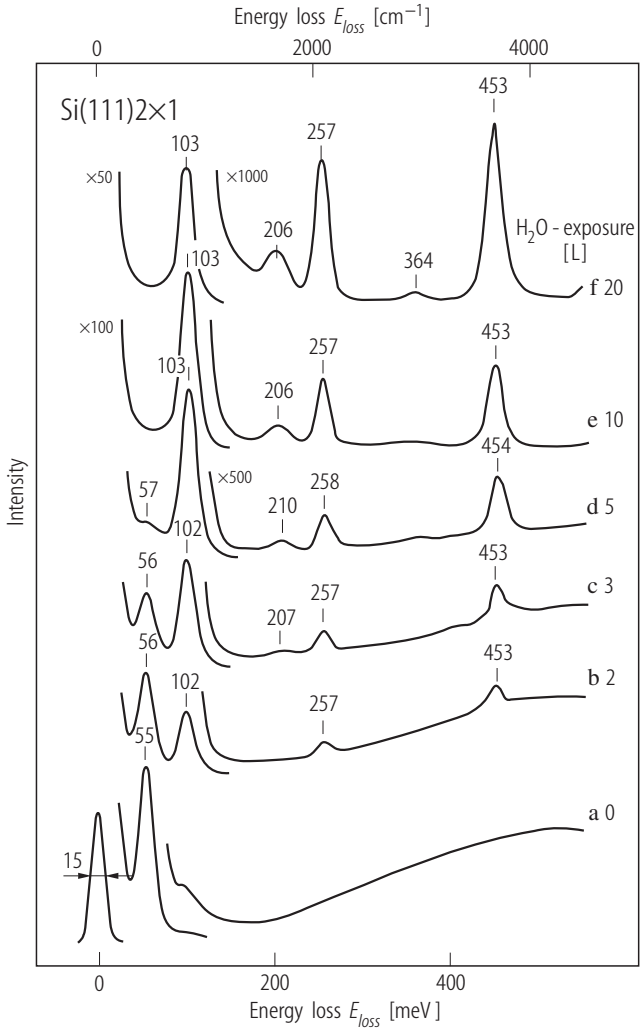

Fig. 39. EELS spectra for (a) clean cleaved and (b)-(f) water exposed Si(111)2×1 at room temperature, E_0 = 6.5 eV, $\theta_i = \theta_s$ = 65° [84S1].

3.8.2.15 References for 3.8.2

55H Hauffe, K.: Advanced Catalysis **7** (1955) 213.
57K Kisliuk, P.J.: J. Phys. Chem. Solids **3** (1957) 95.
58K Kisliuk: J. Phys. Chem. Solids **5** (1958) 78.
63W Wolkenstein, T., The Electron Theory of Catalysis on Semiconductors, (Pergamon Press, Oxford, 1963).
68E Ertl, G.: Ber. Bunsenges. Phys. Chem. **72** (1968) 74.
71M Meyer, F.: Surf. Sci. **27** (1971) 107.
73H Henzler, M.,Töpler, J.: Surf. Sci. **40** (1973) 388.
75F Fujiwara, K.,Nishijima, M.: Phys. Lett. **55A** (1975) 211.
75S Sinharoy, S.,Henzler, M.: Surf. Sci. **51** (1975) 75.
75Y Yu, K.Y., McMenamin, J.C., Spicer, W.E.: Surf. Sci. **50** (1975) 149.
77F Fujiwara, K.,Ogata, H.: J. Appl. Phys. **48** (1977) 4360.
77M Morrison, S.R., The Chemical Physics of Surfaces, (Plenum Press, New York, 1977).
79B Büchel, M.,Lüth, H.: Surf. Sci. **87** (1979) 285.
79F Fujiwara, K.,Ogata, H.: Surf. Sci. **86** (1979) 700.
79G Galaev, A.A., Gamosov, L.V., Parkhomenko, Y.N.,Shirkov, A.V.: Sov. Phys. Crystallogr. **24** (1979) 72.
81F1 Fujiwara, K.: Surf. Sci. **108** (1981) 124.
81F2 Fujiwara, K.: Journal of Chemical Physics **75** (1981) 5172.
81T Thornton, G., Rosenberg, R.A., Rehn, V., Green, A.K.,Parks, C.C.: Solid St. Commun. **40** (1981) 131.
82G Gmelin, Handbook of Inorganic Chemistry, H. Koschel ed. ed., (Springer Verlag, 1982).
82I1 Ibach, H., Bruchmann, D.,Wagner, H.: Appl. Phys. A **29** (1982) 113.
82I2 Ibach, H., Wagner, H.,Bruchman, D.: Solid St. Commun. **42** (1982) 457.
82M Montgomery, V.,Williams, R.H.: J. Phys. C **15** (1982) 5887.
82W Webb, C.,Lichtensteiger, M.: J. Vac. Sci. Technol. **21** (1982) 659.
83B Black, J.E., Bopp, P.,Wolfsberg, M.: Surf. Sci. **134** (1983) 257.
83C1 Ciraci, S., Erkoc, S.,Ellialioglu, S.: Solid St. Commun. **45** (1983) 35.
83C2 Ciraci, S.,Wagner, H.: Phys. Rev. B **27** (1983) 5180.
83K1 Kahn, A.: Surf. Sci. Rep. **3** (1983) 193.
83K2 Kobayashi, H., Kubota, T., Onchi, M.,Nishijima, M.: Phys. Lett. **95A** (1983) 345.
83S1 Schmeisser, D., Himpsel, F.J., Holliger, G., Reihl, B.,Jacobi, K.: Phys. Rev. B **27** (1983) 3279.
83S2 Schmeisser, D., Himpsel, F.J., Hollinger, B.: Phys. Rev. B **27** (1983) 7813.
84C1 Chabal, Y.J.: Phys. Rev. B **29** (1984) 3677.
84C2 Chabal, Y.J.,Christman, S.B.: Phys. Rev. B **29** (1984) 6974.
84C3 Childs, K.D., Luo, W.-A.,Lagally, M.G.: J. Vac. Sci. Technol. A **2** (1984) 593.
84M Mokwa, W., Kohl, D.,Heiland, G.: Surf. Sci. **139** (1984) 98.
84O Oellig, E.M., Butz, R., Wagner, H.,Ibach, H.: Solid St. Commun. **51** (1984) 7.
84S1 Schaefer, J.A., Stucki, F., Frankel, D.J., Göpel, W.,Lapeyre, G.J.: J. Vac. Sci. Technol. B **3** (1984) 359.
84S2 Schmeisser, D.: Surf. Sci. **137** (1984) 197.
84S3 Stucki, F., Anderson, J., Lapeyre, G.J.,Farrell, H.H.: Surf. Sci. **143** (1984) 84.
85C Chabal, Y.J.: J. Vac. Sci. Technol. A **3** (1985) 1448.
85N Nishijima, M., Edamota, K., Kobayashi, H.,Onchi, M.: Surf. Sci. **158** (1985) 422.
85R1 Ranke, W.,D.Schmeisser: Surf. Sci. **149** (1985) 485.
85R2 Ranke, W., Schmeisser, D.,Xing, Y.R.: Surf. Sci. **152/153** (1985) 1103.
85R3 Ranke, W.,Xing, Y.R.: Surf. Sci. **157** (1985) 339.
85S Schäfer, J.A., Anderson, J.,Lapeyre, G.J.: J. Vac. Sci. Technol. A **3** (1985) 1443.
85T Takayanagi, K., Tonishiro, Y., Takahashi, M.,Takahashi, S.: J. Vac. Sci. Technol. A **3** (1985) 1502.
86B Broughton, J.Q., Schaefer, J.A., Bean, J.C.,Farrel, H.H.: Phys. Rev. B **33** (1986) 6841.
86N Nishijima, M., Edamoto, K., Kubota, Y., Tanaka, S.,Onchi, M.: J. Chem. Phys **84** (1986) 6458.

86S1 Schaefer, J.A., Anderson, J.,Lapeyre, G.J.: J. Electr. Spectr. Rel. Phen. **38** (1986) 21.
86S2 Schmeisser, D.,Demuth, J.E.: Phys. Rev. B (1986) 4233.
87B Barone, V., Lelj, F., Russo, N.,Toscano, M.: Journal de chimie physique **84** (1987) 5.
87F Feenstra, R.M., Strodcio, J.A.,Fein, A.P.: Surf. Sci. **181** (1987) 295.
87J Jaegermann, W.,Schmeisser, D.: J. Vac. Sci. Technol. A **5** (1987) 627.
87K1 Katircioglu, S.: Surf. Sci. **187** (1987) 569.
87K2 Kuhr, H.J.,Ranke, W.: Surf. Sci. **189/190** (1987) 420.
87K3 Kuhr, H.J.,Ranke, W.: Surf. Sci. **187** (1987) 98.
87L1 Larsson, C.U.S., Flodström, A.S., Nyholm, R., Incoccia, L.,Senf, F.: J. Vac. Sci. Technol. A **5** (1987) 3321.
87L2 Larsson, C.U.S., Johnson, A.L., Flodström, A.,Madey, T.E.: J. Vac. Sci. Technol. A **5** (1987) 842.
87R Russo, N.,Toscano, M.: Surf. Sci. **180** (1987) 599.
87T Thiel, P.A.,Madey, P.E.: Surf. Sci. Rep. **7** (1987) 211.
88D Dong, G., Ding, X., Hou, X.,Wang, X.: Surf. Sci. **201** (1988) 531.
88F Froitzheim, H., in: The Chemical Physics of Solid Surfaces and Heterogeneous Catalysis, Vol. 5, Eds. D. A. King, D. P. Woodruff, (Elsevier, Amsterdam, 1988), pp. 183.
88H Hansson, J.G.V.,Uhrberg, R.I.G.: Surf. Sci. Rep. **9** (1988) 197.
88J Jaegermann, W.,Tributsch, H., in: Progress in Surface Sciences, Vol. 29, Ed. S. G. Davison, (Pergamon Press, New York, 1988), p. 1.
88M McGrath, R., Cimino, R., Braun, W., Thornton, G.,McGovern, I.T.: Vacuum **38** (1988) 251.
89F Fives, K., McGrath, R., Stephens, C., McGovern, I.T., Cimino, R., Law, D.S.-L., Johnson, A.L.,Thornton, G.: J. Phys.: Condens. Matter **1** (1989) SB105.
89H Hamers, R.J.,Köhler, U.K.: J. Vac. Sci. Technol. A **7** (1989) 2854.
89K Koehler, B.G., Mak, C.H.,George, S.M.: Surf. Sci. **221** (1989) 565.
89L Larsson, C.U.S., Flodström, A.S., Karlsson, U.O.,Yang, Y.: J. Vac. Sci. Technol. A **7** (1989) 2044.
89O Ong, C.K.: Solid St. Commun. **72** (1989) 1141.
89P Papagno, L., Caputi, L.S., Anderson, J.,Lapeyre, C.J.: Phys. Rev. B **40** (1989) 8443.
89S Seebauer, E.G.: J. Vac. Sci. Technol. A **7** (1989) 3279.
90E Engler, C.: phys. stat. sol. (b) **159** (1990) 721.
90S Schröder-Bergen, E.,Ranke, W.: Surf. Sci. **236** (1990) 103.
91A Avouris, P.,Lyo, I.: Surf. Sci. **242** (1991) 1.
91L1 Larsson, C.U.S.,Flodström, A.S.: Vacuum **42** (1991) 297.
91L2 Larsson, C.U.S.,Flodström, A.S.: Phys. Rev. B **43** (1991) 9281.
91P1 Papagno, L., Frankel, D., Chen, Y., Caputi, L.S., Anderson, J.,Lapeyre, G.J.: Surf. Sci. **248** (1991) 343.
91P2 Pettenkofer, C., Jaegermann, W.,Bronold, M.: Ber. Bunsenges. Phys. Chem. **95** (1991) 560.
91P3 Podolsky, B.S., Ukraintsev, V.A.,Chernov, A.A.: Surf. Sci. **251/252** (1991) 1033.
91P4 Podolsky, B.S., Ukraintsev, V.A.,Chernov, A.A.: Sov. Phys. Solid State **33** (1991) 65.
91S Shao, Y.,Paul, J.: Vacuum **42** (1991) 313.
91U Ukraintsev, V.A., Podolsky, B.S.,Chernov, A.A.: Appl. Surf. Sci. **48/49** (1991) 151.
92B Brillson, L.J., Handbook of Semiconductors, Vol. I, North Holland, 1992).
92C Cohen, S.M., Yang, Y.L., Rouchance, E., Jin, T.,D´Evelyn, M.D.: J. Vac. Sci. Technol. A **10** (1992) 2166.
92D Dai, D., Zhu, F., Luo, Y.,Davoli, I.: J. Phys.: Condens. Matter **4** (1992) 5855.
92L Landemark, E., Karlsson, C.J., Chao, Y.-C.,Uhrberg, R.I.G.: Phys. Rev. Lett. **69** (1992) 1588.
92M Mayer, T., Klein, A., Lang, O., Pettenkofer, C.,Jaegermann, W.: Surf. Sci. **269/270** (1992) 909.
92S Sander, M., Jaegermann, W.,Lewerenz, H.J.: J. Phys. Chem. **96** (1992) 782.
92W Wolkow, R.A.: Phys. Rev. Lett. **27** (1992) 2636.
93A Andersohn, L.,Köhler, U.: Surf. Sci. **284** (1993) 77.
93C1 Carlson, C.R., Buechter, W.F., Che-Ibrahim, F.,Seebauer, E.G.: J. Chem. Phys **99** (1993) 7190.
93C2 Chander, M., Li, Y.Z., Patrin, J.C.,Weaver, J.H.: Phys. Rev. B **48** (1993) 2493.
93J Jacobi, K., Myler, U.: Surf. Sci. **284** (1993) 223.

93L Lacharme, J.P., C. Sébenne, Chérif, S.M., Safta, N.,Zaibi, M.A.: Appl. Surf. Sci. **65/66** (1993) 598.
93M Mayer, T.: Ph.D. Thesis, Technische Universität Berlin, 1993.
93R1 Ranke, W.: J. Electr. Spectr. Rel. Phen. **61** (1993) 231.
93R2 Ranke, W.,Wasserfall, J.: Surf. Sci. **292** (1993) 10.
94B Bu, H.,Rabalais, J.W.: Surf. Sci. **301** (1994) 285.
94G Gao, Q., Z. Dohnalek, Cheng, C.C., W.J. Choyke,J.T. Yates, J.: Surf. Sci. **312** (1994) 261.
94H Himpsel, F.H., in: Handbook of Semiconductors, Vol. II, Eds. T. S. Moss, M. Balkowski, Amsterdam, 1994), pp. 161 .
94K Karlsson, C.J., Landemark, E., Chao, Y.-C.,Uhrberg, R.I.G.: Phys. Rev. **B 50** (1994) 5767.
94L Lay, G.l., Göthelid, M., Grekh, T.-M., Björkquist, M., Karlsson, K.O.,Aristov, U.Y.: Phys. Rev. **B 50** (1994) 14277.
94S1 Schulze, R.K.,Evans, J.F.: Appl. Surf. Sci. **81** (1994) 449.
94S2 Sebenne, C., in: Handbook of Semiconductors, Vol. II, Eds. T. S. Moss, M. Balkowski, Amsterdam, 1994), pp. 33 .
95L Lüth, H., in: Surfaces and Interfaces of Solid Materials 3 Ed. Springer-Verlag, Berlin, 1995).
95M Mönch, W., in: Semiconductor Surfaces and Interfaces 2nd ed., (Springer-Verlag, Berlin, 1995).
95P Poncey, C., Rochet, F., Dufour, G., Roulet, H., Sirotti, F.,Panaccione, G.: Surf. Sci. **338** (1995) 143.
95V Vittadini, A., Selloni, A.,Casarin, M.: Phys. Rev. B **52** (1995) 5885.
95W1 Waltenburg, H.N.,Yates, J.T.J.: Chemical Reviews **95** (1995) 1589.
95W2 Wise, M., Okada, L., Sneh, O.,George, S.: J. Vac. Sci. Technol. A **13** (1995) 1853.
96F Flowers, M.C., Jonathan, N.B.H., Morris, A.,Wright, S.: Surf. Sci. **351** (1996) 87.
96H Henrion, O., Löher, T., Klein, A., Pettenkofer, C.,Jaegermann, W.: Surf. Sci. **366** (1996) L685.
96I Ikeda, H., Yamada, T., Hotta, K., Zaima, S.,Yasuda, Y.: Appl. Surf. Sci. **100/101** (1996) 431.
96J Jaegermann, W., in: Modern Aspects of Electrochemistry Ed. R. E. White, New York, 1996).
96K Katircioglu, S.,Ercoc, S.: phys. stat. sol. (b) **196** (1996) 77.
96M Mayer, T., Pettenkofer, C.,Jaegermann, W.: J. Phys. Chem. **100** (1996) 16966.
96R1 Raghavachari, K., Chabal, Y.J.,Struck, L.M.: Chem. Phys. Lett. **252** (1996) 230.
96R2 Ranke, W.: Surf. Sci. **369** (1996) 137.
96R3 Rincón, R., García-Vidal, F.J.,Flores, F.: Appl. Surf. Sci. **92** (1996) 216.
96S1 Scholz, S.M.,Jacobi, K.: Surf. Sci. **369** (1996) 117.
96S2 Sloan, D.W., Sun, Y.-M.,White, J.M.: J. Vac. Sci. Technol. A **14** (1996) 216.
97E Ezzehar, H., Stauffer, L., Leconte, J.,Minot, C.: Surf. Sci. **388** (1997) 220.
97H Henrion, O.: Ph.D. Thesis, Technische Universität Berlin, 1997.
97K Konecny, R.,Doren, D.J.: Journal of Chemical Physics **106** (1997) 2426.
97M1 Mitchell, W.J., Chung, C.-H., Yi, S.I., Hu, E.L.,Weinberg, W.H.: Surf. Sci. **384** (1997) 81.
97M2 Mitchell, W.J., Chung, C.-H., Yi, S.I., Hu, E.L.,Weinberg, W.H.: J. Vac. Sci. Technol. B **15** (1997) 1182.
97P Piancastelli, M.N., Paggel, I.J., Weindel, C., Hasselblatt, M.,Horn, K.: Phys. Rev. **B 56** (1997) R 12737.
97R Ranke, W.,Xing, Y.R.: Surf. Sci. **381** (1997) 1.
97S1 Self, K.W., Yan, C.,Weinberg, W.H.: Surf. Sci. **380** (1997) 408.
97S2 Struck, L.M., Jr., J.E., Bent, B.E., Flynn, G.W., Chabal, Y.J., Christman, S.B., Chaban, E.E., K.Raghavachari, Williams, G.P., Radermacher, K.,Mantl, S.: Surf. Sci. **380** (1997) 444.
97W Weldon, M., Stefanov, B., Raghavachari, K.,Chabal, Y.J.: Phys. Rev. Lett. **79** (1997) 2851.
97Z Zaibi, M.A., Lacharme, J.P.,Sebénne, C.A.: Surf. Sci. **377-379** (1997) 639.
98C Chung, C.-H., Yi, S.I.,Weinberg, W.H.: J. Vac. Sci. Technol. A **16** (1998) 1785.
98F Franco, N., Chrost, J., Avila, J., Müller, C., Dudzik, E., Patchett, A.J., McGovern, I.T., Giebel, T., Lindsay, R., Fritsche, V., Bradshaw, A.M.,Woodruff, D.P.: Appl. Surf. Sci. **123/124** (1998) 219.
00H Henrion, O., Klein, A.,Jaegermann, W.: Surf. Sci. **457** (2000) L337.